THE UNIVERSITY OF ALBERTA

Geometrical Effects in the Closed Tube Thermosyphon

by

©

Gary Simpson

A THESIS

SUBMITTED TO THE FACULTY OF GRADUATE STUDIES AND RESEARCH

IN PARTIAL FULFILMENT OF THE REQUIREMENTS FOR THE DEGREE

OF Master of Science

Mechanical Engineering

EDMONTON, ALBERTA

Fall 1986

ISBN 0-315-32312-4

THE UNIVERSITY OF ALBERTA

RELEASE FORM

NAME OF AUTHOR Gary Simpson

TITLE OF THESIS Geometrical Effects in the Closed Tube Thermosyphon

DEGREE FOR WHICH THESIS WAS PRESENTED Master of Science

YEAR THIS DEGREE GRANTED Fall 1986

(SIGNED) G. Simpson

PERMANENT ADDRESS:

#206 939 19 Avenue S.W.

Calgary, Alberta

T2T 0H8

DATED Sept. 19 1986

THE UNIVERSITY OF ALBERTA

FACULTY OF GRADUATE STUDIES AND RESEARCH

The undersigned certify that they have read, and recommend to the Faculty of Graduate Studies and Research, for acceptance, a thesis entitled Geometric Effects in the Closed Tube Thermosyphon submitted by Gary Simpson in partial fulfillment of the requirements for the degree of Master of Science.

....

Supervisor

....

....

....

Date Sept. 19, 1986

ABSTRACT

An experimental and analytical study of the single phase closed thermosyphon is presented. Emphasis is placed on large length to diameter ratios (L_H/d) and unequal heated and cooled lengths (L_H/Lc).

The experimental study utilized a 10 cm diameter steel thermosyphon with L_H/d values of 10, 30, and 50 and L_H/L_C ranging from 1 to 20. Methyl alcohol ($Pr \approx 6.9$) was used as the working fluid. Results for a temperature difference between the heated and cooled sections ranging from 3^o to 50^oC were found to lie entirely in the turbulent mixed flow regime. Increasing L_H/d or L_H/L_C had a detrimental effect on the heat transfer. A design correlation is given relating the effect of L_H/d and L_H/L_C on the Nusselt number.

The analytical study consisted of developing a coupling model such that the laminar open thermosyphon solution can be used to predict the results for the closed system. A coupling parameter, K, was introduced, thus providing results for pure advection (K=0), pure mixing (K=1), and refluent mixing tending towards pure conduction (1<K<2).

ACKNOWLEDGEMENTS

The author would like to express his appreciation and gratitude to Dr. G.S.H. Lock for his guidance, patience, and understanding throughout this research.

I would also like to take this opportunity to thank the Department of Mechanical Engineering and Dome Petroleum Ltd. for supplying financial assistance.

Special thanks is also due to A. Muir and T. Nord for their experimental assistance and to A. Liu for his help in recording the experimental data.

TABLE OF CONTENTS

LIST OF FIGURES

Figure | Page

Figure | Page

NOMENCLATURE

a	tube radius, inside [m]
b	ordinate intercept value for linear correlation
c	positive coefficients in the difference equation
c_p	specific heat (constant pressure) [J/kg·K]
d	tube diameter, inside [m]
g	gravitational acceleration [m/s^2]
h	convective heat transfer coefficient [w/m^2·K]
k	thermal conductivity [w/m·K]
K	coupling coefficient for closed thermosyphon
L	tube length of open thermosyphon or heated or cooled length of closed thermosyphon [m]
$\dot{m}$	mass flow rate [kg/s]
n	distance between nodes [m]
$\dot{q}$	heat flux density [w/m^2]
$\dot{Q}$	heat flux [w]
R	radius [m]
S	source term
T	temperature [oC]
ΔT	temperature difference [^{o}C]
U	velocity in axial direction [m/s]
V	velocity in axial or radial direction based on subscript [m/s]
X	axial length [m]
z	axial length [m]
β	coefficient of thermal expansion [1/K]
δ	momentum boundary layer thickness [m]

θ temperature difference [°C]

κ thermal diffusivity = $k/\rho c_p$ [m^2/s]

λ convergence criterion

μ viscosity, dynamic [Ns/m^2]

ν viscosity, kinematic [m^2/s]

ρ density [kg/m^2]

ϕ dependent variable = ψ, ω/r, or T

ψ stream function

ω vorticity

Nondimensional Groups

Gr Grashof number = $\beta g \Delta T a^3/\nu^2$

Pr Prandtl number = $\mu c_p/k$

Ra Rayleigh number = GrPr

Nu_a Nusselt number (open system) = $ha/k = Q/2\pi(T_1-T_0)kL$

Nu_d Nusselt number (closed system) = hd/k
$= Q/\pi(T_{1,1}-T_{1,2})kL$

t_a $\beta g a^4(T_1-T_0)/\nu\kappa L$

t_d $\beta g d^4(T_{1,1}-T_{1,2})/\nu\kappa L$

Subscripts

a based on radius

C cold

CA cold annulus

CC cold core

d based on diameter

E nodal point east of node of interest

H hot

HA	hot annulus
HC	hot core
i	adjacent interior node
N	nodal point north of node of interest
o	at point which velocity changes direction
p	boundary node
r	reservoir or radial direction depending on context
S	nodal point south of node of interest
w	at the wall
W	nodal point west of node of interest
z	axial direction
1	condition at wall
0	condition at reservoir or core entry
1,2	denotes bottom or top half respectively of closed thermosyphon; second element denotes tube half

1. INTRODUCTION

1.1 Definition and classifications

A thermosyphon is a device which transfers heat, mass, and momentum by utilizing the buoyancy forces on a fluid enclosed in a vessel. All major studies so far, in which the name thermosyphon has been used, are based on systems which have a specific function of removing heat from a source, carrying it along a specific path and depositing it in a sink. Natural convection from a heated plate or cylinder has the function of removing heat but the subsequent transportation is unprescribed thereby eliminating it from the thermosyphon classification.

Thermosyphons can be classified by the nature of their boundaries, the number of phases present, and the type of body forces. The boundary classifications are usually either a) Open, b) Closed or c) Closed Loop. Figure 1 illustrates the three types of boundaries. The phases are gas and liquid and the types of body forces are primarily gravitational or centrifugal.

Motivation for study of the thermosyphon is fuelled by it being a simple device which can transfer heat without power sources or moving parts. The thermosyphon also has the favourable property that it operates as a thermal "diode".

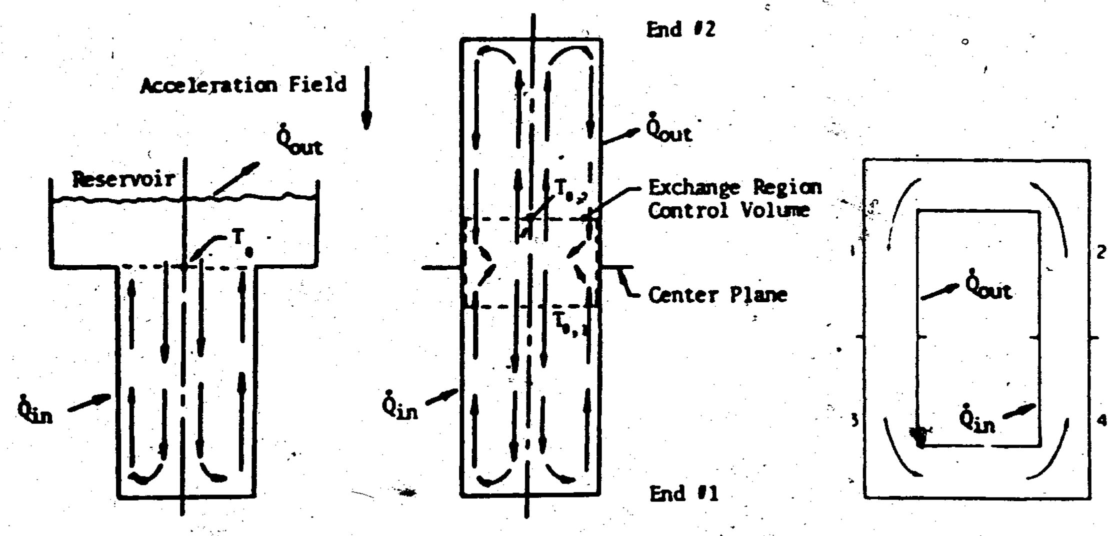

1a. Open Thermosyphon   1b. Closed Thermosyphon   1c. Closed Loop

Figure 1. The open, closed, and closed loop thermosyphons. (following Japikse [14]).

In a gravitational field, with the upper section cooler than the lower section, thermal buoyancy forces are set up which drive the flow and transfer energy by advection* from the lower section to the upper section. However, if the upper section is at a temperature higher than the lower section, no buoyancy forces are induced and heat transfer occurs by the much less efficient mechanism of conduction.

On a mathematical basis the thermosyphon can be described by the equations of conservation of mass, momentum, and energy. For this set of elliptical partial differential equations, an initial condition and boundary conditions on all of its physical boundaries are required to prescribe the problem. The present study is concerned with steady-state operation, thereby eliminating the requirement for an initial condition. If the flow may be further simplified to a boundary layer type then the specifications can be reduced to prescribing the reservoir or core entry temperature, T_0, for the open thermosyphon, or T_{01} and T_{02} for the closed thermosyphon, plus the physical boundary conditions.

The non-dimensional group used to describe the flow are defined as:

Nusselt number: $Nu_a = \dfrac{\dot{q}a}{\Delta T k}$, where $\dot{q} = \dfrac{\dot{Q}}{2\pi a L}$

* This term implies bulk flow or flux of energy ie. $\rho U C_p T$

Prandtl number: $Pr = \mu c_p/k$

Rayleigh number: $Ra_a = \dfrac{\beta g \Delta T a^3}{\nu\kappa}$

L/a

$t_a = Ra_a a/L$ or $t_d = Ra_d d/L$

which have been previously deduced [1]* from the laminar boundary layer equations.

1.2 Applications

Shortly before the second world war interest was sparked in the thermosyphon for potential use in the cooling of gas turbine blades. The gravitational force field is then replaced by a centrifugal force field which is frequently in the order of 10^4 g. E. Schmidt [2] was the first to develop and build a gas turbine with blades water-cooled by an open thermosyphon. From there work progressed into the use of closed thermosyphons and liquid metals as reported by Bayley and Bell [3]. The closed thermosyphon has the advantage of fluid containment and does not have the vibrational stability problems associated with the open thermosyphon. Most investigators have stressed the importance of the closed system when dealing with gas turbine blade cooling.

* Numbers in square brackets indicate references listed in bibliography.

Another application for the closed thermosyphon is in the cooling of nuclear reactors. This has an additional complication of heat generation. D. Wilkie and S.A. Fisher [4] have studied this problem experimentally and B.S. Larkin [5] has presented a general summary of this application. Larkin also mentions the use of thermosyphons for cooling transformer cores and dissipating heat from electronic equipment.

Exploration and development of the arctic has brought about several new northern applications. Larkin [5] and G.H. Johnston [6] have reported on the application of preserving the permafrost beneath heated buildings by using the cold winter air as a heat sink. In 1973 the Alyeska hot oil pipeline provided the largest single application of the closed thermosyphon. Over 120,000 of them were used to provide a freeze "bulb" in the soil around the vertical support members of the elevated sections of the pipeline. A two phase model was selected with ammonia used as the working fluid. An extruded aluminum radiator was press fitted onto the upper portion of the thermosyphon to improve the heat transfer between the atmosphere and the cooled section. C.E. Heuer [7] reports that after one winter season, freeze bulb radii of 1-1.5m were obtained.

The single phase thermosyphon has been preferred over the two phase model by the Soviets. G.F. Biyanov et al [8] report that the single phase model has been used to freeze and stabilize large earthen dams in the U.S.S.R.'s northern areas. It has also successfully been used there to stabilize permafrost under heated buildings.

There are several new arctic proposals for the use of the thermosyphon. The concept of constructing an ice veil to provide greater hydrological control of northern rivers has been reported by G.S.H. Lock [9]. A row of thermosyphons would be vertically driven into the riverbed and would extend several meters above the water surface. The relatively warm water would extend over the heated length and the cold winter atmosphere would envelop the cooled length. Ice growth around the tubes should eventually form into a curtain of ice.

Hydrocarbon production and development in the offshore arctic has also provided several new conceptual uses for thermosyphons. Preliminary engineering of oil production structures in the Beaufort Sea often call for freezing of the foundation immediately beneath the structure to increase the shearing resistance from an ice island collision. Thermosyphons have been proposed as one method to achieve this. Thaw subsidence around hot oil wells in permafrost is another Arctic petroleum problem. A ring of thermosyphons could be used radially around the well to prevent the degradation of the permafrost. In both of the above applications thermosyphons with large length to diameter ratios would be required.

1.3 Literature survey

a) Open system

In 1953 M.J. Lighthill [1] produced an analytical study on the single phase open thermosyphon which has provided a foundation for all future thermosyphon work. Lighthill introduced six basic flow regimes; three laminar and three turbulent. In the laminar regime for large t_a (Gr Pr a/L) ie. large ΔT or large a/L, he hypothesized that a boundary layer type of flow would occur where the boundary layer occupies a small portion of the tube. As t_a is decreased the boundary layers grow until eventually they approach the centerline and restrict the opposing flow. As t_a is further reduced, the wall effects reach a maximum where there is no longer a change in profile shapes, only in their scale. This region he called the similarity regime.

Lighthill started his analysis with laminar boundary layer flow and $Pr=\infty$ (neglecting inertia terms). He later determined that his results would only be about 10% in error for $Pr=2$. A Pohlhausen integral technique was used with equal thermal and momentum boundary layer thicknesses: parabolic temperature and cubic velocity profiles were chosen. Lighthill determined that the volume flow rate is no longer a maximum at the orifice when $t_a<3400$. This marks the transition into the impeded regime. He also stated that for large values of a/L the flow would tend asympotically to flow on a flat plate.

For smaller values of t_a, where the boundary layer fills the tube, integral techniques were again used in his solution. Lighthill predicted that when $t_a=311$ the velocity and temperature profiles showed no change in shape, only in scale. They had become linear functions of L. Below $t_a=311$ a stagnant region would exist in the tube.

For turbulent boundary layer flow the relationship of an earlier investigator was used which gave the Nusselt number as:

$$Nu_a=0.11Gr_a^{1/3}$$

Lighthill predicted for large t_a that a turbulent boundary layer flow would exist. Lowering t_a would result in turbulent flow filling the entire tube. Finally for a further reduction in t_a he predicted that a turbulent similarity solution would occur. Figure 2 shows all of Lighthill's predicted results. B.W. Martin [10] published his experimental results on the open thermosyphon shortly after Lighthill's work was presented. Martin used an opaque

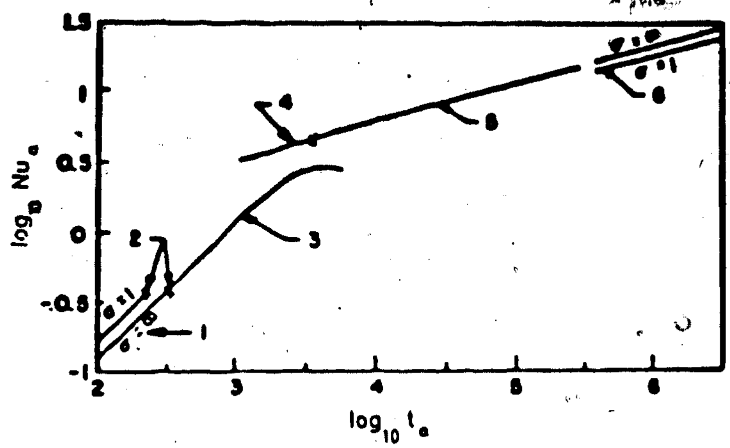

Notes:

1) Similarity flow with stagnant portion
2) Similarity solutions
3) Non-similarity flow with boundary layer filling the tube, Pr=0→∞
4) To the left of the cross involves a physical impossibility
5) Boundary layer flow, Pr=0→∞
6) Limiting case, free convection on vertical flat plate

Figure 2. Heat transfer for the open thermosyphon in laminar flow (following Lighthill [1]).

test cell of variable length heated electrically to obtain a reasonable isothermal wall boundary condition. The experimental results provided an excellent verification of the laminar results of Lighthill. Martin observed the boundary layer flow, the laminar impeded flow, and for low values of t_a; a stagnant portion in the bottom of the tube. Periodic fluctuations or surges in the flow were observed between the boundary layer flow regime and the impeded regime.

Martin also reported on two distinct modes of turbulence. For viscous fluids he observed a turbulent boundary layer and a laminar core. As t_a was increased a fully mixed turbulent flow occurred with lower heat transfer results due to the mixing of the hot and cold fluids. For less viscous fluids (water) the turbulent boundary layer regime was absent. Martin also investigated the effect of the L/a parameter. He discovered that as L/a increased for a given t_a, the Nusselt number decreased. For large values of L/a the flow would avoid the turbulent boundary regime and proceed directly into the fully mixed turbulent flow.

J.P. Hartnett and W.E. Walsh [11] conducted experiments on the open thermosyphon using a constant heat flux wall condition rather than the usual isothermal condition. The results were plotted using the orifice temperature subtracted from an average wall temperature. By comparison with Martin's results the authors concluded that the average performance for constant heat flux is equivalent to the isothermal case.

Quite recently Gosman, Lockwood, and Tatchell [12] presented a numerical study on the open thermosyphon. A finite difference solution was obtained to the full set of elliptic equations for laminar flow. The predictions are about 20% higher than Lighthill's results, for the similarity and impeded regime and slightly below Lighthill's for the boundary layer regime. The numerical solution predicted a continuous Nu vs. t_a curve as shown in Figure 3. Martin's experimental results for rapeseed oil (69<Pr<1107) with L/a=47.5 are also presented. The change in the Nusselt number for increasing L/a was found to be negligible, contrary to Martin's experimental observations.

b) Closed system

Lighthill first proposed that the closed thermosyphon be treated as two open thermosyphons joined together. He predicted that under turbulent flow the ramming of the two opposing boundary layers would cause a uniform core temperature. F.J. Bayley and G.S.H. Lock [13] presented the first experimental and analytical study on the closed thermosyphon. Emphasis was placed on the effect of L/a and on the exchange region between heated and cooled lengths.

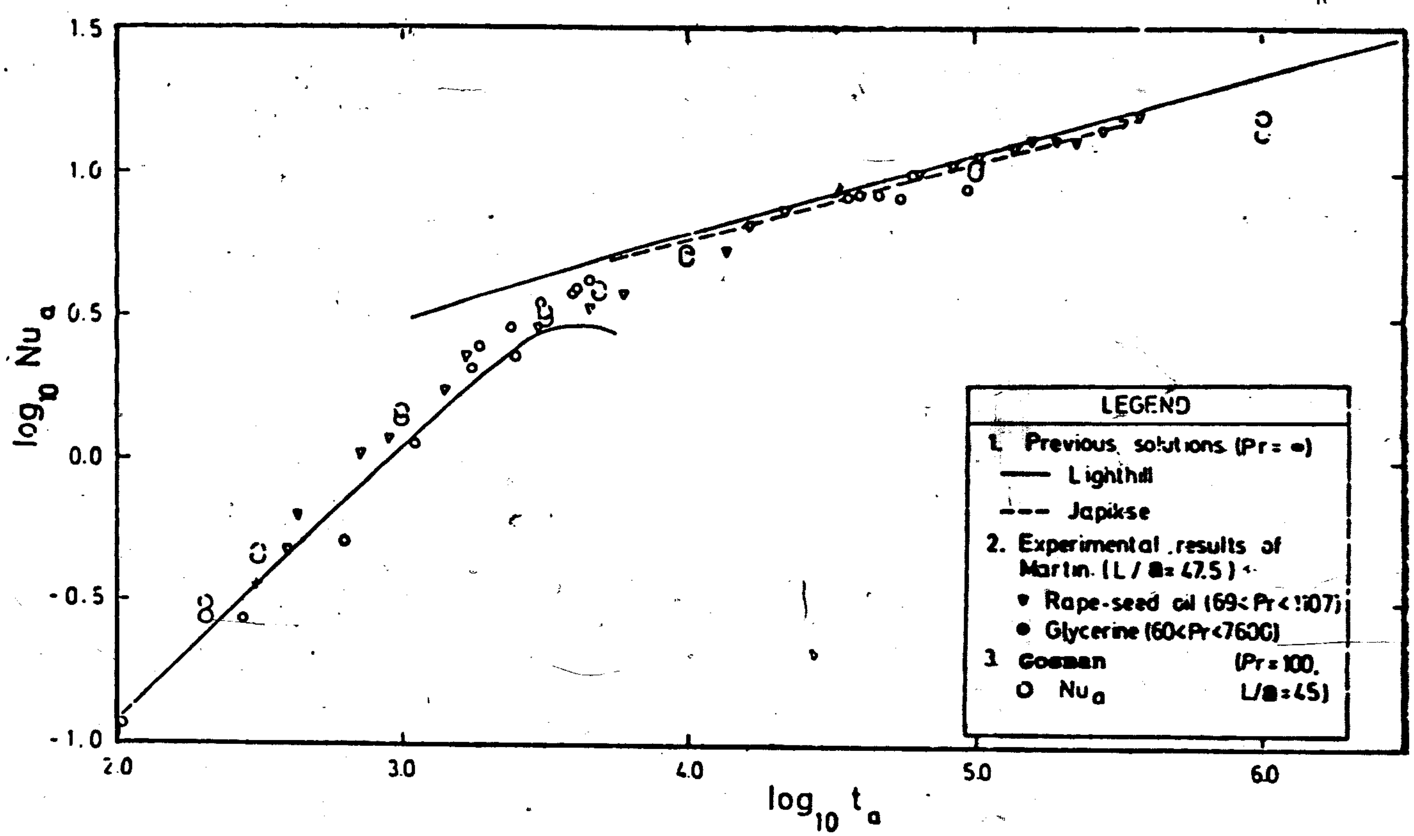

Figure 3. Heat transfer performance: comparison of Gosman et al. [12] results with others.

Tests were run using air, water, ethylene glycol, and glycerine in a vertical test cell of variable length, heated electrically and cooled by water jackets. Results are presented in figures 4-6.

The flow regimes of the open thermosyphon are also evident in the closed system. As t_d is increased a laminar impeded regime is seen to give rise to a laminar boundary layer regime. Turbulence was found to occur approximately at $t_d=10^{7.0}$ and a turbulent impeded regime arose at $t_d=10^{7.6}$. Increasing the L_H/d ratio is seen to have the effect of lowering the heat transfer.

Bayley and Lock proposed three idealized exchange mechanisms to help interpret their results. The first mechanism is called "mixing" which would occur from a violent ramming of the two opposing boundary layers giving rise to vigorous mixing in the exchange region. This in turn produces an isothermal pool of fluid which each core draws upon for its fluid requirements. Bayley and Lock provided evidence for the mixing mode by placing a forced convective coupling device in the exchange region. Figure 4 shows a small increase in the heat transfer when the device is present. This was thought to be due to the device guiding the boundary layers to the opposite core before mixing was complete.

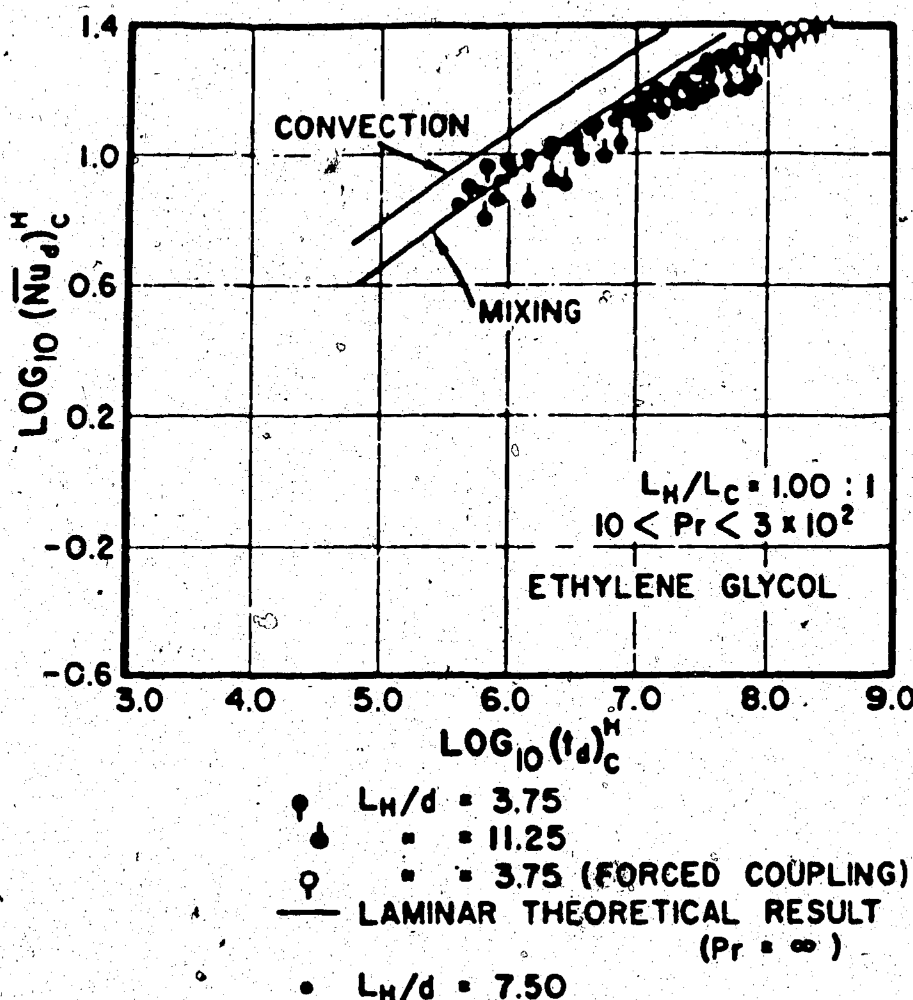

Figure 4. Effect of L_H/d on heat transfer rate in the closed thermosyphon (following Bayley and Lock [13]).

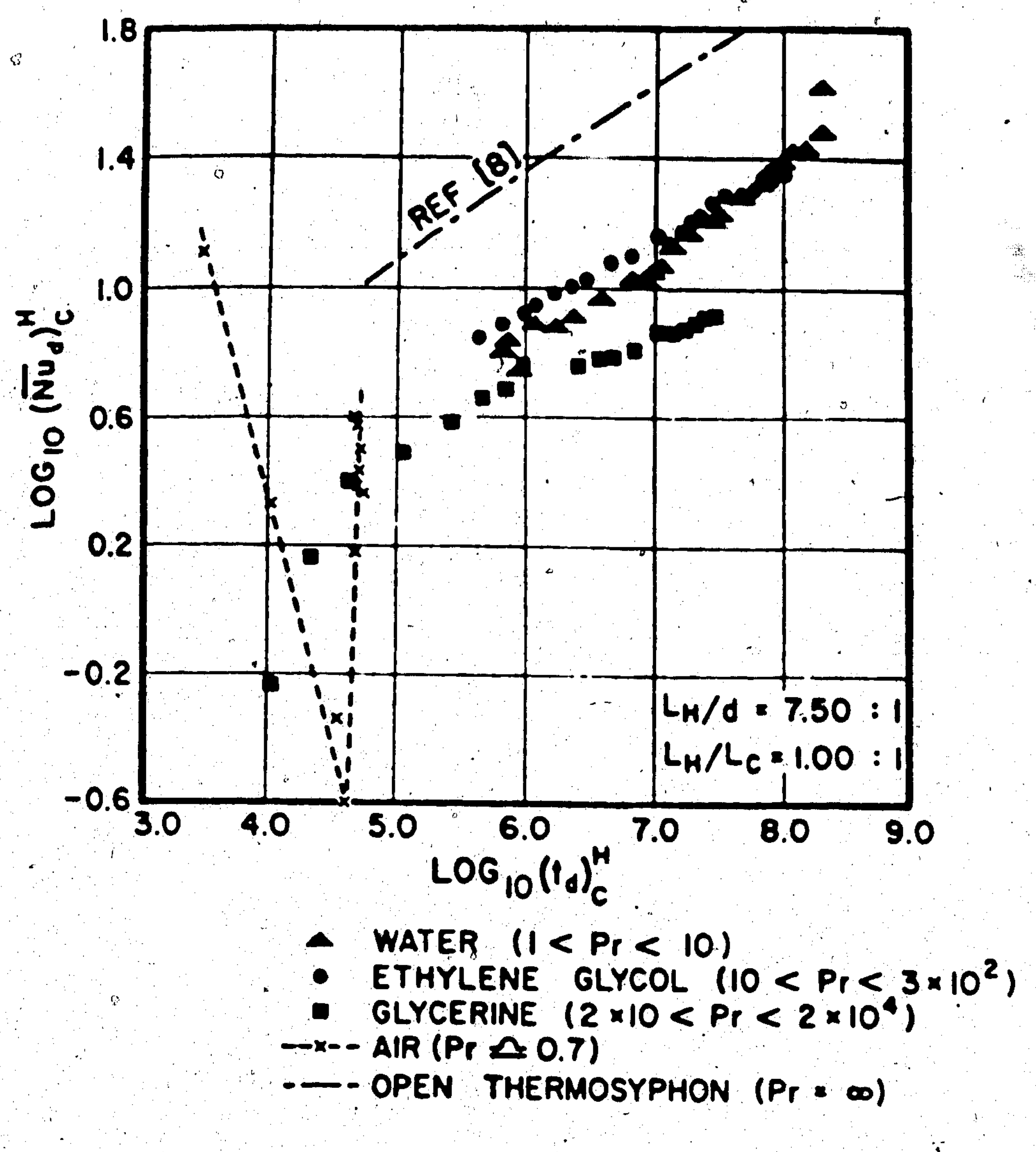

Figure 5. The effect of Prandtl number on heat transfer rate (following Bayley and Lock [13]).

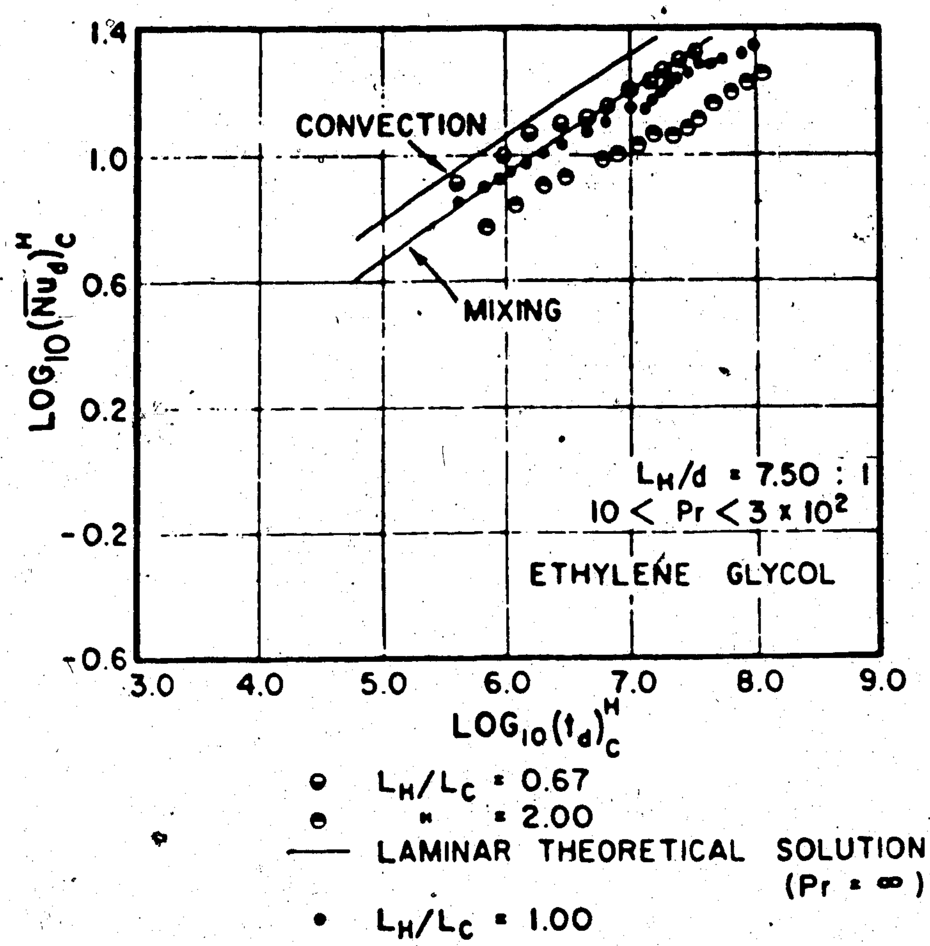

Figure 6. The effect of L_H/L_C on heat transfer rate (following Bayley and Lock [13]).

Bayley and Lock hypothesized a second exchange mode called "convection" which involves a crossing over of the boundary layers in an advective type flow, each becoming the core of the opposite section. Here it is visualized that the boundary layers break up into streamlines or fingers and the two opposing layers of fluid pass through each other much as the fingers from one hand can interlace through the fingers of the opposite hand. The advective or convective mode was thought to occur for large temperature differences and large Pr numbers. Secondary conduction through the hot and cold streams would reduce the efficiency of the mechanism. Experimental evidence of the center-line temperature indicated that the temperature in the heated section core was considerably lower than that in the cold section core, thus verifying such a convective coupling mechanism.

Bayley and Lock also used a Karman-Pohlhausen integral solution to the laminar boundary layer flow with either pure mixing or pure advection. Mixing gave very good results for ethylene glycol but was poor for glycerine. They suggested that since mixing lies between the optimum for advective coupling and the minimum for the conductive mode, it should provide a useful approximation for most laminar boundary layer flows.

D. Japikse [14] and Japikse and E.R.F. Winter [15] presented an analytical and experimental study of the closed thermosyphon. Flow visualization techniques were applied to a transparent closed cell for fluids ranging in Pr number from 4 to 940. The two opposing boundary layers met and exchanged basically in an advective mode. Distinct flow streams were observed flowing into the opposite core. These streams alternated one up, one down, and so on. Mixing and conduction were seen to play secondary roles. Japikse used a thermosyphon with $L_H/d=4$ and t_d ranging from $10^{5.25}$ to $10^{7.0}$. Turbulence occurred at approximately $10^{7.0}$.

Japikse also developed a numerical solution of the open thermosyphon by integrating the governing equations directly with cubic temperature and velocity profiles and employing an iterative procedure to obtain the Nusselt number. Good agreement was obtained with the results of Martin. Japikse then used an overall energy balance and applied the mechanical energy equation in the control volume of the exchange region in the closed thermosyphon to solve for the temperatures T_{01} and T_{02}. A simplified convective model was used with an exchange parameter ζ. Agreement of better than 10% was found with the heat transfer data from Bayley and Lock [13].

Quite recently, G.D. Mallinson, A.D. Graham, and G. de Vahl Davis [19] produced a numerical and flow visualization study of a rectangular closed thermosyphon. Numerical results for a three-dimensional flow model are presented for $t_d<4x10^5$ which augment the results of Japikse. These confirmed the conduction regime ($Ra<10^3$) with the flow separating and returning to its own half. An advective regime was evidenced for increasing Ra. The numerically produced streamlines were in good agreement with the experimental flow visualization carried out in the study. For the case of $t_d>4x10^5$ their numerical scheme became unstable.

1.4 Scope of thesis

The development of the far north has brought along a new range of problems that can be classified under the inter-disciplinary title of arctic engineering. One of the newest problems involves using the natural cold reservoir of the arctic to transfer heat from the warmer earth's surface. Permafrost stabilization, the growth of ice dams, the freezing of artificial islands all provide promising new applications for thermosyphons. However, these thermosyphons will require a relatively large heated length and thereby from economic and structural considerations a large L_H/d ratio. Also of interest will be the case of unequal heated and cooled lengths. The major object of this work is to explore the effect of these parameters on the heat transfer rate. In most situations it will be desirable for the cooled length to be considerably shorter than the heated length. The heat transfer from this shorter length can be augmented somewhat by the use of fins.

The single phase thermosyphon has been chosen for this study due to its inherent simplicity. Once the single phase model is better understood the results should provide a greater understanding and a lower bound to the more efficient two phase model. From an operational standpoint the single phase thermosyphon does not require sealed, pressurized tubes like its two phase counterpart. It can be easily field installed by vibration or pile driving with the filling fluid simply being poured into the tube and a cap placed over its top. If desirable, the heat transfer can be considerably increased by the simple addition of a compressor and some rubber tubing to form an aerosyphon [16]. The heat transfer results for the aerosyphon have been reported to equal and ~~surpass~~ those of the two phase model.

This thesis has been divided into two main parts: experimental results and numerically generated theoretical results. The experimental section consists of heat transfer curves generated for a 10 cm diameter single phase closed tube thermosyphon with L_H/d ranging from 10 to 50. The heated/cooled length ratio was also varied from a minimum value of one to a maximum value of 20. A vertical orientation was chosen for the thermosyphon so that results may be easily compared to those of past investigators. Thermophysical property values of several easily obtainable fluids were examined in order to select a likely candidate for future arctic applications. Methyl alcohol (methanol) was chosen as the test fluid since it remains in a liquid state over typical ambient temperatures, has a relatively constant Prandtl number, and is reasonably priced.

The theoretical work was performed on an open system with a closed thermosyphon coupling model applied to it. Isothermal walls and an adiabatic base were prescribed for the boundary conditions and constant properties for the fluid were assumed. A vertical orientation of the thermosyphon was selected such that the governing equations could be reduced to the simpler two-dimensional axi-symmetric form.

2. DESIGN OF EXPERIMENTS

2.1 Objectives

Three main objectives were kept in mind when performing the experimental portion of this thesis. They were:

1) To obtain heat transfer data for a closed thermosyphon with the large L_H/d (slenderness) ratios that would be characteristic of an arctic application.

2) To obtain heat transfer data to explore the effect of unequal heated and cooled lengths, specifically for the case of large heated lengths.

3) To study the coupling mechanism between the heated and cooled sections.

The first two objectives were achieved by constructing an experimental rig and measuring the wall temperatures and the supplied heat flux. The third objective required a probe to scan inside the thermosyphon and observe fluid behaviour in the immediate vicinity of the coupling plane.

2.2 Experimental rig

In a characteristic arctic application such as the formation of a winter ice veil in a river or the stabilization of permafrost beneath heated structures, it is likely that the L_H/d ratio of a thermosyphon would be in the range of 20-50. Once above the ratio 50:1 the delicate structural considerations of the tube would begin to make a field installation, such as pile driving into foundation material, difficult and expensive. In addition there is the heat transfer benefit of keeping the diameter as large as practicable since t_d is proportional to the diameter raised to the fourth power and only inversely proportional to the length. (See Introduction).

Keeping the above in mind, thermosyphon tubes consisting of a 4 inch nominal steel pipe (102.3 mm I.D., 114.3 mm O.D.) in heated lengths of 1.0, 3.0, and 5.0 m were selected for the experimental rig. Brass has been the usual choice of past investigators for the tube material due to its high thermal conductivity (111 W/m^{o}C). However, it is unlikely that it would be used in a major field application due to its high cost. The thermal conductivity of the steel pipe is 45 W/m^{o}C which, as will be shown later, produces a maximum error in the thermocouple temperature readings of only 0.7^{o}C or 1.6% of the difference between the hot and cold wall temperatures.

Heating was supplied by wrapping nichrome electrical resistance ribbon around the pipe wall. Electrical insulation between the steel pipe and the nichrome was achieved by using high temperature (200°C) electrical resistance tape. Several electrical shorts occurred as a result of small nicks in the tape but these were readily detectable from the overall resistance of the system and easily repaired.

The electrical wiring of the nichrome ribbon was arranged such that for the 1.0, 3.0, and 5.0 m heated lengths, there were two, three, and five resistors in parallel. This lowered the total resistance of the system such that the power requirements could be met by the 220 V line voltage. Unfortunately, separate power supplies for each resistor were unavailable, therefore some altering of the resistances was performed in an attempt to achieve a better approximation to an isothermal wall condition (see section 2.3). Figure 7 illustrates the wiring details used for the 5.0 m length. The other two heated lengths had a similar configuration.

Power was fed from the 220 V line power into a 2 kVA variac power controller. The drift in power readings in the 50 W to 2kW range was found to be less than 2%. For power readings of less than 50 W a Hewlett-Packard 6286 A d.c. power supply was used. The drift in the steady state power

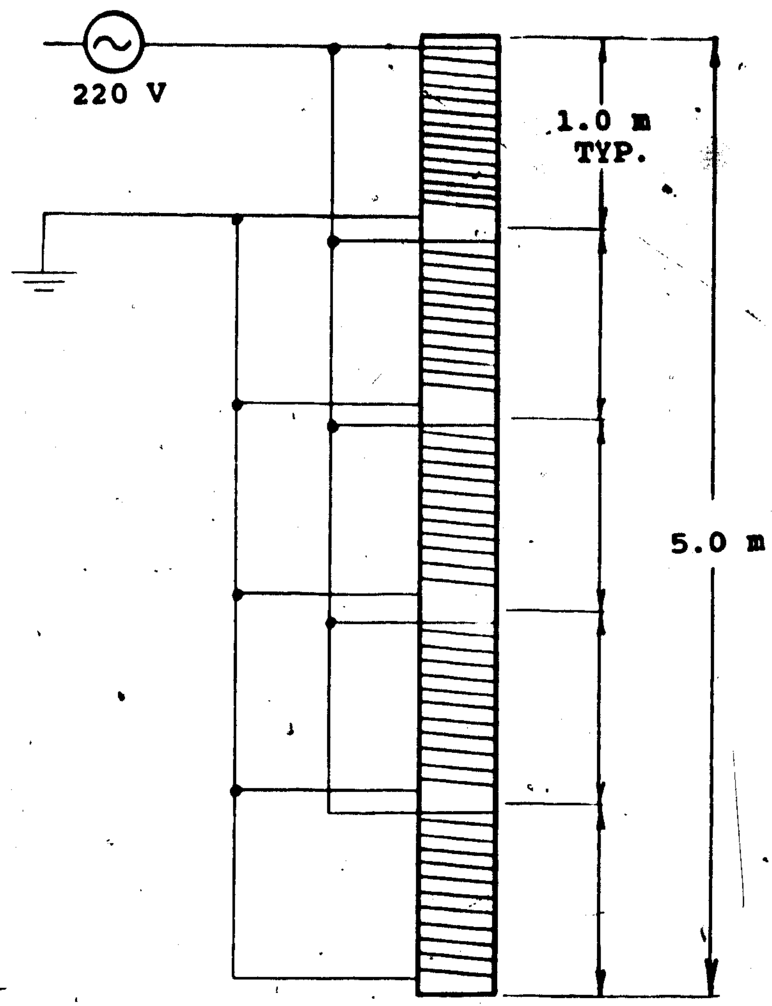

Figure 7. Electrical wiring and wrapping of the 5.0 m heated length.

supply for this unit was observed to be less than 1%.

Due to the large number of turns in the 5.0 m heated length it was thought prudent to check if the alternating current power supply could be inducing eddy currents in the tube. The induction in the nichrome wire was measured to be 0.040 mH, which with the 11 Ω total resistance of the windings, resulted in a negligibly small power factor angle of 0.08°. Thus the reactive power dissipated through the nichrome resistance differed from the supplied power by less than 0.0001%.

The bottom of the steel pipe rested on a 100 mm thick piece of blue STYROFOAM SM (k=0.029 W/m°C) which provided the adiabatic boundary condition for the base of the tube. A 10 mm thick styrofoam disc that fitted inside the 4 inch pipe and rested on top of the methanol was used to provide an approximation to an upper adiabatic boundary condition. Insulation for the walls of the heated section was supplied by 50 mm thick formed fiberglass steam pipe insulation (k=0.09 W/m°C). An 18 mm thick insulating ring of hard rubber (k=0.15 W/m°C) was placed in the joint between the hot and cold sections in an attempt to reduce axial conduction.

Cooling of the upper part of the thermosyphon was effected by the use of a waterjacket. This was constructed from a

1.0 m length of 16 ga. galvanized sheet steel rolled and welded watertight to provide a 12 mm annular gap. The waterjacket was then securely sealed to the outside of the 4 inch pipe by the use of "O" rings. Tube fittings of 3/4 inch diameter were located at each end of the waterjacket for the cold water inlet and outlet. Figure 8 illustrates the general arrangement of the thermosyphon rig.

Cooling of the thermosyphon through the waterjacket was accomplished by using the cold water supply of the building. The water supply was found to have a slow drift in its temperature of 2 or 3 ^{o}C every few hours. This was not thought to significantly affect the "instantaneous" results because the time response of the thermosyphon to an approximate $10^{o}C$ step change in the temperature of the cooling water was measured and found to be in the order of minutes, while a significant drift in the cooling water temperature required a time span in the order of one hour.

2.3 Instrumentation and calibration

Copper-constantan thermocouples were attached to the outside of the tube wall using a high thermal, but low electrical conduction thermocouple paste. The thermocouples for the 1.0, 3.0, and 5.0 m heated lengths were arranged in a diametric plane as shown in Figure 9: their signals were fed into an Omegaswitching box, from which the

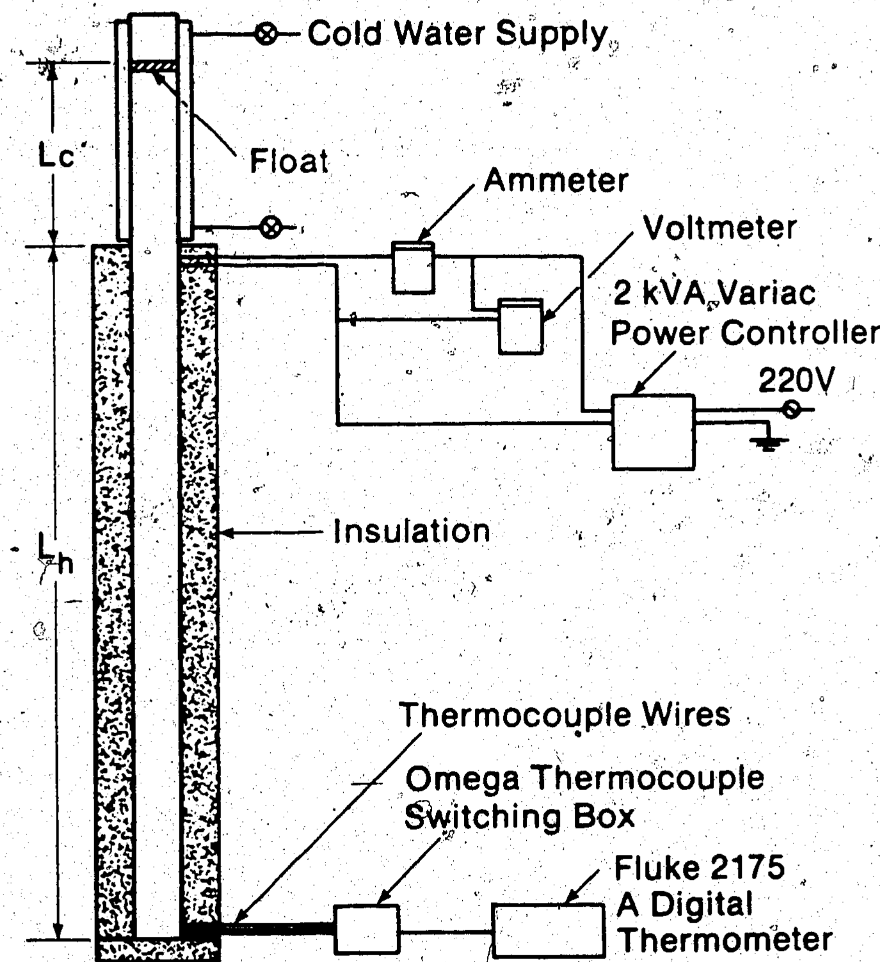

Figure 8. General arrangement of thermosyphon rig.

output was fed into a Fluke 2175 A digital thermometer, factory calibrated for copper-constantan thermocouples. Figure 9 illustrates the thermocouples that were operational over all of the tests and that were used in the analysis of Chapter 3.

The accuracy of the temperature readings depends on the uniformity of the thermocouple wire and the calibration and integration capabilities of the digital thermometer. The specifications for the thermocouple wire is 1% of the temperature, referenced to 0°C, and the accuracy of the Fluke digital thermometer is rated at 0.2°C. Therefore for the minimum 12° and the maximum 70°C wall temperatures recorded, errors of ±0.3°C and ±0.9°C respectively could be expected. A check on the accuracy of the thermocouples was performed using a 50% glycol-water bath with a temperature range of 24°C to 43°C. It was found that all of the thermocouples consistently read the same temperatures to within 0.1°C. However, the magnitude of the thermocouple readings when compared with two mercury thermometers (accurate to 0.2°C) showed a consistent offset* of 1.9°C. Since this offset was constant over the entire temperature range, and all data is processed using a temperature difference, the temperature offset will only have a minor effect essentially limited to the property values of the

* The effect has been attributed to the digital thermometer calibration.

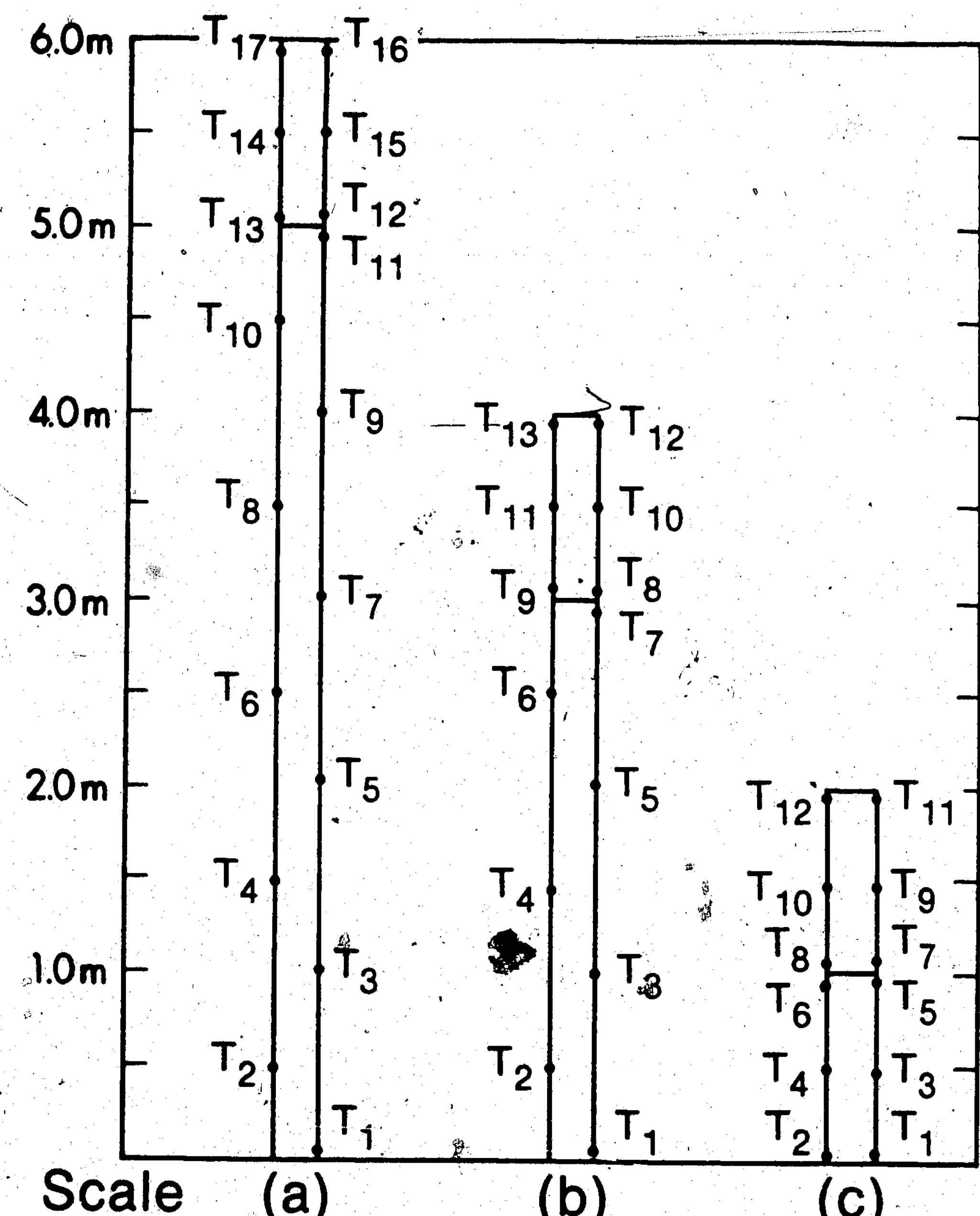

Figure 9. Thermocouple arrangements for a) 5.0 m heated length, b) 3.0 m heated length, and c) 1.0 m heated length.

fluid. The accuracy of ΔT for the outside wall temperatures should be about $0.1^{o}C$.

An initial calibration curve to measure the "heat leak" was performed for each of the heated lengths of the thermosyphon. For these tests the thermosyphon was filled with styrofoam chips (aggregate conductivity $k \approx 0.1\ W/m^{o}C$)* the cooling water was turned on, and the wall temperatures were recorded for various amounts of electrical power. A plot of the power supplied and the hot wall and room temperature difference resulted in a calibration curve, approximately linear, passing through the origin. Appendix 1 contains the calibration curves for the 1.0, 3.0, and 5.0 m heated lengths.

As part of a more detailed analysis of heat transfer from a representative point A in the tube wall (see Figure 10) a numerical solution of conduction in a solid cylinder of insulating material was performed to verify the assumption that the "heat leak" was primarily radially outward (route 1) and not being conducted axially into the cold section (route 2). Isothermal boundary conditions were prescribed on the cylinder walls with a temperature step change between the hot and cold sections. A finite difference method as outlined by Patankar [17] was used for the

* Based on the mean of air ($k=0.09\ W/m^{o}C$) and styrofoam ($k=0.12\ W/m^{o}C$)

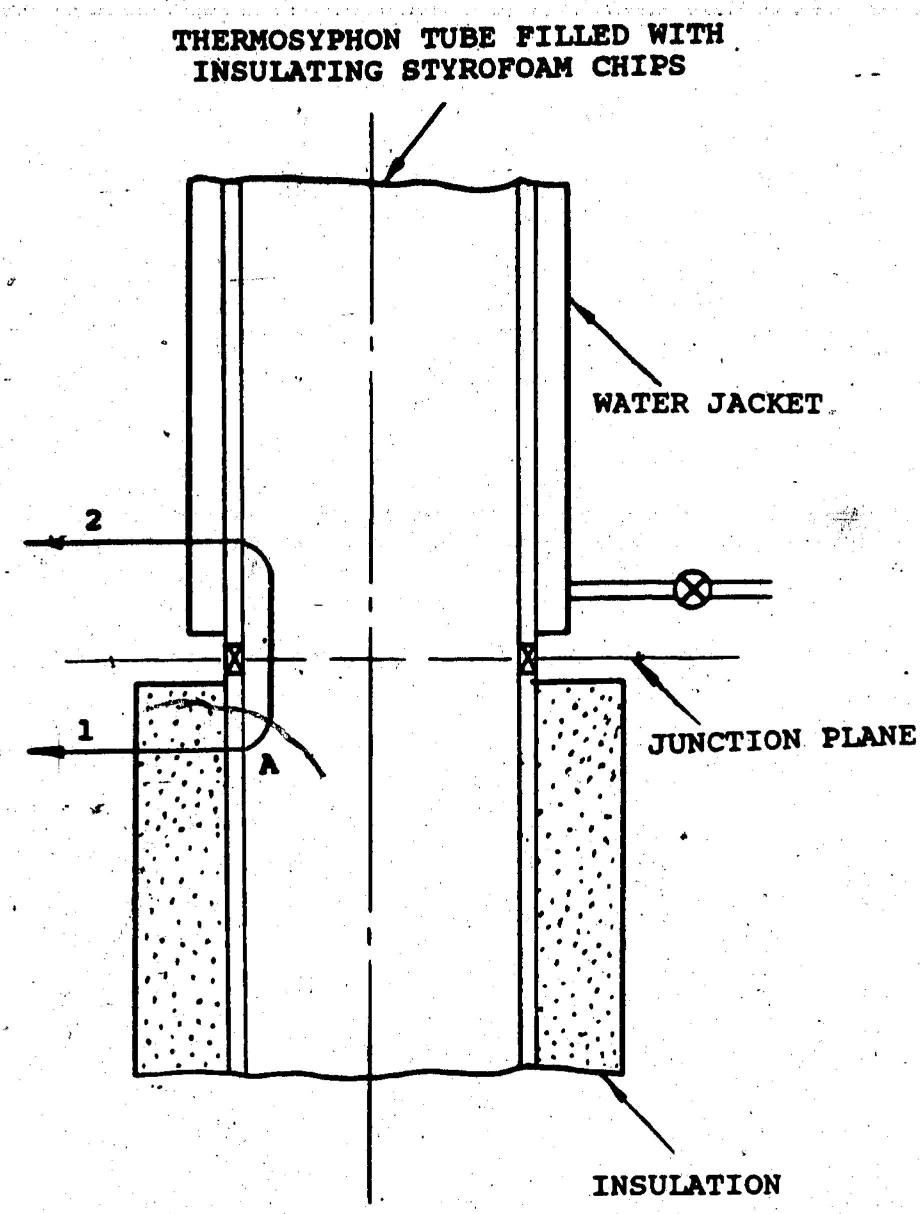

Figure 10. Possible "heat leak" routes during thermosyphon calibration.

numerical algorithm. For a typical case of T_h=50°C, T_c=15°C and k=0.1 W/m°C, the numerical solution indicated that a heat flux of approximately 1.0 W would be transferred axially through the styrofoam chips at the junction between the hot and cold walls. The magnitude of this heat flux remained constant for the three heated lengths. However, the percentage of the "heat leak" that axial conduction represented in flux supplied to the rig was 5.9%, 3.4% and 2.1% for the 1.0, 3.0 and 5.0 m heated lengths respectively. These percentages of the "heat leak" did not significantly vary with the magnitude of the temperature step change, thus verifying that the "heat leak" was primarily radial. The "heat leak" typically comprised about 5% of the total heat supplied.

The nichrome resistance wire used for heating the lower section of the tube was wired in parallel. Since the power is inversely proportional to the resistance in a parallel circuit, the resistance of the upper coils of nichrome was reduced by the selected use of jumper wires in an effort to increase the power supplied to the upper portions of the heated section. In addition the rubber gasket used for thermal insulation between the hot and cold tubes was increased in thickness from 6 mm to 18 mm in order to reduce axial conduction through the steel tube. Typical wall temperature distribution curves for the thermosyphon filled with styrofoam chips and with the working fluid,

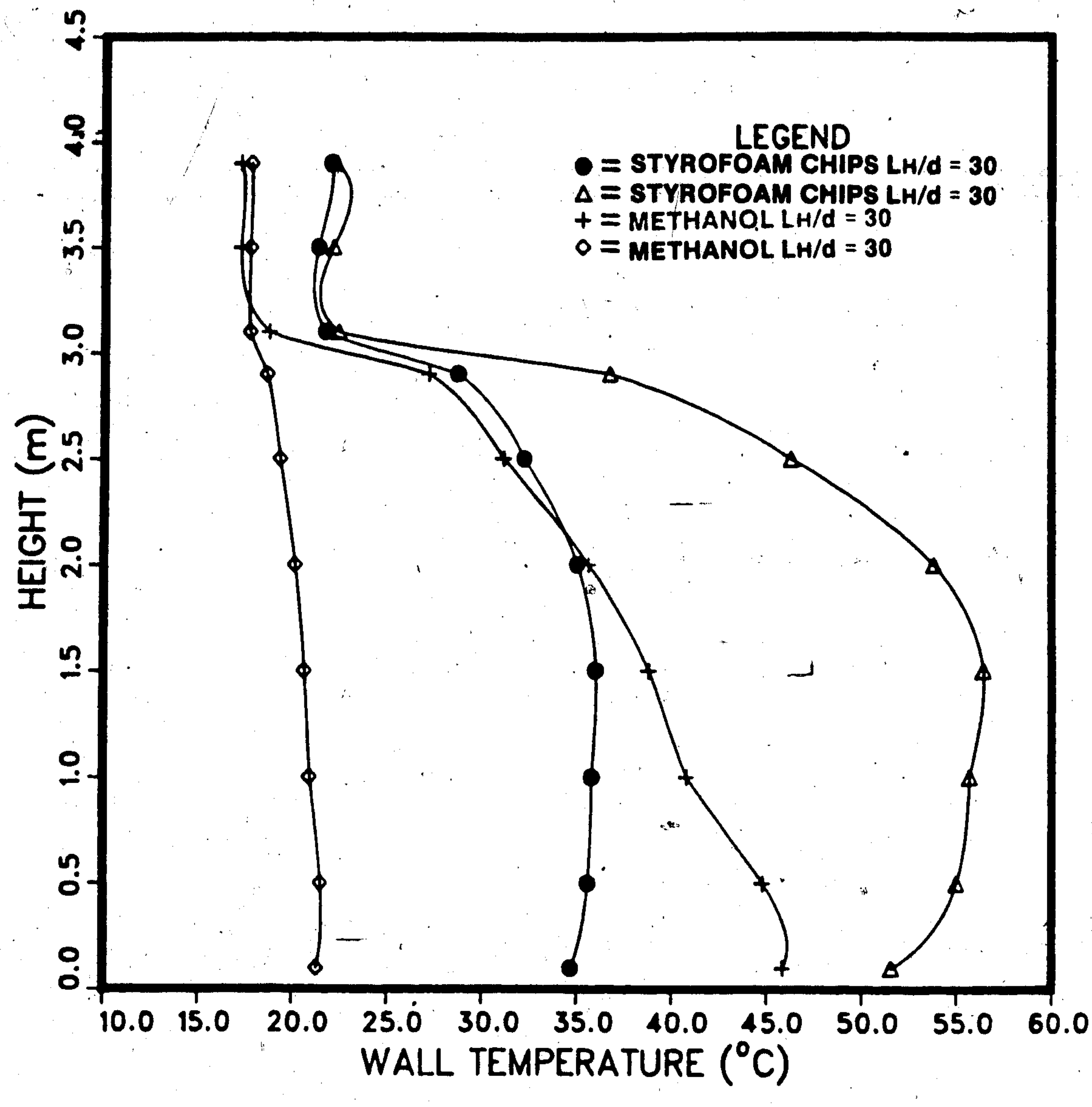

Figure 11. Comparison of wall temperature profiles for two fillings ($L_H/d=30$).

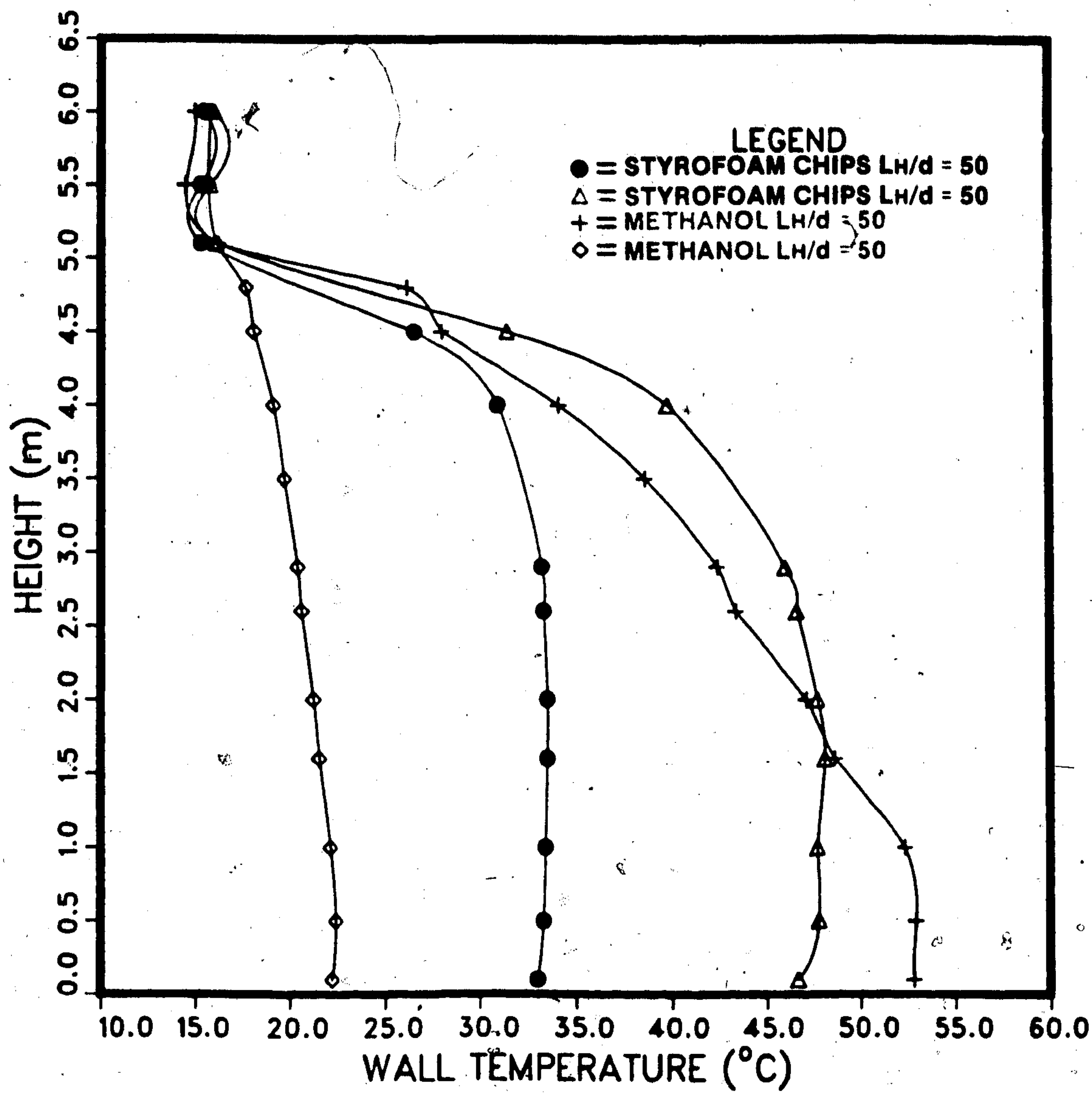

Figure 12. Comparison of wall temperature profiles for two fillings ($L_H/d=50$).

methyl alcohol, are illustrated in Figures 11 and 12.

As indicated, the desired isothermal walls with a step change at the junction plane was not achieved with the thermosyphon filled with methanol. However, for a typical field application the expected boundary conditions would likely involve a smooth temperature change between the hot and cold sections and some compromise between isothermal and constant heat flux wall conditions. The figures indicate that the hot wall temperature is closer to a linearly decreasing function of distance from the tube bottom than an isothermal function.

Hartnett and Welsh [11] have experimentally studied the case of constant heat flux for the open thermosyphon. Their measured wall temperature profile as shown in Figure 13 was similar to the profile obtained for the 5.0 m heated length in this study. In their analysis they used an average wall temperature in calculating the Nu number and determined that this was equivalent to the isothermal case as studied by past investigators. This procedure is also followed in this thesis.

To test the hypothesis that a linearly decreasing wall temperature merely reflects a constant flux boundary condition, the numerical solution (Chapter 4) was used to generate corresponding data. Contrary to expectations, the

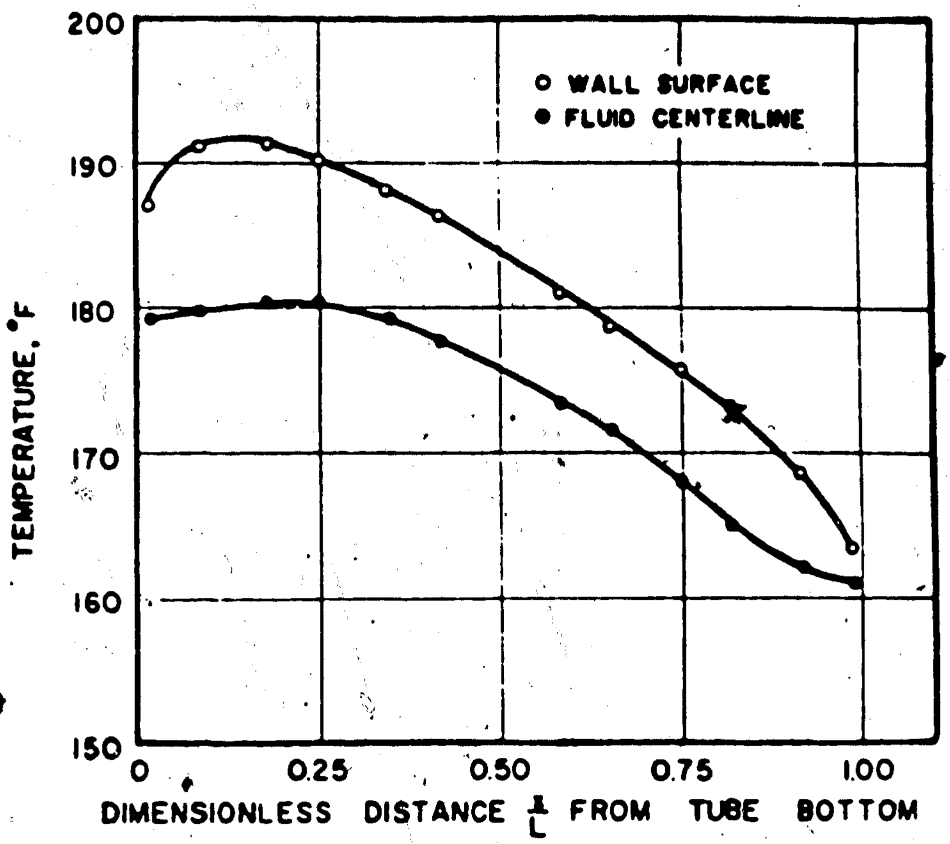

Figure 13. Temperature distribution in the open thermosyphon with a constant heat flux, t_a=6.1, L/a=22.5, [11].

wall temperature distribution was found to be an <u>increasing</u> function of distance from the tube bottom. Therefore the decreasing wall temperature distribution as observed by Hartnett and Welsh and in this study is not simply due to the constant heat flux boundary condition. Some other phenomenon such as junction inter-mixing or core boundary layer inter-action must be involved.

The thermocouples measuring the wall temperature of the thermosyphon were located on the outside of the tube, but the inside tube temperature is used in the heat transfer analysis. A simple conduction calculation was performed to estimate the inside wall temperature and hence the associated error in considering the inside and outside wall temperatures to be equivalent. In the insulated heated section of the thermosyphon the worst case radial "heat leak" was measured to be approximately 100 ~~W~~ ~~across~~ across the tube wall. Using Fourier's law to calculate (T_o-T_i)

$$\dot{Q}=-kA\partial T/\partial R=-k2\pi RL(T_o-T_i)/(\ln R_o/R_i) \ ,$$

where k= thermal conductivity of the tube = 45 W/m^{o}C

R_o= outer radius = 57.15 mm

R_i= inner radius = 51.15 mm

L= 1.0 m ,

resulted in an inner and outer wall temperature difference of less than 0.05^oC.

However, for the uninsulated cooled section all of the heat supplied was transferred radially thereby increasing $\mathring{Q}$ to a worst case value of approximately 1700 W corresponding to an inner and outer wall temperature difference of 0.7^oC. Fortunately the temperature difference between the hot and cold walls was much larger than this, resulting in a maximum error in T_H-T_C of 1.6%. For smaller values of $\mathring{Q}$, the percentage error in ΔT by taking the outside wall temperature equal to the inside wall temperature was reduced to a lower limit of about 0.5%.

As part of the coupling region studies, an axial copper-constantan thermocouple probe was constructed to examine the coupling mechanism between the heated and cooled lengths of the thermosyphon. The probe, illustrated in Figure 14, consisted of a 3.1 mm diameter stainless steel tube that ran axially along a piece of piano wire anchored at both ends of the tube. The piano wire was situated 12 mm from the tube wall enabling the thermocouple on the probe tip to take both axial and radial profiles. The probe was able to extend 1.0 m from the junction plane downward into the heated section and 150 mm upwards into the cooled section. The thermocouple emf was recorded by a Hewlett-Packard 7101 B strip chart recorder. The response time of the thermocouple and recorder was measured to be

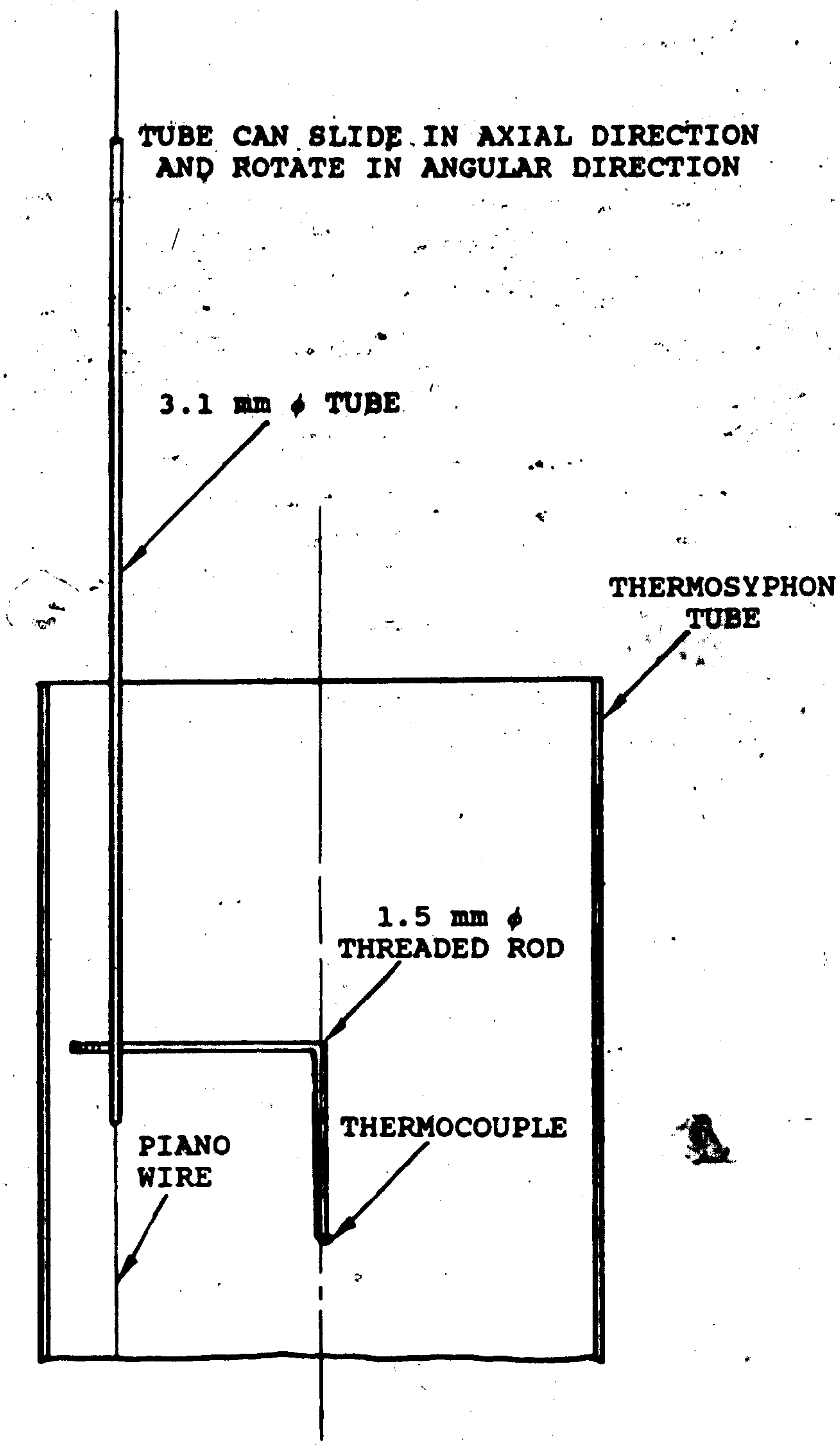

Figure 14. General arrangement of thermocouple probe.

less than 0.2 seconds. The resolution of the recorder was 0.001 mV corresponding to 0.025 °C.

2.4 Test schedule

An experimental program was initiated to extend the earlier work of Bayley and Lock [13] by obtaining heat transfer data for the closed tube thermosyphon. As noted previously the primary objectives were to investigate the effect of large L_H/d ratios and unequal heated and cooled lengths. Table 1 provides a list of the experimental configurations.

	L_H (m)	L_C (m)	d (mm)	L_H/d	L_H/L_C	$\log_{10} t_d$
#1 *	1.0	1.0	102	10	1	7.6-9.2
#2	3.0	1.0	102	30	3	6.9-8.5
#3	3.0	0.6	102	30	5	7.2-8.5
#4	3.0	0.3	102	30	10	7.3-8.5
#5 *	3.0	1.0	102	30	3	7.2-8.4
#6	5.0	1.0	102	50	5	7.1-8.3
#7	5.0	0.5	102	50	10	6.9-8.3
#8	5.0	0.25	102	50	20	6.9-8.3

Table 1 Experimental configurations

* Indicates a free surface boundary condition.

3. EXPERIMENTAL RESULTS

3.1 Preliminary observations

The first experimental test ($L_H/d=10$, $L_H/L_C=1$) was performed with a free surface as the upper boundary condition. It was thought that due to the large length to diameter ratio that the upper boundary condition would not significantly affect the results. Nevertheless, an exploratory test was undertaken to check the influence of the upper free surface as revealed in Figure 15. All other tests were performed with a 12 mm thick styrofoam float which rested on top of the working fluid. As seen, no discernible difference exists between the experimental results with and without the float.

In the lower ranges of t_d a large amount of scatter (40%) exists in the experimental results. Some of this is attributable to the higher percentage error in thermocouple measurements when operating at small ΔT values, but the largest uncertainty results from the measurement of the heat flux at these low power readings. Since the cold wall temperature is fixed by the domestic cold water supply ($\approx 12^oC$), typical hot wall temperature readings in the lower t_d range were $7-10^oC$ below the average room temperature of 24^oC. The calibration curve for the "heat leak" was measured for temperatures above room temperature. In order

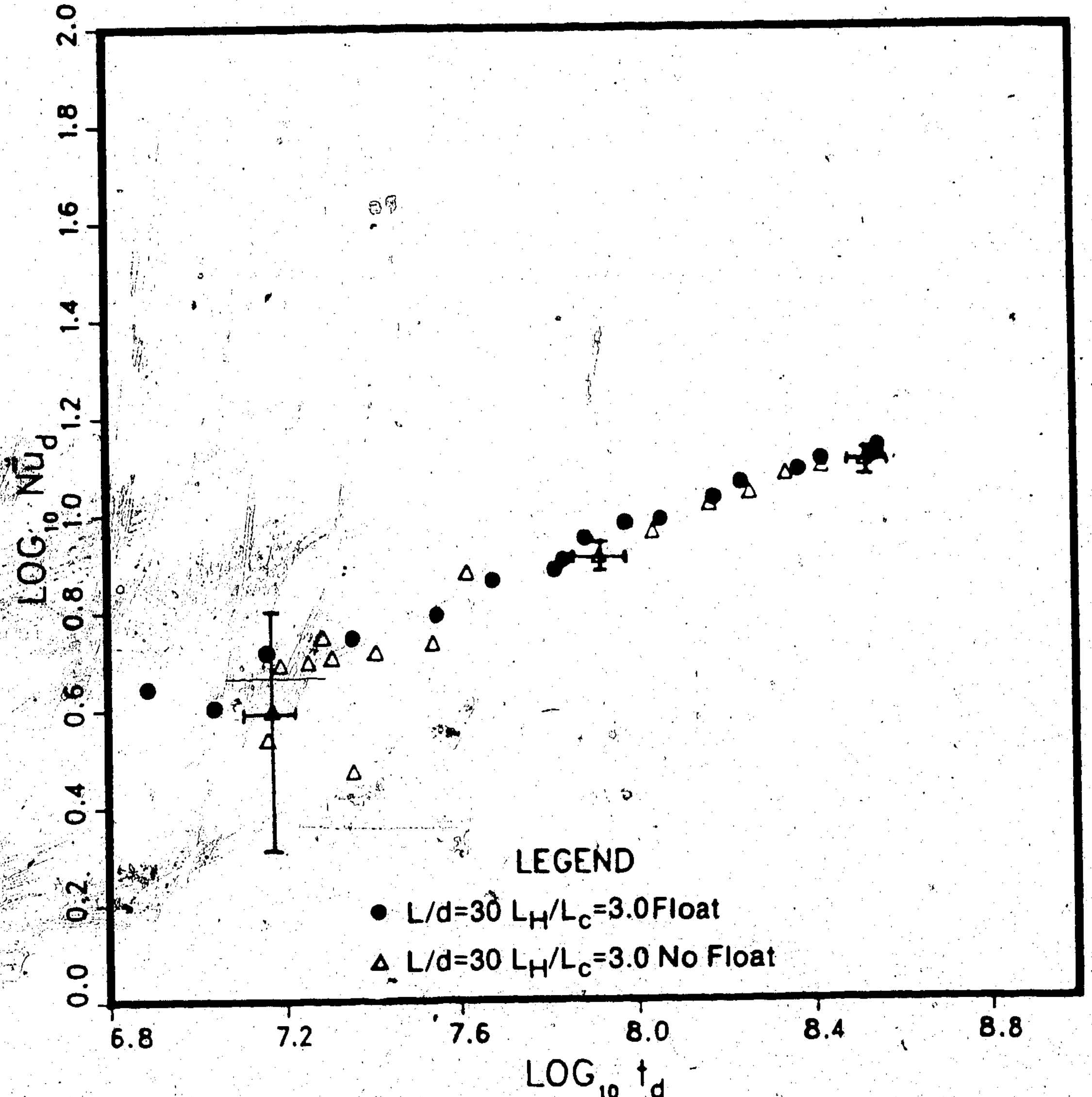

Figure 15. Effect of upper boundary condition on heat transfer rate.

to adjust for the heat gain for hot wall temperatures below room temperature, the calibration curve was linearly extrapolated through the origin to supply values for a negative T_H-T_{room}. The calibration correction was then added to the measured power supply to result in the total heat flux to the hot wall.

An error analysis was performed on data points at the low end, mid-range, and upper end of the Nu_d-t_d curve. The large vertical error bars for the small t_d values reflect the approximate 50% uncertainty in the supplied heat flux. As the hot wall temperature increases above the room temperature ($t_d \approx 10^{7.7}$), the uncertainty in the supplied flux decreases to approximately 2%. This is reflected in the dramatic decrease in the magnitude of the vertical error bars. The horizontal error bars, being largely due to temperature uncertainties, remain relatively constant with respect to the log scale.

For a change in T_H-T_C of about 5^oC, a time span of approximately six hours was sufficient for the system to reach a steady-state temperature distribution relative to the resolution of the digital thermometer. This long length of time can largely be attributed to the heat absorbing capacity of the thermal insulation surrounding the heated section of the tube. For a larger increment in the hot and cold wall temperature difference, a correspondingly larger time span was required for the system to reach steady-state as measured by the resolution of the digital thermometer.

3.2 Comparison with results of Bayley and Lock

Test No. 1 in this study had a length/diameter ratio of 10 and equal heated and cooled lengths. The heat transfer results are presented in Figure 16 along with those of Bayley and Lock's [13] for $L_H/d=7.5$. The Pr number for water used in [13] is assumed to be about 7, slightly higher than the average value of 6.9 for methyl alcohol used in this study. The results of this study compare favourably with the results from Bayley and Lock. Both the slope and the magnitude are seen to be in agreement.

The thermocouple probe that was described in Chapter 2 was used to obtain center-line temperature profiles and radial profiles in an attempt to classify the flow regime of the thermosyphon. It was found that the flow was turbulent and mixed over the entire range of t_d values ($10^{7.2}<t_d<10^{9.2}$). This is also in agreement with the observations of Bayley and Lock who observed a transition to turbulence at $t_d \approx 10^7$.

3.3 Effect of L_H/L_C

The cooled length of the apparatus was easily altered for a

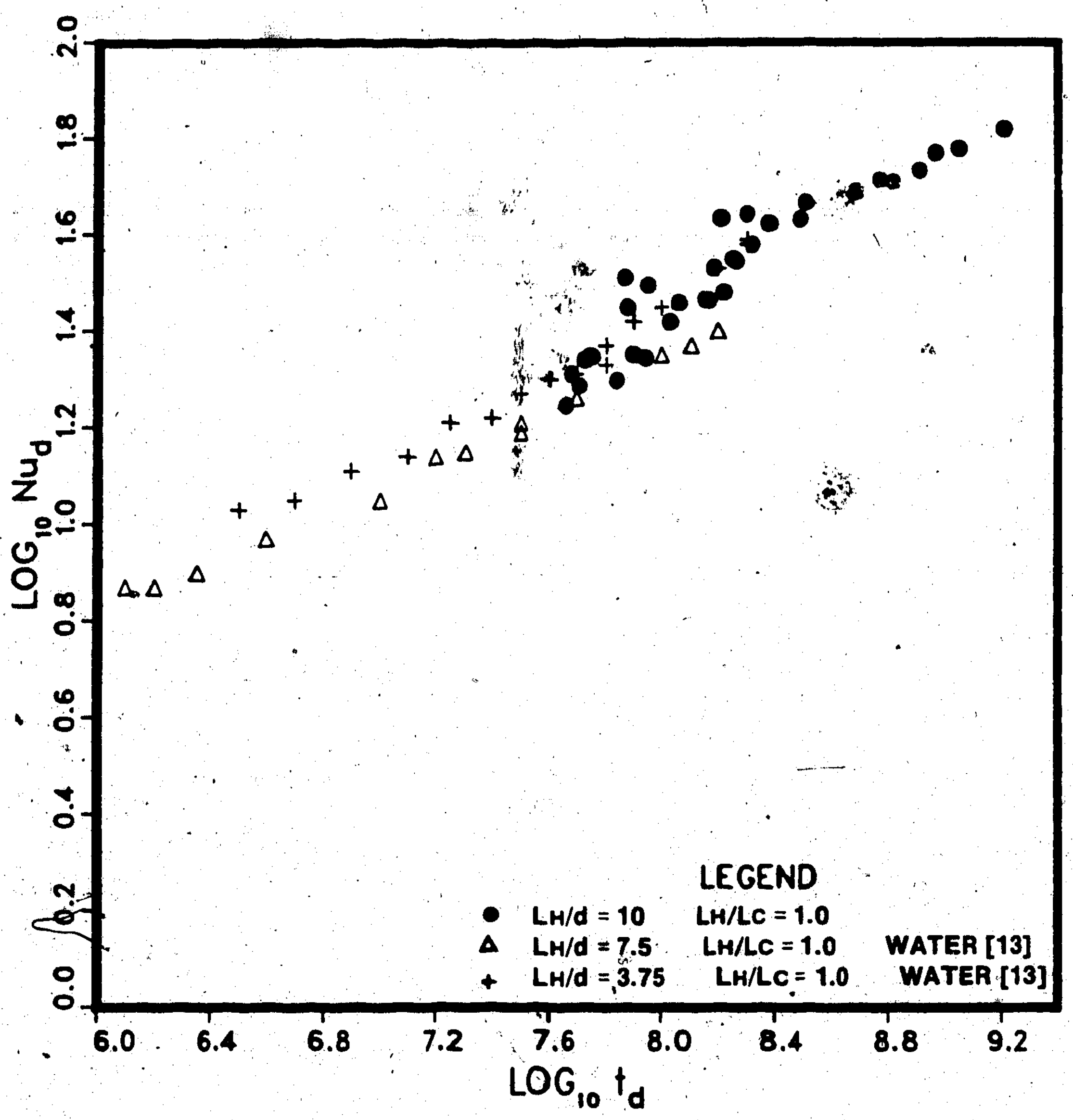

Figure 16. Comparison of heat transfer with results of Bayley and Lock.

given heated length by lowering the fluid level in the tube (see Figure 8). The results for $L_H/d=30$ and $L_H/d=50$ are presented in Figures 17 and 18 respectively. As the heated/cooled length ratio is increased the Nusselt number decreases. The magnitude of this decrease is dependent on both L_H/L_C and L_H/d.

Referring to Figure 17 with $L_H/d=30$, a small decrease of approximately 0.02 in the $Log_{10}Nu_d$ number can be observed between $L_H/L_C=3$ and $L_H/L_C=5$. Between $L_H/L_C=5$ and $L_H/L_C=10$ the reduction increases to approximately 0.1. Increasing the L_H/d ratio to 50 (Figure 18) and comparing the L_H/L_C ratios for 5 and 10, there appears to be very little difference in the middle and upper sections of the curves. Not until L_H/L_C is increased to 20 is a noticeable reduction in the heat transfer evident. The lower portion of the $L_H/L_C=5$ ($L_H/d=50$) curve drops below the values for $L_H/L_C=10$. No explanation can be given for this other than the large amount of uncertainty that occurs for values in this lower t_d range.

For laminar flow in short tubes (small L/d ratios) insight into the effect of decreasing the cooled length with the heated length and t_d (ΔT) held constant can be obtained by considering the normalized relations for axisymmetric boundary layer flow. The characteristic velocity and thickness of the boundary layer are governed by the

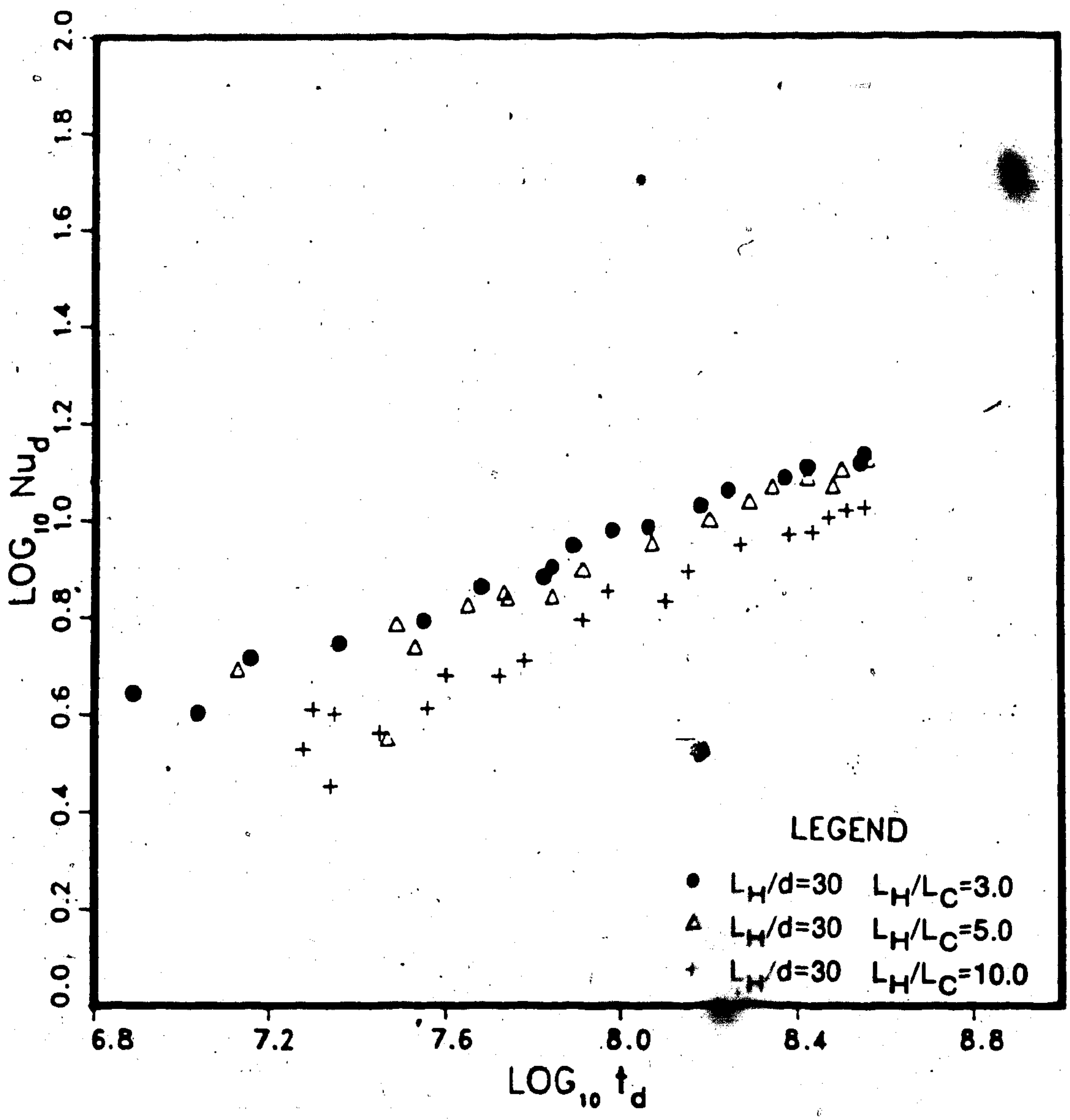

Figure 17. Effect of L_H/L_C on heat transfer (L_H/d=30).

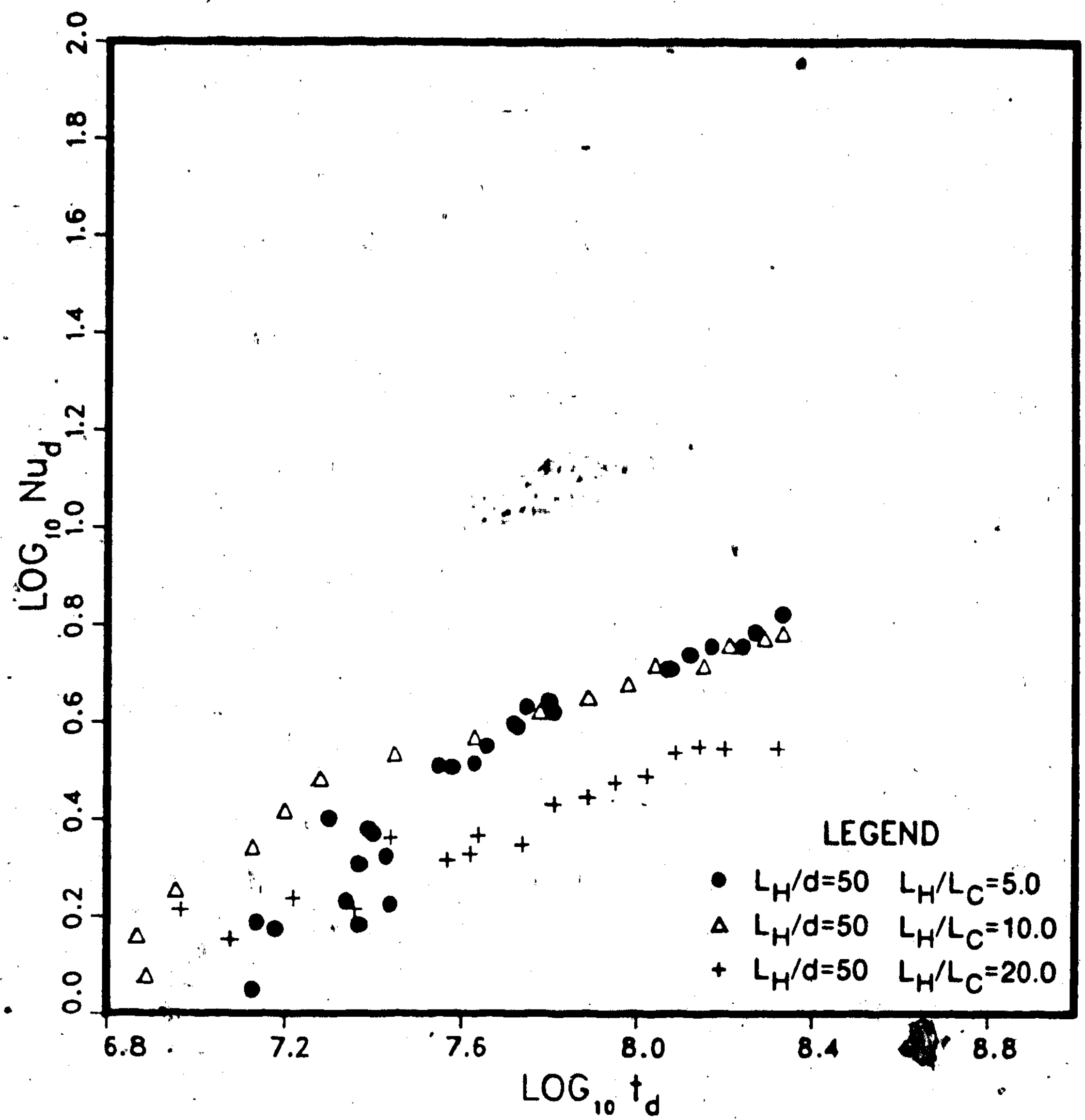

Figure 18. Effect of L_H/L_C on heat transfer ($L_H/d=50$).

following relationships: (See Appendix 2)

$$U_C \sim \left[\frac{\beta g \theta X}{Pr}\right]^{1/2} \tag{3.1}$$

$$\delta_C \sim \left[\frac{\nu \kappa X}{\beta g \theta}\right]^{1/4} \tag{3.2}$$

where X is the heated length and θ is the temperature difference between the tube centerline and the wall. Since the temperature of the tube centerline has been reported to be approximately constant [14] and equal to the "reservoir" temperature. θ can also be thought of as the temperature difference between the "reservoir" and the hot wall.

For a constant θ both the velocity and the thickness of the cold boundary layer decrease with a shorter cooled length, hence lowering the mass flow rate of the cooled annulus. This has the effect of decreasing the amount of cold fluid available to travel down the heated length's core, thereby lowering the ΔT between the centerline and the wall for the heated length. Since the core temperature has now been increased in the heated length, the heat flux will be decreased resulting in a lower Nu number for the same value of t_d.

In tubes with large L/d ratios, it is hypothesized that the increased velocity gradient promotes mixing. The intensity

intensity of the mixing is expected to increase as L_H/d increases. The experimental results indicate that shortening the cooled length has little effect on the heat transfer until L_H/L_C=10 for L_H/d=30 and L_H/L_C=20 for L_H/d=50. Therefore the heat transfer effectiveness must be largely controlled by the lower portion of the cooled length: ie. by the region close to and including the coupling region.

The experimental results tend to support the effect of L_H/L_C diminishing as the L_H/d ratio increases. Further data from Bayley and Lock [13] for L_H/d=7.5 indicates a decrease of 0.1 in the $Log_{10}Nu_d$ number for a small L_H/L_C ratio of 2. Again this suggests the decreasing importance of L_H/L_C as L_H/d is increased.

3.4 Effect of L_H/d

The length/diameter ratio of the heated length was extended by the attachment of two 2.0 m long additional heated lengths. For each of three cases a calibration curve (see Appendix 1) was completed to measure the heat leak and thus modify the supplied heat flux. The heat transfer results for L_H/d=10, 30, and 50 are shown in Figure 19. Heated and cooled lengths are equal for L_H/d=10, while for L_H/d=30 and 50 the heated lengths are five times the cooled length. From the preceeding section it was seen that the effect of

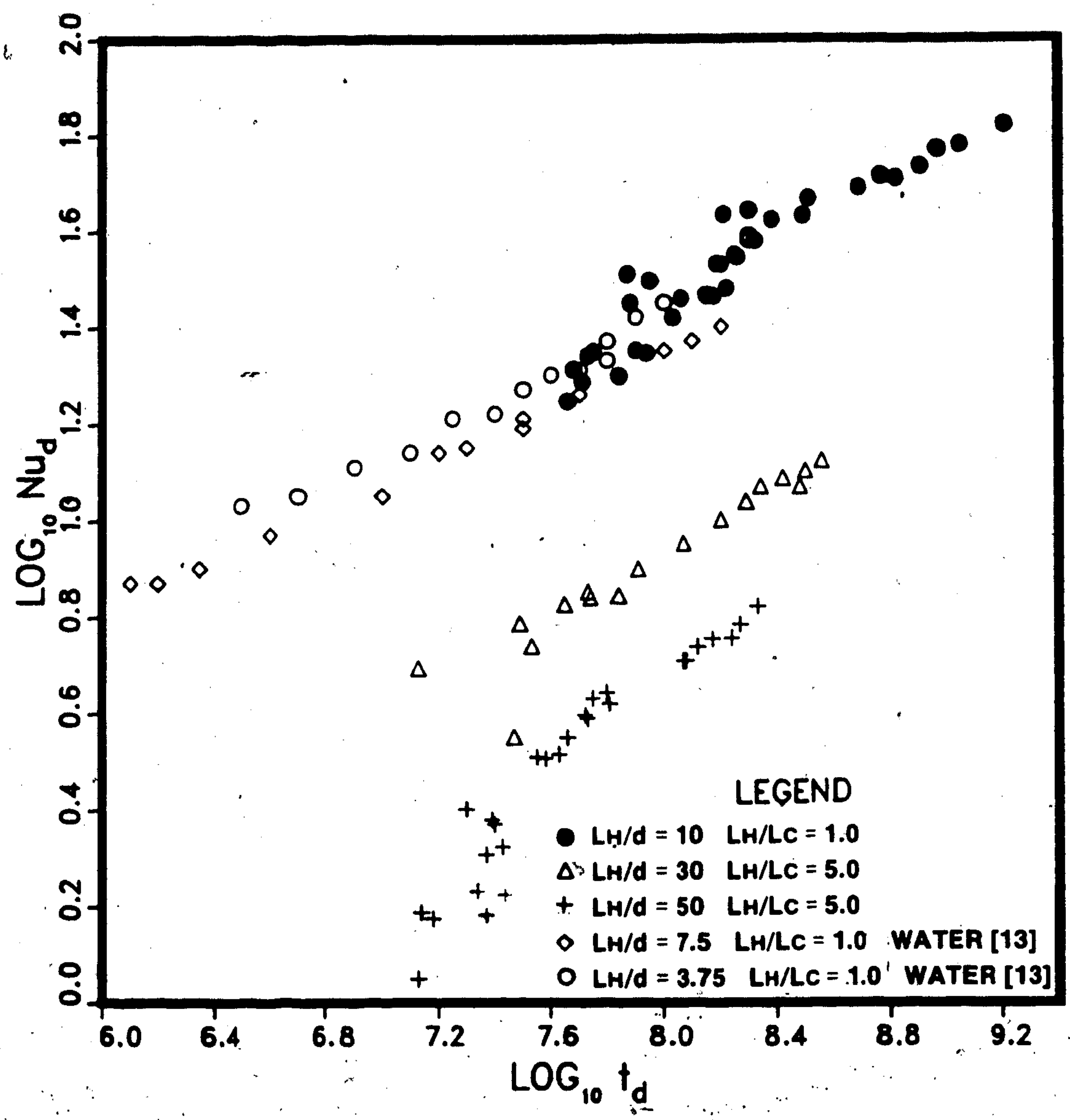

Figure 19. Effect of L_H/d on heat transfer.

L_H/L_C diminishes as the length/diameter ratio is increased. Since the results for $L_H/d=30$ showed negligible change between $L_H/L_C=3$ and $L_H/L_C=5$ and the results for $L_H/d=50$ showed negligible change between $L_H/L_C=5$ and $L_H/L_C=10$, it is probable that these results would also be comparable to those with equal heated and cooled lengths. Unfortunately obtaining experimental data for verification is beyond the capacity of the present rig.

The effect of increasing L_H/d is to produce a downward shifting of the heat transfer curve. The L_H/d parameter is included in the t_d variable; however, its entire effect is evidently not contained within t_d. Figure 19 also includes the results from Bayley and Lock [13] for two smaller L_H/d values. The same trend of shifting the heat transfer curve downward is evident but not to the same extent as the results from this study.

The numerical results of Gosman et al. [12] and the analytical results of Lighthill [1] have indicated that only the Pr number and the t_d parameter should affect the heat transfer for an open system. However, experimental observations of Martin [10] have indicated that for a constant value of t_d the Nusselt number is inversely proportional to L_H/d. Such is also the case for the closed system where adverse mixing of the core and boundary layer flow is likely the cause of the effect. The laminar flow equations used by Gosman et al. in their analysis would be unable to predict this mixing, thus their results do not reflect a separate dependence on L_H/d.

The laminar velocity profile inside the thermosyphon contains a point of inflection thereby characterizing it with an inherent low level of stability. As L_H/d is increased, the boundary layer velocity is increased thus increasing the magnitude of the velocity gradient and hence shear. This should promote turbulent mixing between the core and the boundary layer flow. Further increasing of L_H/d will increase both the magnitude of the mixing and the extent that the mixing extends down the tube. Probe studies from Bayley and Lock [13] and from this study have suggested that as L_H/d is increased the transition to turbulence will occur at a lower value for t_d. This is discussed further in the following section.

3.5 Transition to turbulence

A steady-state laminar flow regime was not achieved with the present rig. However, the thermal time constant of the rig, including the insulation and the waterjacket, was observed to be approximately 2 hours. By shutting off the power and the waterjacket supply, a quasi-steady laminar flow regime could be produced as the wall temperature difference gradually decreased to zero. The procedure was then reversed to explore the transition to turbulence.

The tip of the traversing thermocouple probe discussed in Chapter 2 was placed 75 mm below the physical coupling plane at an approximate radius of 45 mm (ie. 5 mm from the heated wall). The probe was connected to a Hewlett-Packard 3108 B strip chart recorder with a resolution of 0.025°C. Figure 20 shows the onset of turbulent flow in the boundary layer area for $L_H/d=50$. No evidence of a periodic instability was found. The thermocouple probe was used to estimate both the hot wall and cold wall temperatures at the transition point indicating a 0.4°C temperature difference corresponding to a t_d value of $1.2x10^6$. The transition to turbulence for $L_H/d=10$ occurred at a (T_H-T_C) value of 0.5°C corresponding to a t_d value of $7.5x10^6$. Bayley and Lock [13] in their experiments with water also noted a decreasing value for the transition to turbulence as the L_H/d parameter was increased. They observed a transitional t_d value of $4.0x10^7$ for $L_H/d=3.75$ and $7.6x10^6$ for $L_H/d=7.5$.

As pointed out in the preceding section, increasing L_H/d increases the velocity of the boundary layer without affecting its thickness for a given value of t_d. Therefore from the conservation of mass, the core flow must also increase in velocity. The net effect will be a substantial increase in the velocity gradient where the boundary layer

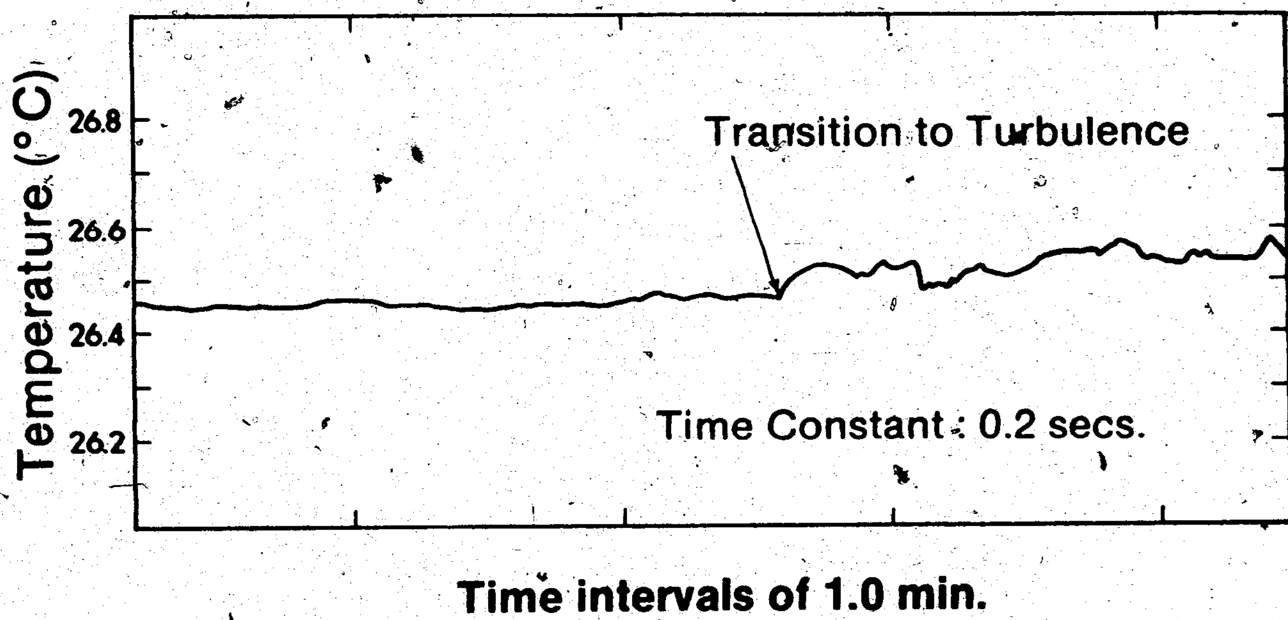

Figure 20. Onset of turbulent flow in the boundary layer for $L_H/d=50$

meets the core flow. Since the Reynolds or turbulent stresses are proportional to the square of the velocity gradient, increasing L_H/d should have a substantial effect on both the transition to turbulence and the intensity of turbulence.

3.6 Coupling Region

The closed thermosyphon can be treated in the manner first suggested by Lighthill by considering two open thermosyphons coupled together. The heated section will be comprised of a thin rising boundary layer adjacent to the heated wall and a slowly moving central core travelling in the opposite direction. A similar situation exists in the cooled length. In the coupling region the boundary layers must somehow transpose themselves into the slower moving core flows. To achieve this Bayley and Lock [13] hypothesized three possibilities as described earlier in Chapter 1. These are:

1) Mixing
2) Advection
3) Conduction

or a combination of the above.

Consider the case of increasing L_H/d with equal heated and cooled lengths for laminar flow with advective coupling. As seen from equations 3.1 and 3.2 the boundary layer velocity and thickness will both increase giving rise to mixing rather than the advective coupling. A further increase in L_H/d will further increase the velocity, causing core and boundary layer mixing to occur both below and above the junction plane. This should have the effect of reducing the heat transfer below that for pure mixing in the absence of impeded flow.

Center-line temperature profiles for the range of t_d covered by this study indicated that the flow was fully mixed turbulent. The magnitude of the fluctuations were approximately in proportion to the hot and cold wall temperature difference. Figure 21 is supplied as reference indicating typical center-line temperature fluctuations for $t_d=10^{8.6}$ and $L_H/d=50$.

However, as mentioned previously, a quasi-steady laminar flow was achieved by letting the thermosyphon reach the ambient room temperature and then slowly increasing the power of the heat source. Figure 22 shows a typical laminar centerline temperature profile for $t_d \approx 1\times10^6$, $L_H/d=50$, and $L_H/L_C=5$.

A slight decrease in temperature is apparent as the temperature profile is followed upwards from the base of the tube. At approximately 3 diameters below the coupling plane the temperature decrease is replaced by an isothermal

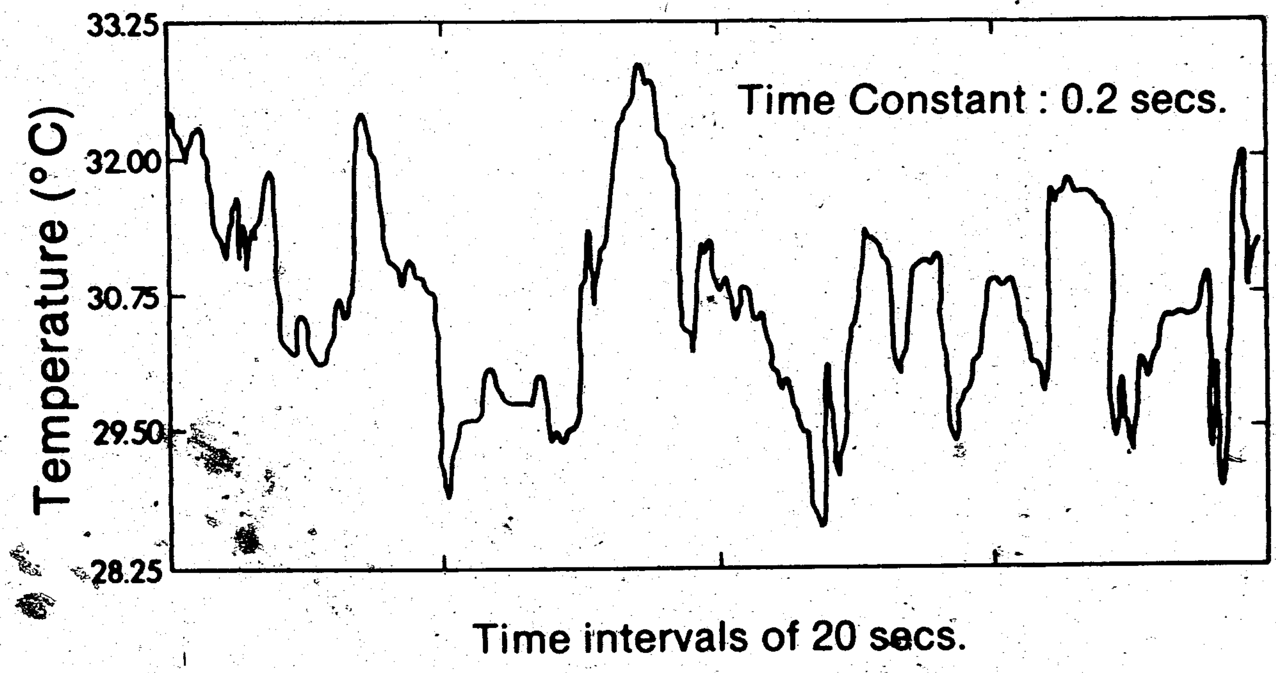

Figure 21. Typical center-line temperature fluctuations in fully mixed turbulent regime

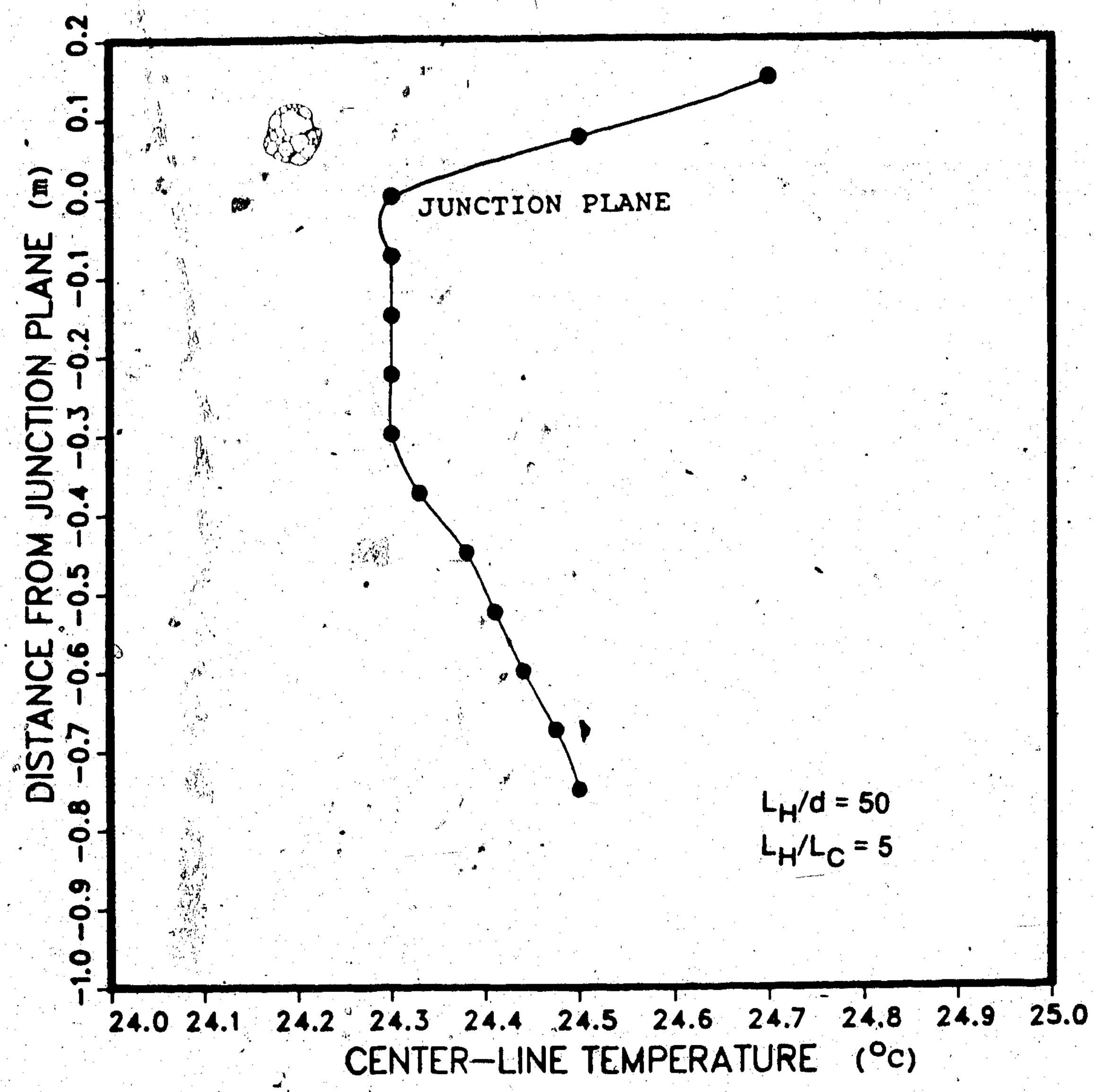

Figure 22. Center-line temperature profile for laminar flow, $L_H/d=50$, $L_H/L_C=5$.

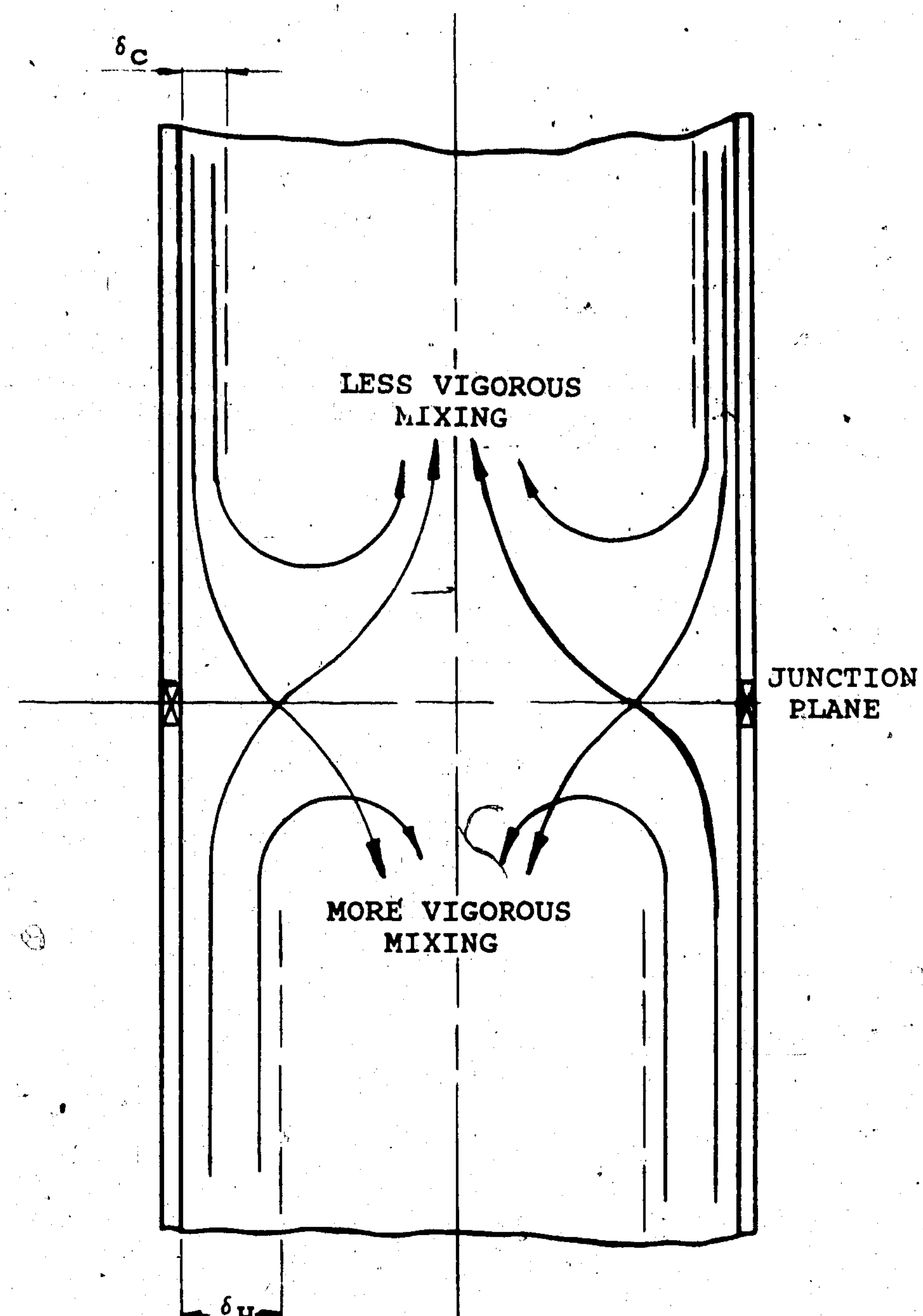

Figure 23. Assumed flow pattern [illegible] $L_H/D_c>1$.

region extending to the junction plane. Immediately above this plane a sharp increase in temperature is observed.

These results can best be interpreted by recalling that the boundary layer velocity in a tube of given diameter is proportional to L_H/d for a constant t_d. Equations 3.1 and 3.2 imply that the heated boundary layer for $L_H/L_C=5$ will have a substantially larger mass flow rate and thickness than its cooled counterpart. As the two boundary layers collide in the coupling region, continuity will require that much of the heated boundary layer return to its own core (see Figure 23). However, the remainder of the heated fluid, having a larger thickness than the opposing cold stream, would be likely to push its way, relatively unimpeded, to the core of the cooled section. Meanwhile the cold boundary layer and the returning heated fluid would combine and move towards the heated section's core. The final temperature profile could likely result in an isothermal section below the coupling plane and an advective effect above it as seen in Figure 22.

3.7 Design Correlations

Probe studies have indicated that all of the experimental results in this study lie entirely in the turbulent mixed regime. According to the analysis by Lighthill [1], the data is expected to lie along a single curve on a log-log plot. A least squares regression was used to fit the data in the form

$$Nu_d = bt_d^n \qquad (3.3)$$

Since there was a great deal of uncertainty in the data in the lower t_d ranges, only the data in the middle and upper ranges of the curves was used in an attempt to curve-fit. Table 3 lists the eight experimental curves with their minimum t_d value used in curve-fitting and their respective slopes and intercepts.

L_H/d	L_H/L_c	t_d (Min)	b	n	b*
10	1	$10^{8.1}$	0.135	0.29	0.0674
30	3	$10^{7.2}$	0.020	0.33	0.0209
30	5	$10^{7.5}$	0.016	0.34	0.0195
30	10	$10^{7.5}$	0.004	0.40	0.0154
30	3	$10^{7.2}$	0.008	0.38	0.0209
50	5	$10^{7.5}$	0.004	0.38	0.0110
50	10	$10^{7.2}$	0.023	0.29	0.0110
50	20	$10^{7.5}$	0.005	0.35	0.0070

Table 3 Experimental Curve Fitting ($t_d<10^{9.1}$)

The average value for the slopes of the curves after curve-fitting is 0.34. For turbulent flow on a flat plate a slope of 1/3 is expected. The intercept was found to be very sensitive to the slope of the curve as can be seen by the large variation in values for b. A new intercept, b^*, was calculated using a slope of 1/3 applied through the midpoint of the data.

Further curve-fitting was performed by assuming b^* is a function of L_H/L_C and L_H/d. The Nusselt number can be described by the power law

$$Nu_d = 1.19\left[(d/L)^3(L_C/L_H)t_d\right]^{0.29}$$

and was seen to reasonably fit the data on a single curve as shown in Figure 24. The entire data, including that with a large uncertainty ie. low t_d values, is presented in Figure 25.

Extrapolation of the data for larger values of t_d should not present a problem since the flow is already turbulent and likely to keep the same slope of for larger temperature differences. Extrapolation for lower values of t_d than the ones listed in Table 3 is not recommended since the flow will now have the tendency to change to a laminar boundary layer type. The experimental results from Bayley and Lock [13] and Japikse [14] provide a better guide in the laminar regime. Only three cases for the curve-fitting were available for the effect of L_H/d and four cases for L_H/L_C, therefore equation (3.4) is recommended only for the range of L_H/d and L_H/L_C listed in Table 3.

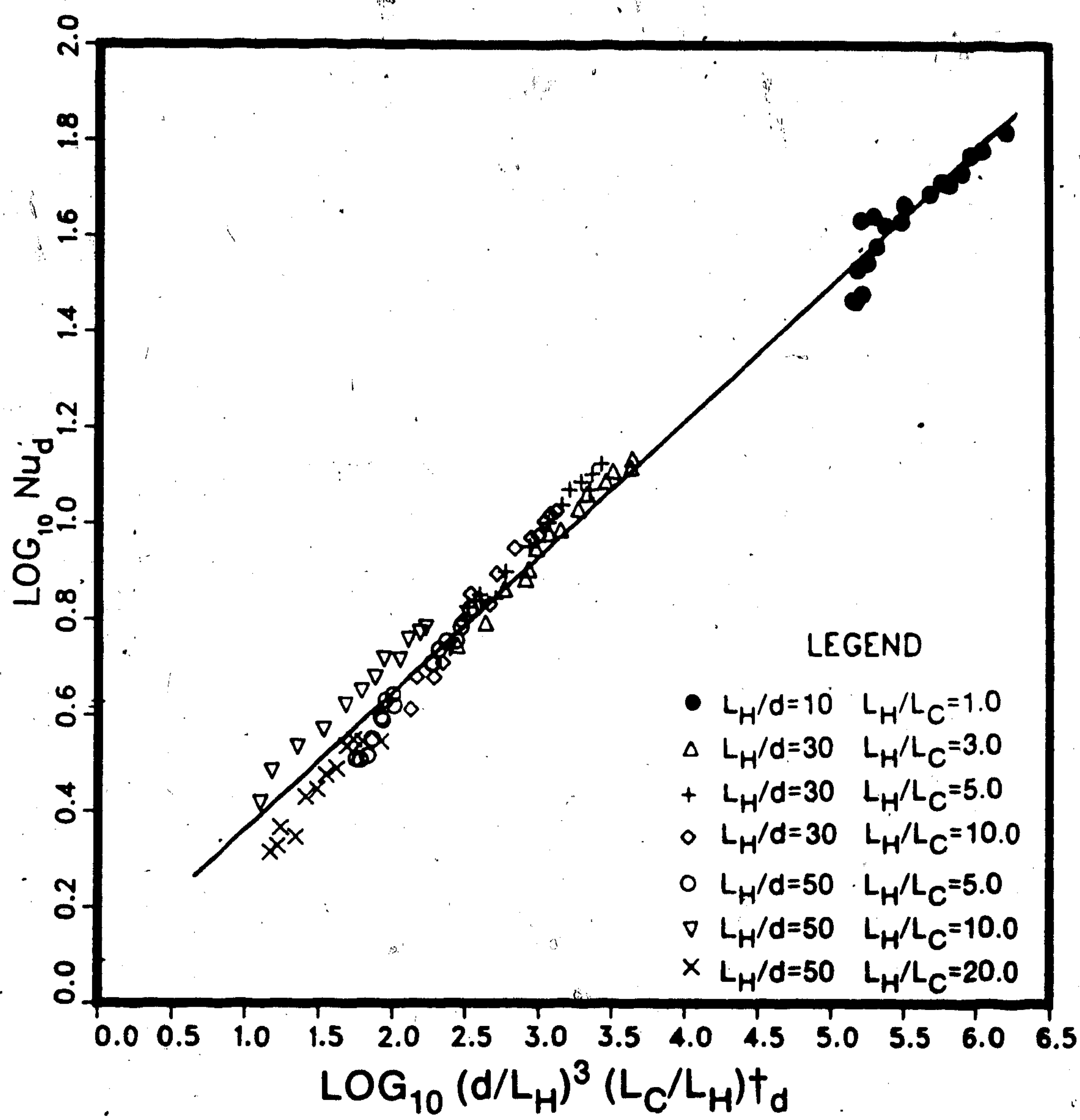

Figure 24. Experimental data used for curve-fitting.

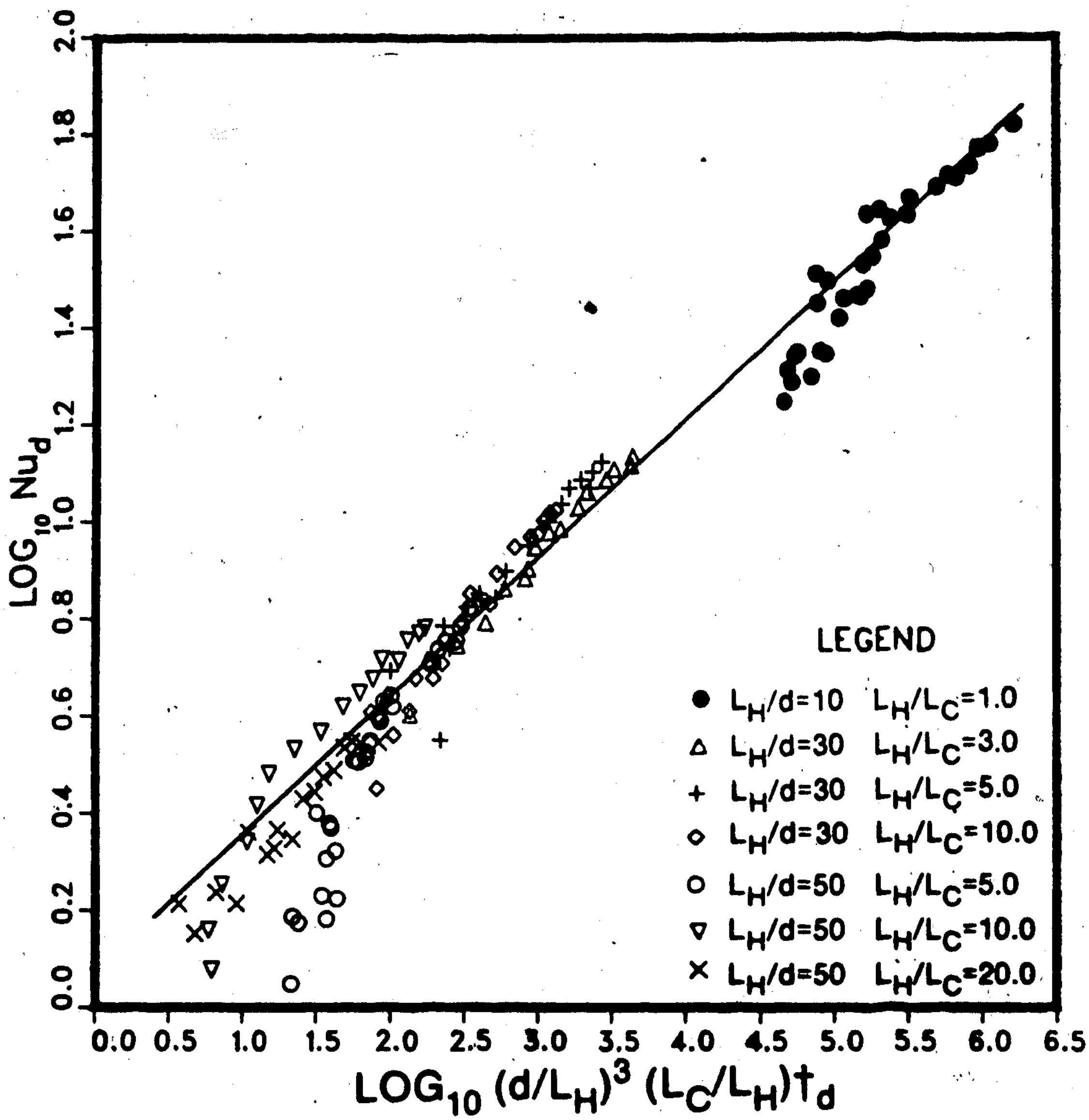

Figure 25. All experimental data for the closed thermosyphon.

4. NUMERICAL SOLUTION FOR THE LAMINAR CLOSED THERMOSYPHON

4.1 Previous theoretical work

M.J. Lighthill provided the initial groundwork for the analytical predictions for the open thermosyphon by using an integral-profile technique on the boundary layer equations. His results in the laminar regime were seen to agree within 10% of the experimental results but no attempt was made to predict the behaviour of the closed thermosyphon. Further extensions on Lighthill's work was performed by Bayley and Lock [13] and Japikse [14] on the open and closed thermosyphon. Japikse used a simplified convection model with an arbitrary coupling parameter, ς, which represented the conductive loss from a convecting stream as it passes through the coupling region. Therefore, $\varsigma=0$ was used for pure mixing and $\varsigma=1$ for pure advection. Japikse was able to match Bayley and Lock's experimental results within 10%.

However, integral-profile techniques suffer the shortcomings of becoming complex for any but ~~the simplest~~ of boundary conditions and of having to predict the profile shape prior to solving the problem. A further problem also exists as L_H/d is increased. As seen in the previous chapter the heat transfer results in turbulent flow drop well below those for shorter tubes due to mixing of the core and boundary layer. The coupling parameter in Japikse's model has a limiting case of pure mixing corresponding to $L_H/d \approx 10$ and thus would only be of limited use for large L_H/d ratios.

Finite difference methods for the numerical solution have the advantage of easily varying the boundary conditions without adding more complexity to the solution method. A second benefit is that the full set of elliptic equations can be solved rather than the approximate parabolic ones. Gosman, Lockwood, and Tatchell [12] used a two-dimensional axi-symmetric finite difference procedure to solve the conservation equations for the open thermosyphon. Their technique was employed and expanded in the present study to include the coupling of two open thermosyphons to model the closed thermosyphon.

4.2 The open thermosyphon equations and solution procedure

The two dimensional conservation equations for mass, energy, and radial and axial momentum under steady laminar conditions are used in the finite difference solution. It is assumed that the gravitational force acts axially and that viscous heating and tangential velocity are negligible. Gosman et al [20] have shown that the pressure can be eliminated by transforming the equations into the stream function and vorticity. This results in three non-linear elliptic partial differential equations which have the common form:

$$a_\phi\left[\frac{\partial}{\partial z}\left(\phi\frac{\partial\psi}{\partial r}\right)-\frac{\partial}{\partial r}\left(\phi\frac{\partial\psi}{\partial z}\right)\right]-\frac{\partial}{\partial z}\left[b_\phi r\frac{\partial(c_\phi\phi)}{\partial z}\right]-\frac{\partial}{\partial r}\left[b_\phi r\frac{\partial(c_\phi\phi)}{\partial r}\right]+rd_\phi=0 \quad (4.1)$$

where r and z are respectively the radial and axial co-ordinates in a circular-cylinder co-ordinate frame. The dependent variable ϕ may stand for:

1) the variable ω/r where the vorticity, ω, is defined by

$$\omega=\frac{\partial V_r}{\partial z}-\frac{\partial V_z}{\partial r} \quad (4.2)$$

2) the streamfunction ψ where

$$\psi=\int[\rho r(V_z dr-V_r dz)] \quad (4.3)$$

3) the fluid temperature, T

The functions a_ϕ, b_ϕ, c_ϕ, and d_ϕ stand for the coefficients which may be deduced from the equations and are given in Table 3.

Variable ϕ	a_ϕ	b_ϕ	c_ϕ	d_ϕ
ψ	0	$1/\rho r^2$	1	$-\omega/r$
ω/r	r^2	r^2	μ	$rg_z\frac{\partial\rho}{\partial r}-\frac{r}{2}\left[\frac{\partial}{\partial z}(V_r^2+V_z^2)\frac{\partial\rho}{\partial r}-\frac{\partial}{\partial r}(V_r^2+V_z^2)\frac{\partial\rho}{\partial z}\right]$
T	1	μ/Pr	1	0

Table 3 **Coefficients for Equation 4.1**

For simplicity the fluid properties have been taken as uniform except for the term $rg_z \partial\rho/\partial r$ which represents the source of vorticity due to buoyancy forces. The Boussinesq approximation has been used to reformulate this term as

$$rg_z\frac{\partial\rho}{\partial r} = -rg_z\rho\beta\frac{\partial T}{\partial r} \qquad (4.4)$$

Boundary conditions for the stream function, vorticity, and temperature must be provided at on all the boundaries of the domain of solution. The conditions imposed by Gosman et al [12] will be used since their results for the open thermosyphon were very close to the experimental results of Martin. The side wall and base boundaries will be considered jointly due to their similarities.

1) Side Wall and Base

a) Stream Function: From the definition (equation 4.3), the stream function assumes a constant value along the wall. This value is arbitrarily taken as zero.

b) Temperature: For the calculations performed in this study the side wall is isothermal and the base is adiabatic.

c) Vorticity: The wall vorticities are calculated from the extrapolation formula

$$\left(\frac{\omega}{r}\right)_p = -\left[\frac{3(\psi_i-\psi_p)}{\rho r_p^2 n_i^2} + \frac{1}{2}\left(\frac{\omega}{r}\right)_i + \frac{a\rho\beta(T_i-T_p)n_i}{8\mu r_p}\right] \qquad (4.5)$$

where the subscripts p and i refer to the boundary node and the adjacent interior node respectively. The symbol n_i stands for the distance between the two nodes and a represents the acceleration parallel to the wall in question. Thus for the side wall $a=g_z$ and for the base a=0. The above equation has been derived by Tatchell [18] from the analytical solution of the differential equations on the assumption that a one-dimensional Couette flow exists very near the wall.

2) Axis of Symmetry

a) Stream Function: Again from the definition it is clear that the stream function must be a constant value along the axis and that this value must be the same as that at the base ie. $\psi=0$

b) Temperature: From symmetry the radial variation of temperature at the axis will be zero ie. $\partial T/\partial r=0$

c) Vorticity: For the region very close to the symmetry axis Tatchell [18] has shown that $\omega=-8br/\rho$ where b is not a function of r. This is in accordance with the observation that in a great many flows the shear stress near a symmetry axis (very similar to ω in this region) varies linearly with r. Therefore the following relation has been used:

$$\left(\frac{\omega}{r}\right)_p = \left(\frac{\omega}{r}\right)_i \quad \text{ie.} \quad \frac{\partial(\omega/r)}{\partial r} = 0$$

3) Core entry

a) Stream Function: The boundary condition at the orifice has been imposed such that the streamlines run parallel to the tube. This implies that $\partial\psi/\partial z=0$

b) Temperature: For the boundary condition for the temperature at the orifice it has been assumed that incoming fluid will be at the reservoir temperature whereas for outflow the temperature does not change with respect to its axial position. ie. Inflow $T=T_r$

Outflow $\partial T/\partial z=0$

c) Vorticity: It has also been assumed that the equi-vorticity lines run parallel to the axis of the tube at the orifice. ie. $\partial\omega/\partial z=0$

Figure 26 provides a summary of the boundary conditions.

The finite difference solution procedure outlined by Gosman et al [12] integrates equation (4.1) over the small control volume shown in Figure 27. This approach ensures that the conservation of the property ϕ is upheld for each individual control volume. "Upwind" differences were used

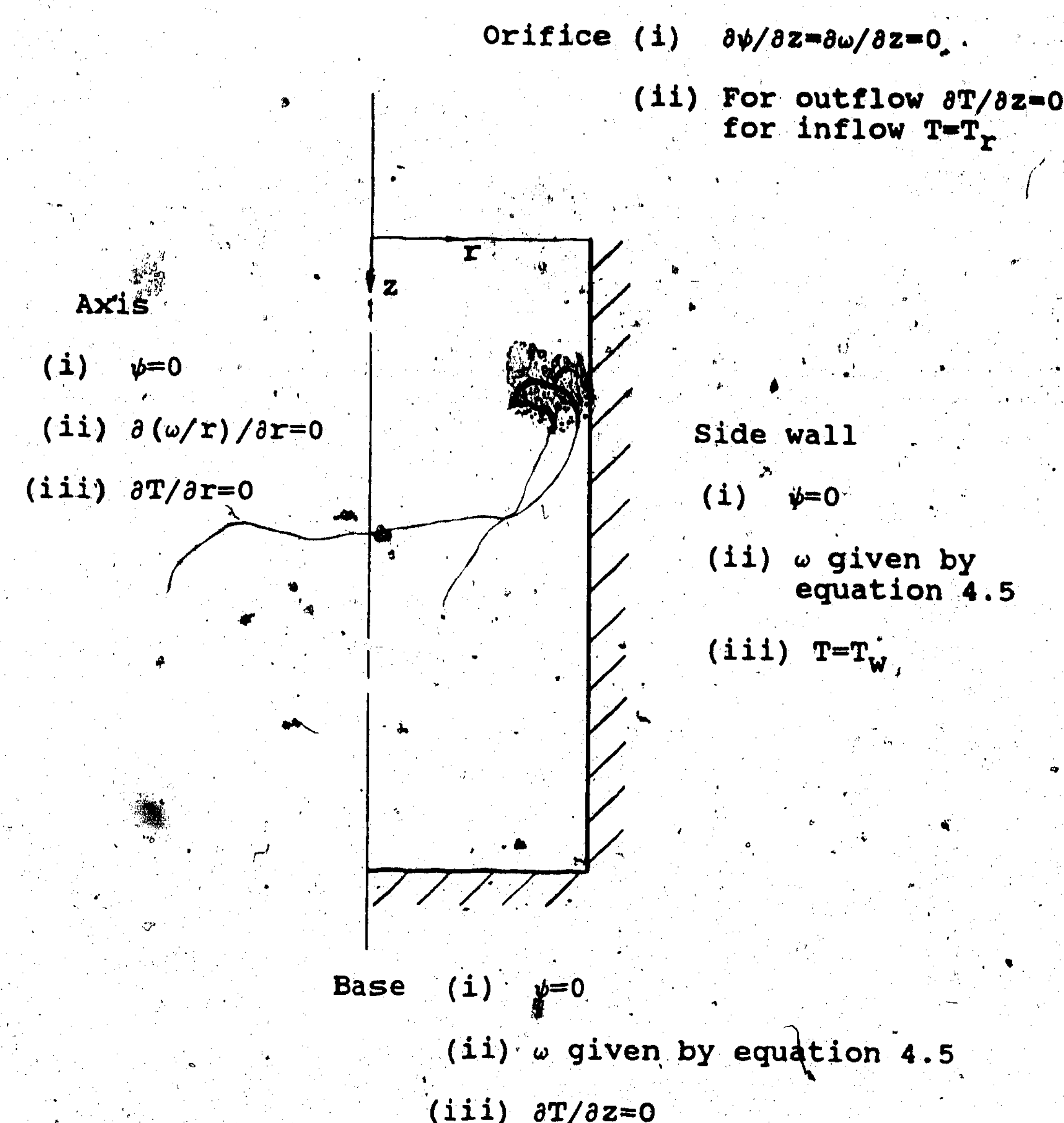

Figure 26. Summary of boundary conditions (following Gosman et al. [12]).

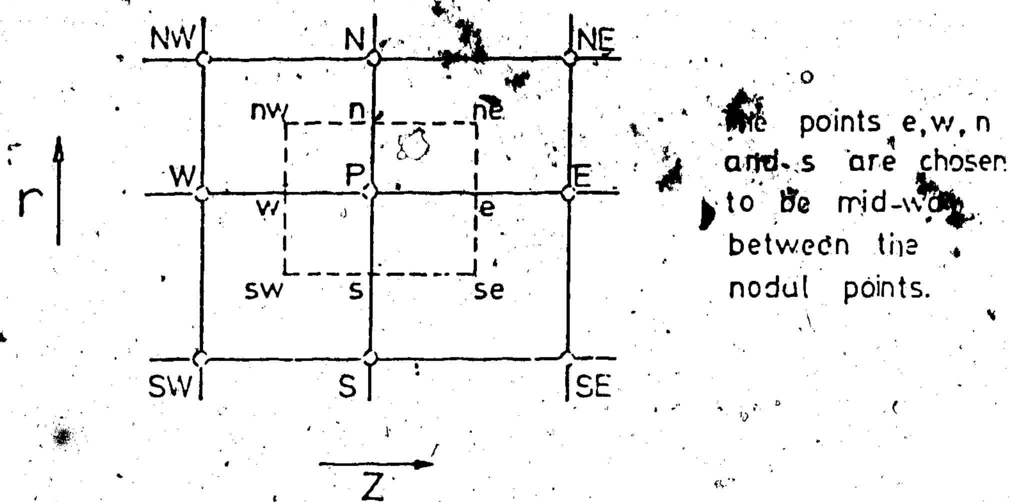

Figure 27. The control volume over which the differential equations are integrated (following Tatchell [18]).

to represent the advective terms in order to ensure convergence of the solution. This results in the general form of the difference equation:

$$C_N(\phi_N-\phi_P)+C_S(\phi_S-\phi_P)+C_E(\phi_E-\phi_P)+C_W(\phi_W-\phi_P)+S=0$$

where the C's are positive coefficients combining the effects of advection and diffusion and S is the source term. The boundary conditions are absorbed into the difference equations for the half control volumes at the boundaries resulting in a set of non-linear algebraic equations with the number of unknowns equal to the number of equations.

The starting values were found not to influence the final results therefore the economical procedure of using the results from the previous calculation as the initial condition for a new calculation was used. The Gauss-Seidel successive substitution method was used to solve for ψ, ω, and T. This meant that the grid was scanned once for all the ψ values, once for all the ω values, and once for all the T values for each iteration. The iterative procedure was halted when the value of the convergence criterion (λ) dropped below 0.01 for every variable and node. The change criterion used was

$$\frac{\phi^N-\phi^{N-1}}{\phi^N} \leq \lambda$$

where ϕ^N is the ϕ value at a grid point after N iterations.

4.3 Open thermosyphon results

Gosman's previous work on the open thermosyphon indicated a grid size of between 15 and 31 lines in each direction would result in a solution that was within 3% of that which would occur for an infinitely fine grid. As a compromise between economy and accuracy a grid size of 20 lines in each direction was chosen for the solutions. In addition the grid size near the wall was further reduced to 1/4 of the normal spacing.

The average Nu_a number was calculated from the temperature distributions in the flow using the relation

$$\overline{Nu} = \frac{\overline{h}a}{k} = -\frac{a\overline{(\partial T/\partial n)}_w}{(T_w - T_r)}$$

where $\overline{h}$ and $\overline{\partial T/\partial n}$ are the average heat transfer coefficient and the average normal temperature gradient on the non-adiabatic walls and k is the thermal conductivity of the fluid. Simpson's rule of integration was used to obtain the average temperature gradient at the walls. Figure 28 compares the results of Lighthill and Gosman et al. with the results from this study. As anticipated the results from this study have nearly duplicated those of Gosman with the exception of the largest value for t_a. Roundoff error

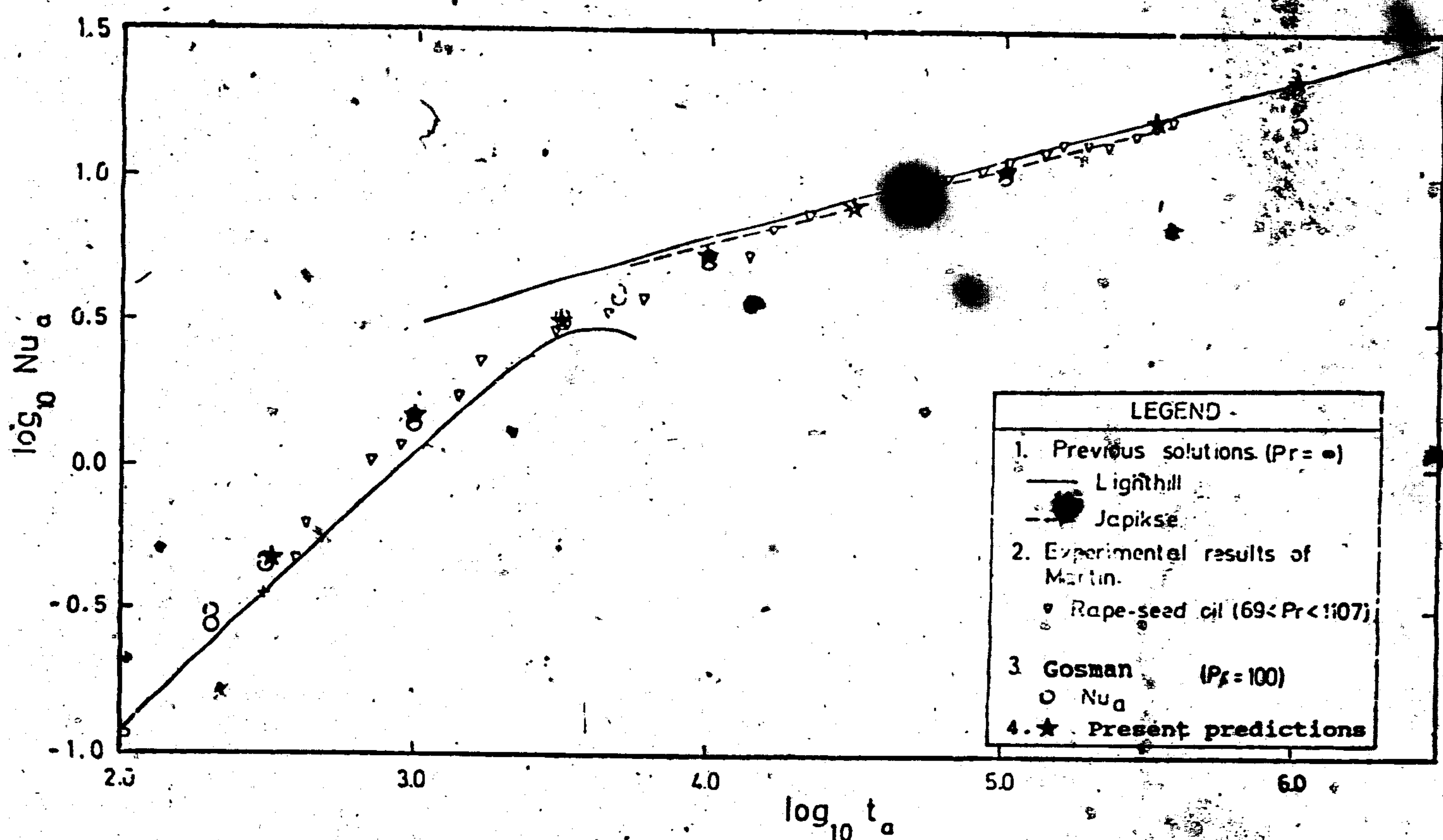

Figure 28. Comparison of present heat transfer predictions with existing results

is likely the cause of this discrepancy.

Increasing L/a for a constant t_a has a negligible effect on the Nu_a number as predicted by Lighthill's dimensional analysis. The boundary layer thickness also remains constant but the velocity is directly proportional to L/a. This is in agreement with the normalized relations given in Chapter 3.

The temperature and velocity profiles determined from the numerical solution are illustrated in Figure 29. In the boundary layer regime the temperature profile is in excellent agreement with Lighthill but the velocity profile does not exhibit the slug type of flow which Lighthill assumed. This indicates that the energy equation is rather insensitive to the type of velocity profile assumed for the core flow. For the case of impeded boundary layer flow, both the velocity and temperature profiles show good agreement with Lighthill's predictions.

4.4 Closed thermosyphon coupling model

The suggestion by Lighthill that the closed thermosyphon be represented by two open thermosyphons will be adopted here together with a coupling model to join the two open tubes together. By considering the velocity profiles as shown in Figure 29, the advective fluxes can be represented by:

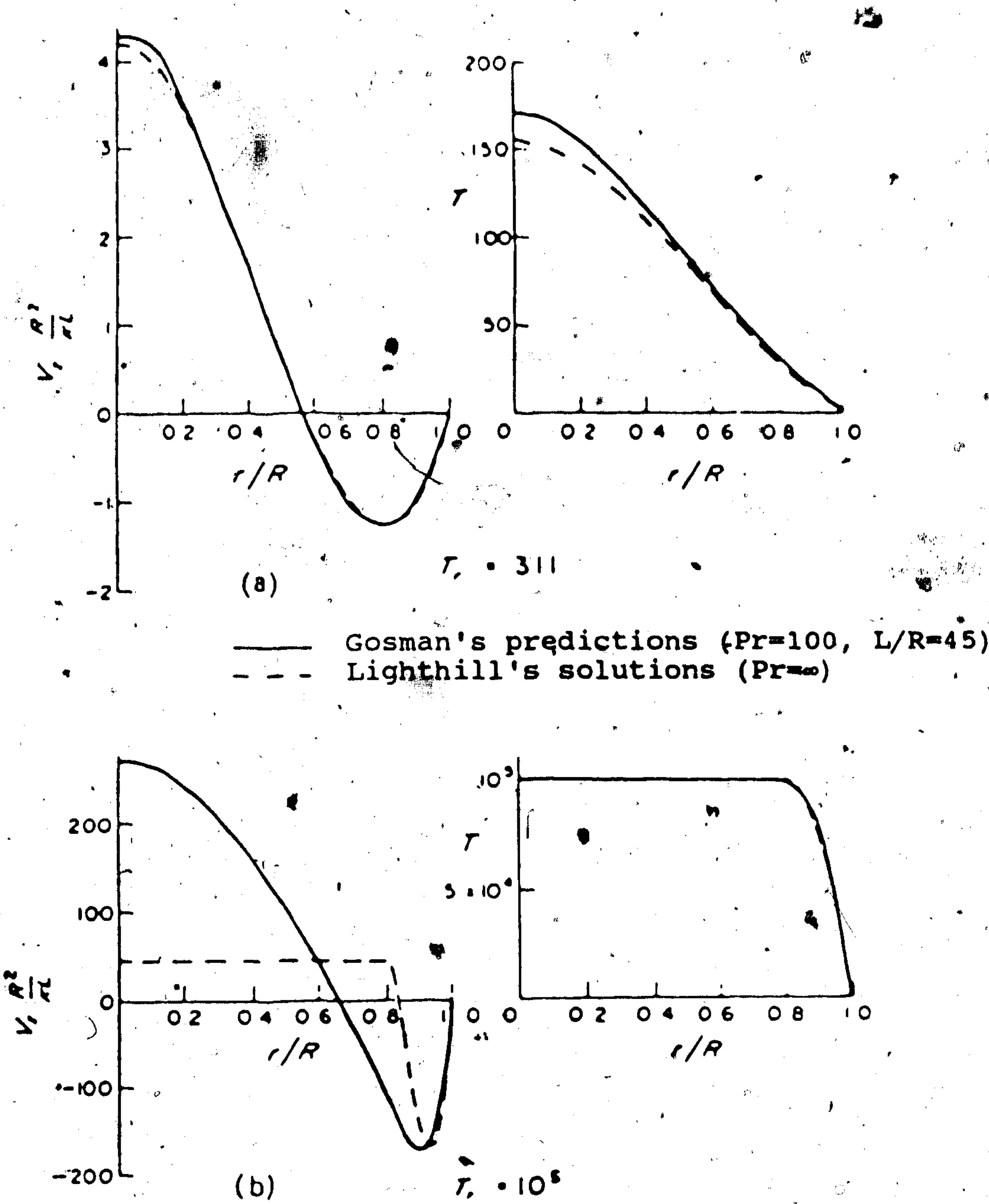

Figure 29. Comparison of predicted velocity and temperature profiles at z/L=0.5 with those of Lighthill, [12]

$$a_{CA} = \left| \rho c_p \int_{R_o}^{R_w} V_z T 2\pi r \, dr \right| \tag{4.9}$$

$$a_{CC} = \left| \rho c_p \int_{0}^{R_o} V_z T 2\pi r \, dr \right| \tag{4.10}$$

where the subscripts CA and CC stand for "cold annulus" and "cold core" respectively, R_o is the radius wh[illegible] velocity changes direction and R_w is the radius of the wall. Similar relations can be written for the "hot annulus" and "hot core".

Ignoring axial conduction, an energy balance on the thermosyphon requires that

$$\dot{Q}_C = a_{CC} - a_{CA} \tag{4.11}$$

$$\dot{Q}_H = a_{HA} - a_{HC} \tag{4.12}$$

and $$-\dot{Q}_H = \dot{Q}_C \tag{4.13}$$

For the case of a purely advective coupling mechanism the "heated core" flux will be equal to the "cold annulus" flux and the "cold core" flux will be equivalent to the "hot annulus" flux. In the situation of a pure mixing coupling mechanism, the heated core flux will be equal to the cold core flux which will be equivalent to the average of the hot annulus and cold annulus fluxes. Equations (4.14), (4.15) and (4.16) represent the cases of pure advection and pure mixing.

$$\text{Advective} \quad a_{HC} = a_{CA} \tag{4.14}$$

$$a_{CC} = a_{CA} \tag{4.15}$$

$$\text{Mixing} \quad a_{HC} = a_{CC} = 0.5(a_{HA}+a_{CA}) \tag{4.16}$$

By considering equations 4.14-4.16 an empirical coupling relation can be written such that

$$a_{HC} = a_{CA} - 0.5K(a_{CA} - a_{HA}) \tag{4.17}$$

$$a_{CC} = a_{HA} - 0.5K(a_{HA} - a_{CA}) \tag{4.18}$$

where K indicates secondary mixing. Thus for pure advection K=0, for pure mixing K=1, and for refluent mixing tending ultimately towards pure conduction, 1<K<2.

Substitution of equations 4.11-4.13 into 4.18 results in

$$a_{CC} = \frac{\dot{Q}(1-K)}{(1-K/2)} + a_{HC} \tag{4.19}$$

and further substitution of the advective fluxes yields

$$\rho c_p \int_0^{R_o} V_z T 2\pi r \, dr = \frac{\dot{Q}_H(1-K)}{(1-K/2)} + \rho c_p \int_0^{R_o} V_z T 2\pi r \, dr \tag{4.20}$$

By defining T_{CC} and T_{HC} as average core temperatures, the temperature may be removed from inside the integral for both the cold and hot core fluxes yielding

$$\rho c_p T_{CC} \int_0^{R_o} V_z 2\pi r \, dr = \frac{Q_H(1-K)}{(1-K/2)} + \rho c_p T_{HC} \int_0^{R_o} V_z 2\pi r \, dr \qquad (4.21)$$

which may be re-written by using the definition of the mass flow rate $\dot{m}$ to yield

$$\dot{m}_{CC} c_p T_{CC} = \frac{\dot{Q}_H(1-K)}{(1-K/2)} + \dot{m}_{HC} c_p T_{HC} \qquad (4.22)$$

It was seen from the experimental results of Chapter 3 that the effect of L_H/L_C is small compared to the effect of the parameter L_H/d. Furthermore, the effect of the length's ratio diminishes as L_H/d increases. Since a major objective of this work is to investigate thermosyphons with large L_H/d ratios, the simplifying assumption of equal heated and cooled lengths will be made. The symmetry of the problem now dictates that $\dot{m}_{HC}=\dot{m}_{CC}$ enabling equation 4.22 to be re-written in its final form as

$$(T_{CC} - T_{HC}) = \frac{\dot{Q}_H(1-K)}{\dot{m} c_p (1-K/2)} \qquad (4.23)$$

where T_{CC} and T_{HC} can also be thought of as the cold and hot core entry temperatures, T_{OC} and T_{OH}, respectively.

The numerical results for the open thermosyphon can now be used to provide results for the closed thermosyphon providing a value for the coupling coefficient, K, is specified. The coupling program listed in Appendix 3 inputs the mass and heat fluxes from the open solution and solves the closed system's core entry temperature and Nusselt number for a range of K values.

Figure 30 illustrates a plot of Nu_d vs. t_d for various values of K. The shape of the curves are very similar to the relations predicted by Gosman et al. [12], as might be expected, since this is an extension of the open system solution. The change in slope of the curve for K=1 (mixing) occurs at about $\log_{10}t_d=5.2$. This is in agreement with the change in slope predicted by Gosman et al. at $\log_{10}t_a=3.7$ which, by assuming pure mixing, also corresponds to $\log_{10}t_d=5.2$ for the closed system. The magnitude of the Nusselt numbers are also in agreement when the diameter, rather than the radius, is used as the characteristic length for Gosman's results.

As K increases beyond one, the knee or bend in the curve is seen to become less distinct and to occur at a larger value for t_d. Since increasing K represents the flow tending ultimately towards pure conduction, it is not unexpected that the bend in the curve, representing the transition from boundary layer flow to impeded flow, should become less pronounced and eventually disappear. However, as $K \rightarrow 2$ the solution is singular and the physical implication is unacceptable.

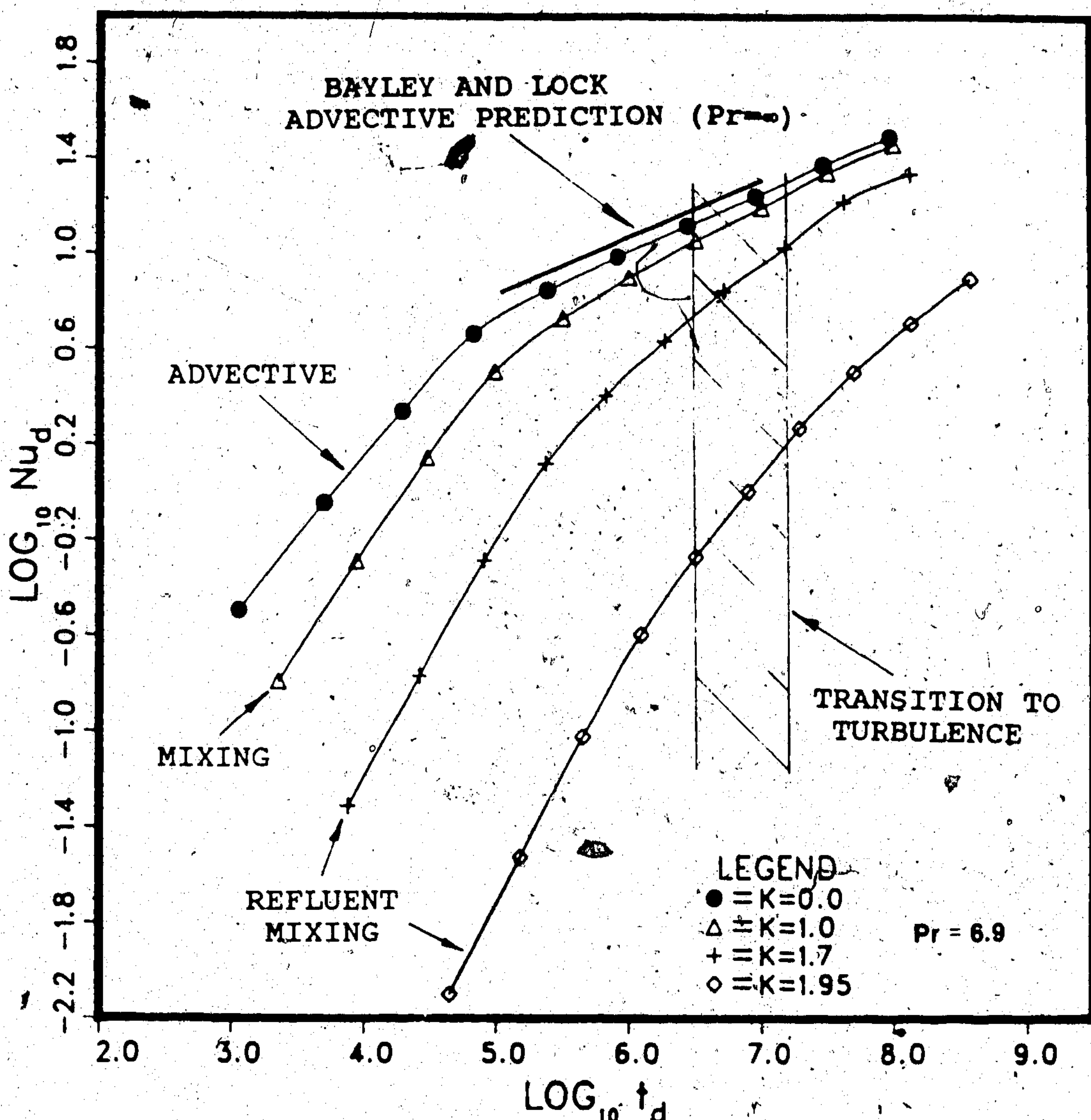

Figure 30. The effect of coupling on the closed thermosyphon model: $L_H=L_C$

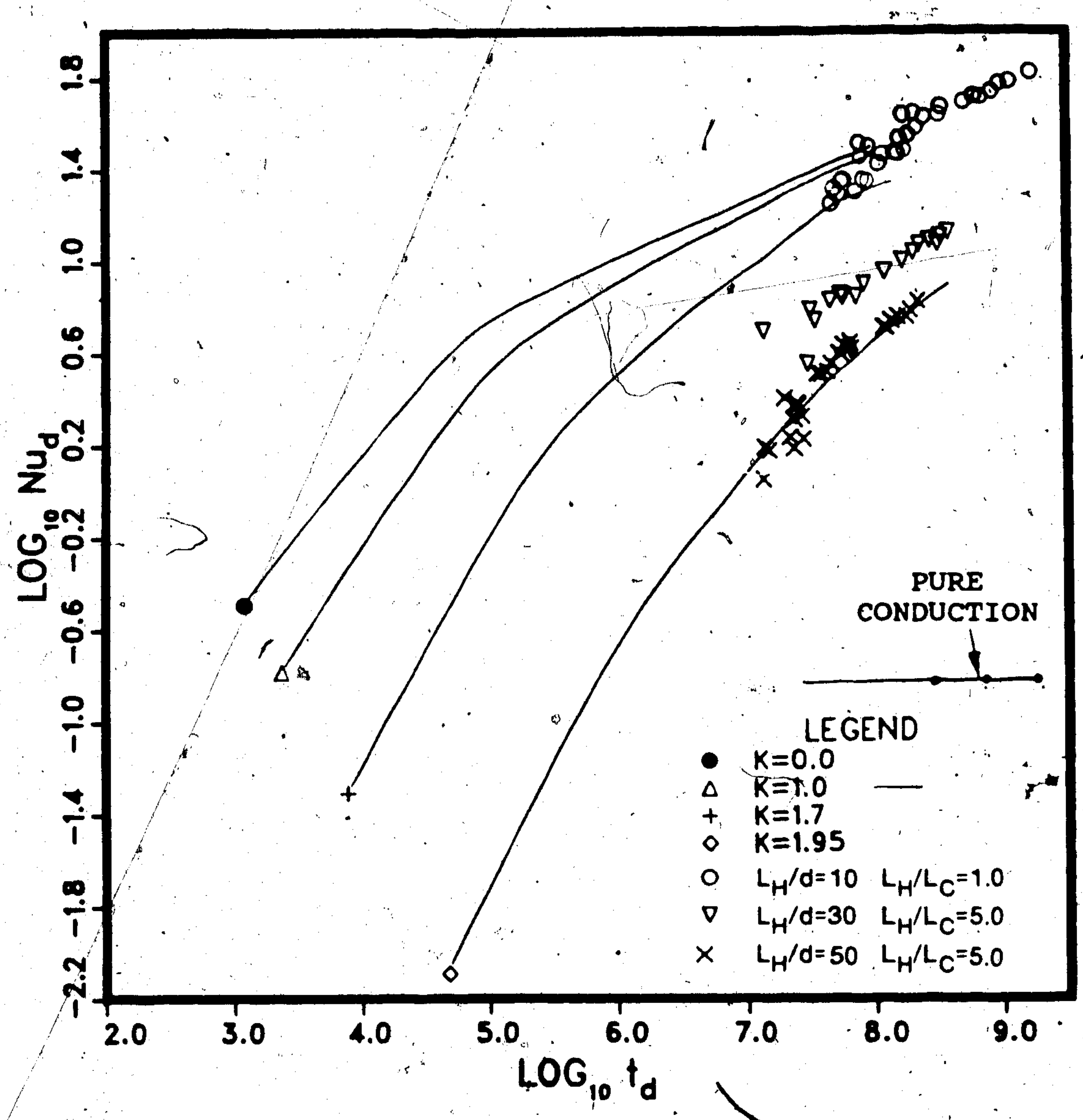

Figure 31. Comparison of laminar thermosyphon model with turbulent experimental results.

The experimental results for $L_H/d=10$, 30, and 50 are superimposed over the numerical results in Figure 31. Although the experimental data is for fully mixed turbulent flow and the theoretical curves are for laminar flow, some similarities are evident. The effect of increasing L_H/d appears to be similar to increasing K. Since K>1 has been defined as refluent mixing tending ultimately towards pure conduction, it appears that an increase in L_H/d causes an increase in the degree of mixing and a corresponding reduction in the heat transfer efficiency. Further studies on the effect of L_H/d in the laminar regime are required to define a relationship between K, L_H/d, and L_H/L_C.

Also included in Figure 31 is the limiting case of pure conduction in a cylinder ($L_H/d=10$). The three points defining the lower limit of the thermosyphon were arrived at from the numerical solution of conduction in a cylinder as outlined in Chapter 2. As expected, the Nusselt number results for the pure conduction case are constant and have a magnitude of approximately 1% of the value for the least efficient experimental case ($L_H/d=50$ $L_H/L_C=20$), thus providing some encouragement for the practicality of long thermosyphons in the turbulent regime.

5. CONCLUSIONS AND RECOMMENDATIONS

This thesis has considered two main areas of research to further our understanding of the closed thermosyphon.

In the first area an experimental investigation of the closed thermosyphon was performed with an emphasis on large L_H/d ratios and unequal heated and cooled lengths. The second area consisted of a coupling model such that the numerical heat transfer results from the laminar open thermosyphon could be used to predict the results for the closed system.

It was observed experimentally that L_H/d had a significant effect on the heat transfer for the closed thermosyphon under turbulent conditions. This is in contrast to the laminar flow predictions of Lighthill who concluded that only t_d and the Pr number would affect the heat transfer for the open thermosyphon. From the thermocouple probe measurements all of the experimental data was seen to be in the fully mixed turbulent regime. As L_H/d increased, the t_d value for the transition to turbulence decreased. It is believed that this is due to the increased velocity gradient brought about by increasing the heated length. The turbulence is thought to have promoted mixing between the core and the boundary layer flow thus resulting in a lowering of the Nu_d-t_d curves.

Increasing L_H/L_C also had a detrimental effect on the Nusselt number but to a much lesser extent than L_H/d. It was found that the effect of L_H/L_C decreased as L_H/d increased. Again this was thought to be due to the increased turbulence and mixing brought about by the larger velocity gradients. As the intensity of turbulence rose, the increased mixing in the flow likely caused a higher percentage of the cooled section's heat transfer to take place in the region immediately above the junction plane, therefore diminishing the effect of L_H/L_C for large L_H/d.

The experimental data for turbulent flow in the closed thermosyphon was reasonably represented by a design correlation taking into account the effect of L_H/d and L_H/L_C.

The second contribution of this thesis was in developing a coupling model such that the laminar numerical results from the open system could be modified to predict the results for the closed thermosyphon. A coupling parameter, K, was introduced which has a value of zero for pure advection, one for pure mixing, and a value between one and two for refluent mixing tending ultimately towards conduction. The case of pure advection should represent the upper bound of performance for a laminar closed thermosyphon. The actual performance is a function of geometry, specifically L_H/d and $L_H/_C$. Further investigation in the laminar flow regime, is required to determine how the coupling parameter, K, relates to geometry and the temperature difference. The lower bound for the performance of the closed thermosyphon is the case of pure conduction in a cylinder.

Several recommendations for future work are listed below:

1) Studies on large L_H/d ratios in both the laminar and turbulent regimes to determine where the transition to turbulence occurs and to demonstrate the dependenceof the coupling coefficient, K, on L_H/d and L_H/L_C.

2) A modification of the existing numerical model to enable it to handle turbulent flow.

3) Studies on convective boundary conditions so that the effects of wind speed on the performance of the thermosyphon can be quantified.

REFERENCES

1. M.J. Lighthill, "Theoretical Considerations on Free Convection in Tubes", Quarterly Journal Mech. and Applied Math, Vol. VI, pt. 4, 1953, pp. 398-439.

2. E. Schmidt, "Heat Transmission by Natural Convection at High Centrifugal Acceleration in Water-Cooled Gas Turbine Blades", Paper submitted to Institute of Mechanical Engineers on Jan. 2, 1951, p.361-363.

3. F.J. Bayley and N. Bell, Heat Transfer Characteristics of a Liquid Metal in the Closed Thermosyphon", Engineering, March, 1957.

4. D. Wilkie and S.A. Fisher, "Natural Convection in a Liquid Containing a Distributed Heat Source", International Dev. in Ht. Trans., Proc. of 1961-62 Ht. Trans. Conf., N.Y. ASME, 1963, 995-1002.

5. B.S. Larkin, "Heat Transfer in a Two-Phase Thermosyphon Tube", National Research Council, Canada, Division of Mechanical Engineering, Quarterly Bulletin of the Division of Mechanical Engineering and the National Aeronautical Establishment, Ottawa, No. 3, 1967, p. 45-53.

6. G.H. Johnston, "Permafrost and Foundations", Canadian Building Digest, CBD 64, National Research Council, Ottawa, Ont., Apr. 1965.

7. C.E. Heuer, "The Application of Heat Pipes on the Trans-Alaska Pipeline", U.S. Army Cold Regions Research and Engineering Laboratory, July 1979.

8. G.F. Biyanov, V.I. Makarov, A.D. Molochnikov, "Liquid Cooling Units for Freezing Thawed Ground and Cooling Plastically Frozen Ground for Construction in Areas with Harsh Climates", Permafrost: The Russian Contribution to the Second International Conference, National Academy of Sciences, Washington, D.C., 1973.

9. Anon, Peace-Athabasca Delta Project Report, Intergovernmental Study Group, Dept. of the Environment, Queen's Printer, Edmonton, 1972.

10. B.W. Martin, "Heat Transfer by Free Convection in an Open Thermosyphon Tube", Brit. J. Applied Physics, Vol. 5, No. 3, March, 1954, p. 91-95.

11. J. P. Hartnett and W.E Welsh, "Experimental Studies of Free Convection Heat Transfer in Vertical Tubes with Uniform Wall Heat Flux", ASME Trans., Vol.79, No. 7, October 1957, p. 1551-7.

12. A.D. Gosman, F.C. Lockwood, and D.G. Tatchell, "A Numerical Study of the Heat Transfer Performance of the Open Thermosyphon", Int. J. Heat Mass Transfer, 14(10), (1971).

13. F.J. Bayley and G.S.H. Lock, "Heat Transfer Characteristics of The Closed Thermosyphon", J. Heat Transfer, Feb., 1965, pp. 30-40.

14. D. Japikse, "Heat Transfer in Open and Closed Thermosyphons", Ph.D. Thesis, Purdue University, U.S.A., October, 1968.

15. D. Japikse and E.R.F. Winter, "Heat Transfer and Fluid Flow in the Closed Thermosyphon", Int. J. Heat Mass Transfer 14(4), pp. 427-441 (1971).

16. G.S.H. Lock and S. Maezawa, "The Aerosyphon: An Exploratory Study", Int. J. Heat Mass Transfer 18, pp. 219-226 (1975).

17. S.V. Patankar, "Numerical Heat Transfer and Fluid Flow", Hemisphere Publishing Corporation, Wash., N.Y., London, Mc-Graw-Hill Book Company, 1980.

18. D.G. Tatchell, "The Prediction of Laminar Flow in The Open Thermosyphon by a Finite-difference Technique", M.Sc thesis, Imperial College of Science and Technology, London, England, 1969.

19. G.D. Mallinson, A.D. Graham, and G. de Vahl Davis, "Three-dimensional Flow in a Closed Thermosyphon", J. Fluid Mech. (1981), vol. 109, pp. 259-275.

APPENDICES

APPENDIX 1

Calibration Curves for the Closed Thermosyphon

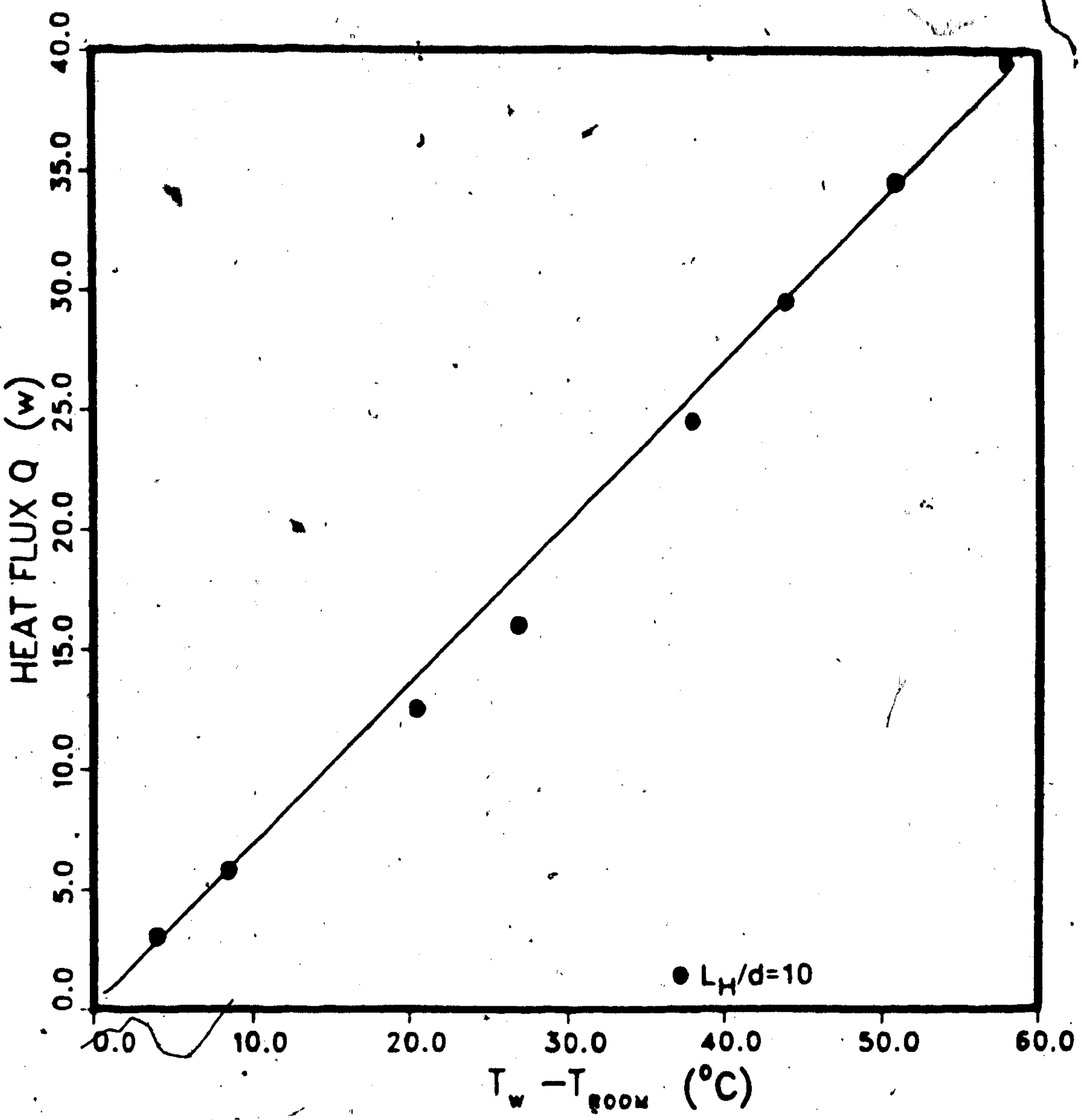

Figure 32. Calibration curve for $L_H/d=10$.

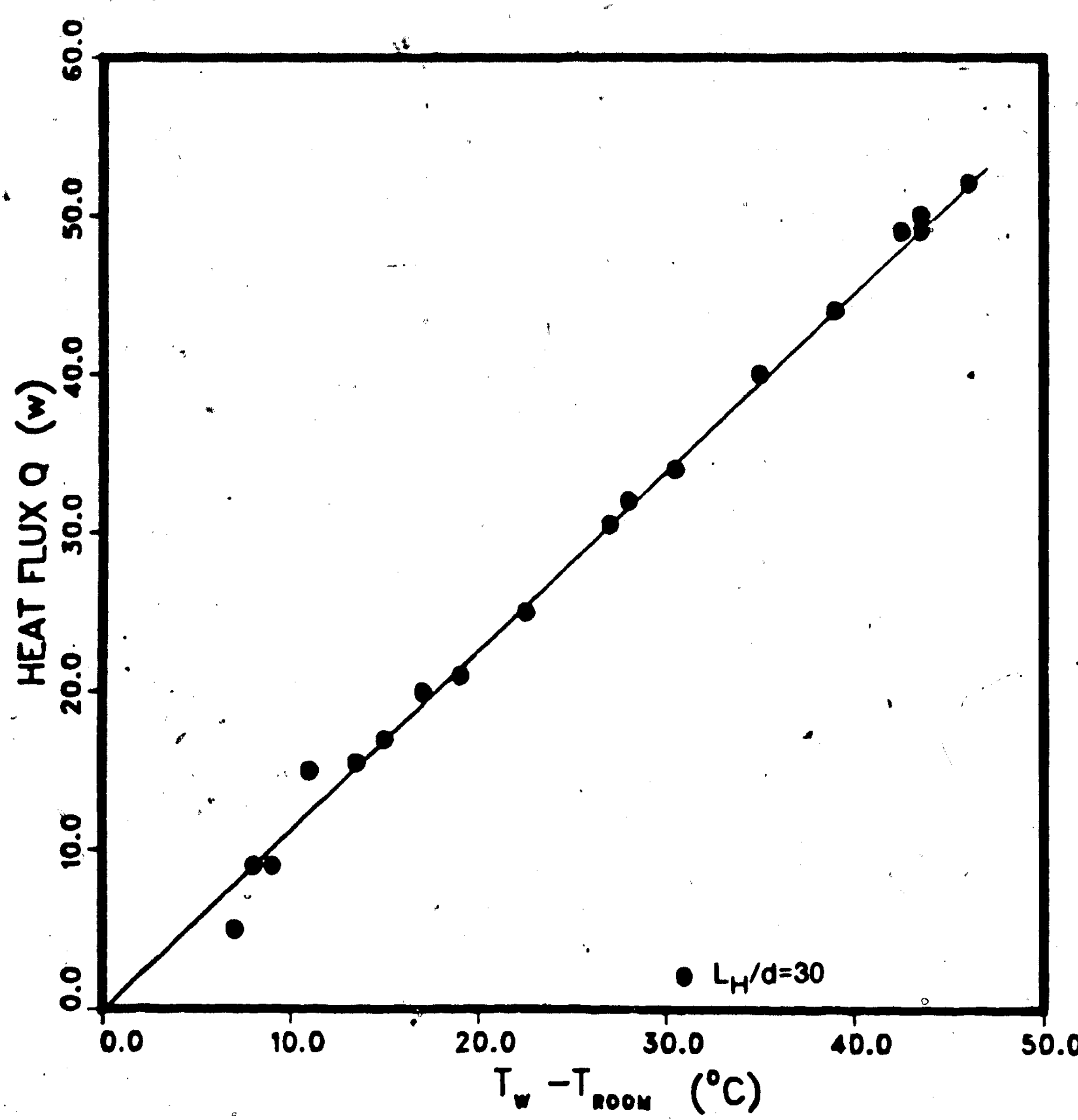

Figure 33. Calibration curve for $L_H/d=30$.

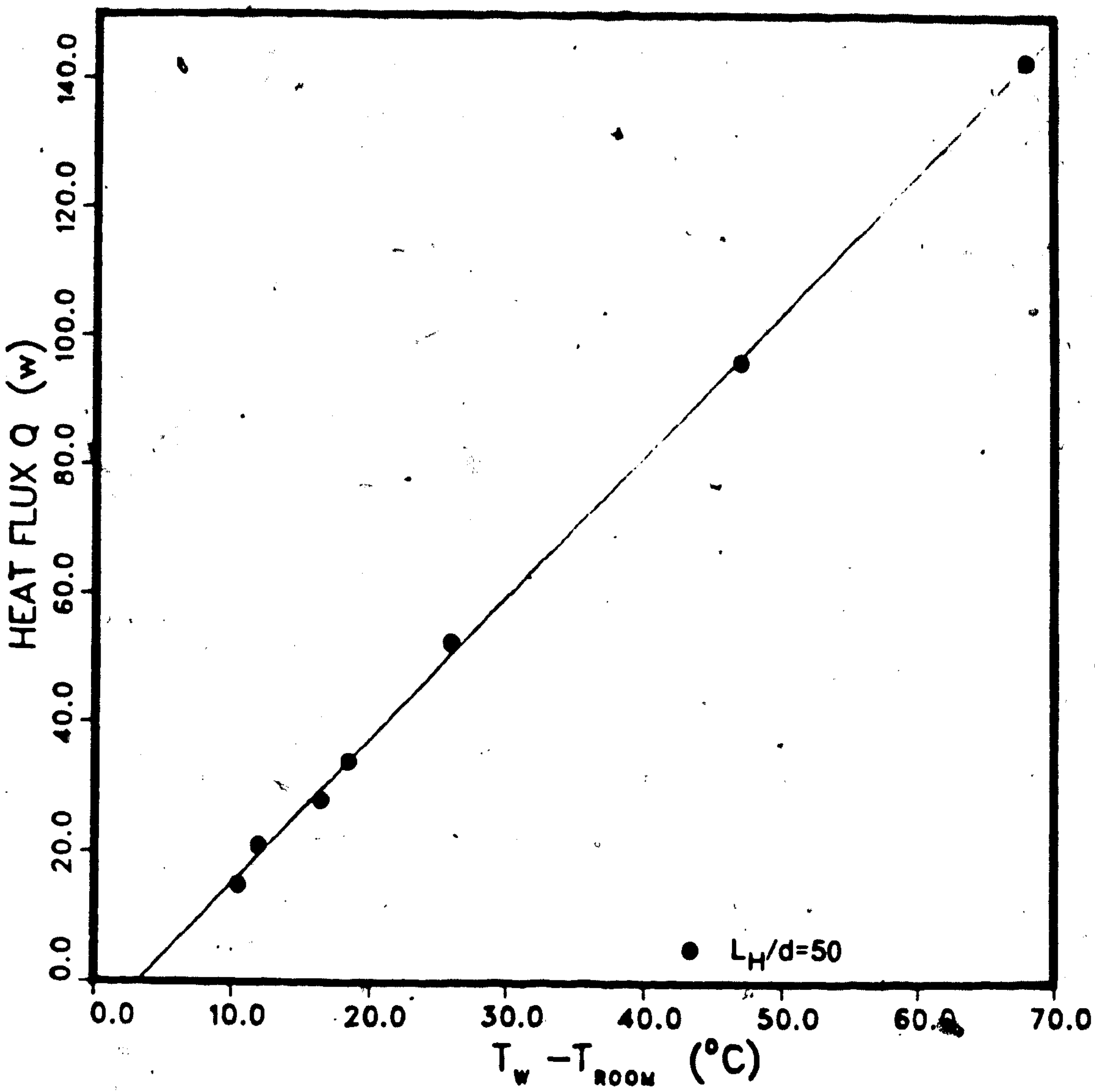

Figure 34. Calibration curve for $L_H/d=50$.

APPENDIX 2

Normalization of the Boundary Layer Equations

Consider the two-dimensional axi-symmetric boundary layer equations:

$$\frac{\partial U}{\partial X} + \frac{\partial V}{\partial R} + \frac{V}{R} = 0 \qquad (1)$$

$$U\frac{\partial U}{\partial X} + V\frac{\partial U}{\partial R} = \beta g\theta + \nu\left[\frac{\partial^2 U}{\partial R^2} + \frac{1}{R}\frac{\partial U}{\partial R}\right] \qquad (2)$$

$$U\frac{\partial T}{\partial X} + V\frac{\partial T}{\partial R} = \kappa\left[\frac{\partial^2 T}{\partial R^2} + \frac{1}{R}\frac{\partial T}{\partial R}\right] \qquad (3)$$

Introduction of the following normalized variables

$$x = \frac{X}{X_c} \quad r = \frac{R}{R_c} \quad u = \frac{U}{U_c} \quad v = \frac{V}{V_c} \quad \phi = \frac{\theta}{\theta_c} = \frac{T-T_\infty}{T_w-T_\infty}$$

into equations (1), (2), and (3) yields

$$\frac{U_c}{X_c}\frac{\partial u}{\partial x} + \frac{V_c}{R_c}\frac{\partial v}{\partial r} + \frac{V_c}{R_c}\frac{v}{r} = 0 \qquad (4)$$

$$\frac{U_c^2}{X_c}\frac{u\partial u}{\partial x} + \frac{U_cV_c}{R_c}\frac{v\partial u}{\partial r} = \beta g\theta_c\phi + \nu\frac{U_c}{R_c^2}\left[\frac{\partial^2 u}{\partial r^2} + \frac{1}{r}\frac{\partial u}{\partial r}\right] \qquad (5)$$

$$\frac{U_c}{X_c}\frac{u\partial\phi}{\partial x} + \frac{V_c}{R_c}\frac{v\partial\phi}{\partial r} = \frac{\kappa}{R_c^2}\left[\frac{\partial^2\phi}{\partial r^2} + \frac{1}{r}\frac{\partial\phi}{\partial r}\right] \qquad (6)$$

From the continuity equation (4), U_c/X_c must be of the same order as V_c/R_c resulting in

$$\frac{U_c R_c}{V_c X_c} = O(1) \qquad (7)$$

Equation (6) may now be re-written as

$$\frac{U_c R_c^{\,2}}{X_c \kappa}\left[\frac{u\partial\phi}{\partial x} + \frac{v\partial\phi}{\partial r}\right] = \frac{\partial^2\phi}{\partial r^2} + \frac{1}{r}\frac{\partial\phi}{\partial r} \qquad (8)$$

By assuming that the advective terms are as important as conduction, it follows that

$$\frac{U_c R_c^{\,2}}{X_c \kappa} = O(1) \qquad (9)$$

By considering equation (5) and assuming that the viscous terms are important

$$\frac{\beta g \theta_c R_c^{\,2}}{\nu U_c} = O(1) \qquad (10)$$

Applying (7) to (10) yields

$$U_c = \left(\frac{\beta g \theta_c X_c}{Pr}\right)^{1/2} \qquad (11)$$

and substituting (11) into (9) results in

$$\delta_c = R_c = \left(\frac{X_c \kappa \nu}{\beta g \theta_c}\right)^{1/4} \qquad (12)$$

APPENDIX 3

Program listings for the Open Thermosyphon Solution, Conduction in a Cylinder, and the Coupling Model.

```
C      OPEN THERMOSYPHON USING STREAM FUNCTION & VORTICITY
C         ISOTHERMAL WALL TEMPERATURES
C
       DIMENSION A(21,21,8),ANAME(6,8),ASYMBL(6),BE(21),BW(21),
     +  BN(21),BS(21),ATITLE(18),FLUX(21),TBAR(21)
       COMMON /CVRBLE/A,ANAME,ASYMBL
       COMMON/CNUMBR/NW,NF,NT,NRO,NMU,NL,NV1,NV2,IE,IV
     +  /CGEO/IN,INM,JN,JNM,IMIN(21),IMAX(21),X1(21),X2(21),
     +  R(21),NCORD/CGEN/ROREF,ZMUREF,NMAX,NPRINT,IP,CC,PR(9),
     +  RP(9),RSDU(9)
       COMMON/CCONST/TR,TW,TL,RR,BETA,COND
C
C  SUBROUTINE FOR INITIALIZATION AND PROGRAM CONTROL
C
C  ENSURE THAT DIMENSIONS OF ARRAYS ABOVE CORRESPOND WITH
C   VALUES ASSIGNED TO N1,N2,N3
       DATA N1,N2,N3/21,21,8/
       INM=IN-1
       JNM=JN-1
C***CALL INITIALIZATION SUBROUTINES
       CALL   GRID (N1,N2,N3,BE,BW,BN,BS)
       CALL   INIT (N1,N2,N3,A)
       WRITE (6,333)
       WRITE (6,334)ROREF,ZMUREF,TL,RR
       TRR=BETA*9.81*(TW-TR)*(RR**4)*PR(3)*ROREF**2/
     +     (ZMUREF**2*TL)
       WRITE (6,335)TR,TW,PR(3),TRR
       NITER=0
C** ITERATION AND PRINTOUT CONTROL LOOP
1      CONTINUE
       NITER=NITER+1
C**  DO ONE ITERATION
       CALL  EQN  (N1,N2,N3,A,BE,BW,BN,BS)
C** TEST IF MAX NUMBER OF ITERATIONS PERFORMED
       IF(NITER.EQ.NMAX) GOTO 8
C      IF(NITER.EQ.10)GOTO 13
C      IF(NITER.EQ.20)GOTO 13
C      IF(NITER.EQ.40)GOTO 13
C      IF(NITER.EQ.80)GOTO 13
C      IF(NITER.EQ.160)GOTO 13
C      IF(NITER.EQ.300)GOTO 13
       IF(NITER.EQ.500)GOTO 13
       GOTO 14
13     WRITE(6,106)NITER
       SUMM=0.0
       DO 88 I=2,INM
       SUMM=SUMM+(3.0*TW-4.0*A(I,JNM,NT)+A(I,JN-2,NT))/
     +    (2.*(X2(JN)-X2(JNM)))
88     CONTINUE
       I=IN
       SUMM=SUMM+0.5*(3.0*TW-4.0*A(I,JNM,NT)+A(I,JN-2,NT))/
     +    (2.0*(X2(JN)-X2(JNM)))
```

```
      I=2
      SUMM=SUMM+0.5*(3.0*TW-4.0*A(I,JNM,NT)+A(I,JN-2,NT))/
     +   (2.0*(X2(JN)-X2(JNM)))
      RNU=SUMM*RR/(TW-TR)/FLOAT(INM)
      WRITE(6,107)RNU
      CALL PRINT(N1,N2,N3,A,ANAME,IN,JN,1,IE)
 14   RES=0
      DO 7 K=1,3
      IF(ABS(RES).LT.ABS(RSDU(K))) RES=RSDU(K)
 7    RSDU(K)=0
C** TEST IF CONVERGENCE CRITERION (CC) SATISFIED
      IF(ABS(RES).GT.CC.OR.NITER.LE.5) GOTO 1
C** END OF LOOP
      GOTO 9
 9    WRITE(6,113)
 8    WRITE(6,106) NITER
      SUMM=0.0
      DO 86 I=2,INM
      SUMM=SUMM+(3.0*A(I,JN,NT)-4.0*A(I,JNM,NT)+A(I,JN-2,NT))/
     +   (2.*(X2(JN)-X2(JNM)))
 86   CONTINUE
      I=IN
      SUMM=SUMM+0.5*(3.0*TW-4.0*A(I,JNM,NT)+A(I,JN-2,NT))/
     +   (2.0*(X2(JN)-X2(JNM)))
      I=2
      SUMM=SUMM+0.5*(3.0*A(I,JN,NT)-4.0*A(I,JNM,NT)+
     +   A(I,JN-2,NT))/(2.0*(X2(JN)-X2(JNM)))
      RNU=SUMM*RR/(TW-TR)/20
      WRITE(6,107)RNU
C** OBTAIN VELOCITY DISTRIBUTIONS
      CALL VELDIS(N1,N2,N3,A)
C** OBTAIN MASS FLOWRATE
      I=2
      FLUXT=0
      TBART=0
      NN=0
      DO 47 J=1,JN
        IF(A(I,J,NV1).LE. 0.0) GOTO 92
 91     FLUX(J)=ROREF*A(I,J,NV1)*2.*3.1416*X2(J)
        FLUXT=FLUXT+FLUX(J)
        TBAR(J)=A(I,J,NT)*2.*X2(J)
        TBART=TBART+TBAR(J)
        NN=NN+1
 92   CONTINUE
 47   CONTINUE
      DR=X2(2)-X2(1)
      FLUXT=(FLUXT-FLUX(1)/2.-FLUX(NN)/2.)*DR
      TBART=DR*(TBART-TBAR(1)/2.-TBAR(NN)/2.)/(X2(NN)*X2(NN))
      QHOT=2.*3.1416*TL*(TW-TBART)*RNU*COND
      WRITE(6,108)FLUXT,TBART,QHOT
      WRITE(6,110)NN
C** FINAL PRINTOUT
```

```
        CALL PRINT(N1,N2,N3,A,ANAME,IN,JN,1,IE)
        DO 44 I=1,IN
        DO 44 J=1,JN
        DO 44 K=1,7
        WRITE(7,133)A(I,J,K)
 44     CONTINUE
        STOP
 133    FORMAT(E13.7)
 318    FORMAT(/,2X,11E10.2)
 106    FORMAT(3X,'NITER= ',I3)
 113    FORMAT(/,3X,'CONVERGENCE OBTAINED')
 107    FORMAT(/,5X,'NU=',E12.3)
 112    FORMAT(5X,4F8.3)
 110    FORMAT(5X,'NN=',I3)
 108    FORMAT(/,5X,'MASS FLOW=',E10.3,'  TEMP CORE=',F9.4,
       +        '  Q=',F10.3)
 333    FORMAT(/,5X,'THERMOSYPHON FINITE DIFFERENCE SOLUTION',/)
 334    FORMAT( 5X,'DENSITY=',F8.2,' ',5X,'VISCOSITY=',E10.4,
       +  ' ',5X,'LENGTH=',F8.3,' ',5X,'RADIUS=',F8.5)
 335    FORMAT(5X,'RESERVOIR TEMP=',F5.2,5X,'WALL TEMP=',F5.2,
       +  5X,'PR=', F8.2,5X,'TRR=',E12.3)
 336    FORMAT(2X,E12.4)
 433    FORMAT(/,2X,4E13.4)
        END
C
C  BLOCK DATA
C
        BLOCK DATA
        COMMON/CNUMBR/NW,NF,NT,NRO,NMU,NL,NV1,NV2,IE,IV
       +  /CGEO/IN,INM,JN,JNM,IMIN(21),IMAX(21),X1(21),X2(21),
       +  R(21),NCORD
       + /CGEN/ROREF,ZMUREF,NMAX,NPRINT,IP,CC,PR(9),RP(9),
       +  RSDU(9)
        COMMON/CCONST/TR,TW,TL,RR,BETA,COND
C
C*****INPUT OF NUMERICAL DATA
C
C** PROGRAM AND PRINTOUT CONTROL DATA
        DATA NW,NF,NT,NV1,NV2,NMU,NRO,NL/1,2,3,4,5,6,7,8/
        DATA IE,IV/3,7/
        DATA NMAX,NPRINT,IP,CC/500,200, 4,0.00100/
        DATA RP(1),RP(2),RP(3)/1.0,0.6,1.1/
C** PHYSICAL DATA
        DATA ROREF,ZMUREF/786.6,0.5514E-03/,PR/9*6.862/
        DATA COND/0.20/
        DATA TR,TW,TL,RR,BETA/20.,29.23,3.0,0.05,1.20E-03/
C** GRID DATA
        DATA NCORD/2/,IN,JN/21,21/,IMIN/21*2/,IMAX/21*20/
        END
C
C**SUBROUTINE FOR BOUNDARY CONDITIONS
C
```

```
      SUBROUTINE BOUND(N1,N2,N3,A)
      DIMENSION A(N1,N2,N3)
      COMMON/CNUMBR/NW,NF,NT,NRO,NMU,NL,NV1,NV2,IE,IV
     + /CGEO/IN,INM,JN,JNM,IMIN(21),IMAX(21),X1(21),X2(21),
     + R(21),NCORD
      COMMON/CCONST/TR,TW,TL,RR,BETA
C*** WALL VORTICITIES
      DO 101 I=1,INM
      DX2=X2(JN)-X2(JNM)
      RW=(R(JN)+R(JNM))/2
      RHO=(A(I,JN,NRO)+A(I,JNM,NRO))/2
101   A(I,JN,NW)=3.*(A(I,JN,NF)-A(I,JNM,NF))/RW/R(JN)/DX2/DX2/
     + RHO-A(I,JNM,NW)*R(JNM)/R(JN)/2.+RHO*9.81*BETA*
     + (A(I,JN,NT)-A(I,JNM,NT))*DX2/8./A(I,JN,NMU)/RW
      DO 102 J=2,JNM
      DX1=X1(IN)-X1(INM)
      RHO=(A(IN,J,NRO)+A(INM,J,NRO))/2
102   A(IN,J,NW)=3.*(A(IN,J,NF)-A(INM,J,NF))/R(J)/R(J)/DX1/DX1
     + /RHO-A(INM,J,NW)/2
C***SYMMETRY AXIS
      DO 301 I=1,INM
      A(I,1,NW)=A(I,2,NW)
301   A(I,1,NT)=A(I,2,NT)
C*** ORIFICE BOUNDARY CONDITIONS
      CALL VELDIS(N1,N2,N3,A)
      DO 109 J=2,JNM
      IF(A(2,J,NV1)) 202,201,201
202   A(1,J,NT)=A(2,J,NT)
      GOTO 203
201   A(1,J,NT)=TR
203   CONTINUE
      A(1,J,NF)=A(2,J,NF)
109   A(1,J,NW)=A(2,J,NW)
C**  ADIABATIC BASE
      DO 103 J=1,JNM
103   A(IN,J,NT)=A(INM,J,NT)
      RETURN
      END
C
C
C*******SUBROUTINE FOR CALCULATION OF AE,AW,AN,AS
C
C
      SUBROUTINE CONVEC (N1,N2,N3,A,AE,AW,AN,AS,I,J,K)
      DIMENSION A(N1,N2,N3)
      COMMON/CNUMBR/NW,NF,NT,NRO,NMU,NL,NV1,NV2,IE,IV
     + /CGEO/IN,INM,JN,JNM,IMIN(21),IMAX(21),X1(21),X2(21),
     + R(21),NCORD
C
      DV=R(J)*(X1(I+1)-X1(I-1))*(X2(J+1)-X2(J-1))
      G1PW=(A(I,J+1,NF)-A(I,J-1,NF)+A(I-1,J+1,NF)
     + -A(I-1,J-1,NF))/DV
```

```
      G1PE=(A(I,J+1,NF)-A(I,J-1,NF)+A(I+1,J+1,NF)
     +   -A(I+1,J-1,NF))/DV
      G2PS=(A(I-1,J,NF)-A(I+1,J,NF)+A(I-1,J-1,NF)
     +   -A(I+1,J-1,NF))/DV
      G2PN=(A(I-1,J,NF)-A(I+1,J,NF)+A(I-1,J+1,NF)
     +   -A(I+1,J+1,NF))/DV
C  COMPUTE AE,AW,AN,AS
      APP=1
      IF(K.EQ.NW)APP=R(J)*R(J)
      AE=0.5*APP*(ABS(G1PE)-G1PE)
      AW=0.5*APP*(ABS(G1PW)+G1PW)
      AN=0.5*APP*(ABS(G2PN)-G2PN)
      AS=0.5*APP*(ABS(G2PS)+G2PS)
      RETURN
      END
C
C
C*****MAIN ITERATION SUBROUTINE
C
C
      SUBROUTINE EQN (N1,N2,N3,A,BE,BW,BN,BS)
      DIMENSION A(N1,N2,N3),BE(N1),BW(N1),BN(N2),BS(N2)
      COMMON/CNUMBR/NW,NF,NT,NRO,NMU,NL,NV1,NV2,IE,IV
     +  /CGEO/IN,INM,JN,JNM,IMIN(21),IMAX(21),X1(21),X2(21),
     +  R(21),NCORD
     +/CGEN/ROREF,ZMUREF,NMAX,NPRINT,IP,CC,PR(9),RP(9),RSDU(9)
      COMMON/CCONST/TR,TW,TL,RR,BETA
C**OBTAIN EFFECTIVE VISCOSITY
      CALL VISCOS (N1,N2,N3,A)
      CALL VELDIS (N1,N2,N3,A)
C**VORTICITY SUB-CYCLE
      DO 11 J=2,JNM
      IL=IMIN(J)
      IH=IMAX(J)
      DO 11 I=IL,IH
C**OBTAIN SOURCE TERM
      CALL SORCE (N1,N2,N3,A,SOURCE,I,J,NW)
C**OBTAIN AE,AW,ETC
      CALL CONVEC (N1,N2,N3,A,AE,AW,AN,AS,I,J,NW)
C**COMPUTE BBE,BBW,BBN,BBS
      RSQ=R(J)*R(J)
      BBE=2.*RSQ*BE(I)
      BBW=2.*RSQ*BW(I)
      BBN=(R(J+1)*R(J+1)+RSQ)*BN(J)
      BBS=(R(J-1)*R(J-1)+RSQ)*BS(J)
      ANUM=(AE+A(I+1,J,NMU)*BBE)*A(I+1,J,NW)
     +  +(AW+A(I-1,J,NMU)*BBW)*A(I-1,J,NW)
     +  +(AN+A(I,J+1,NMU)*BBN)*A(I,J+1,NW)
     +  +(AS+A(I,J-1,NMU)*BBS)*A(I,J-1,NW)+SOURCE
      ADNM=AE+AW+AN+AS+A(I,J,NMU)*(BBE+BBW+BBN+BBS)
      IF (ADNM.EQ.0.)GOTO 11
C**STORE OLD VALUE OF VORTICITY
```

```
 18     Z=A(I,J,NW)
C**CALCULATE NEW VALUE
        A(I,J,NW)=ANUM/ADNM
C**CALCULATE RESIDUAL
        RS=1.-Z/A(I,J,NW)
C**UNDER OR OVER-RELAX IF SPECIFIED
        A(I,J,NW)=Z+RP(NW)*(A(I,J,NW)-Z)
C**STORE MAX RESIDUAL
        IF(ABS(RS).GT.ABS(RSDU(NW)))RSDU(NW)=RS
 11     CONTINUE
C**STREAM FUNCTION SUB-CYCLE
        DO 21 J=2,JNM
        IL=IMIN(J)
        IH=IMAX(J)
        DO 21 I=IL,IH
        CALL SORCE (N1,N2,N3,A,SOURCE,I,J,NF)
C**AVERAGE VALUE OF R USED FOR EVALUATION OF BBN,BBS,BBW,BBE
        RISQ=1./R(J)/R(J)
        ROP=A(I,J,NRO)
        BBE=4./(A(I+1,J,NRO)+ROP)*RISQ*BE(I)
        BBW=4./(A(I-1,J,NRO)+ROP)*RISQ*BW(I)
        BBN=16./(A(I,J+1,NRO)+ROP)/((R(J+1)+R(J))**2)*BN(J)
        BBS=16./(A(I,J-1,NRO)+ROP)/((R(J-1)+R(J))**2)*BS(J)
        ANUM=BBE*A(I+1,J,NF)+BBW*A(I-1,J,NF)+BBN*A(I,J+1,NF)
       +  +BBS*A(I,J-1,NF)+SOURCE
        ADNM=BBE+BBW+BBN+BBS
        IF(ADNM.EQ.0.)GOTO 21
        Z=A(I,J,NF)
        A(I,J,NF)=ANUM/ADNM
        RS=1.-Z/A(I,J,NF)
        A(I,J,NF)=Z+RP(NF)*(A(I,J,NF)-Z)
        IF(ABS(RS).GT.ABS(RSDU(NF)))RSDU(NF)=RS
 21     CONTINUE
        A(1,1,NF)=(A(1,2,NF)+A(2,1,NF))/2
C**SUBCYCLE FOR OTHER VARIABLES
        K=3
        DO 31 J=2,JNM
        IL=IMIN(J)
        IH=IMAX(J)
        DO 31 I=IL,IH
        CALL SORCE (N1,N2,N3,A,SOURCE,I,J,K)
        CALL CONVEC (N1,N2,N3,A,AE,AW,AN,AS,I,J,K)
        BPP=A(I,J,NMU)
        BBE=(A(I+1,J,NMU)+BPP)/PR(K)*BE(I)
        BBW=(A(I-1,J,NMU)+BPP)/PR(K)*BW(I)
        BBN=(A(I,J+1,NMU)+BPP)/PR(K)*BN(J)
        BBS=(A(I,J-1,NMU)+BPP)/PR(K)*BS(J)
        ANUM=(AE+BBE)*A(I+1,J,K)+(AW+BBW)*A(I-1,J,K)
       +  +(AN+BBN)*A(I,J+1,K)+(AS+BBS)*A(I,J-1,K)+SOURCE
        ADNM=AE+AW+AN+AS+BBE+BBW+BBN+BBS
        IF(ADNM.EQ.0.)GOTO 31
        Z=A(I,J,K)
```

```
         A(I,J,K)=ANUM/ADNM
         RS=1.-Z/A(I,J,K)
         A(I,J,K)=Z+RP(K)*(A(I,J,K)-Z)
         IF(ABS(RS).GT.ABS(RSDU(K)))RSDU(K)=RS
   31    CONTINUE
   42    CONTINUE
C**INITIATE ITERATION ON BOUNDARY NODES
         CALL BOUND(N1,N2,N3,A)
         CALL VELDIS(N1,N2,N3,A)
         RETURN
         END
C
C****GRID SUBROUTINE
C
         SUBROUTINE GRID (N1,N2,N3,BE,BW,BN,BS)
         DIMENSION BE(N1),BW(N1),BN(N2),BS(N2)
         COMMON/CNUMBR/NW,NF,NT,NRO,NMU,NL,NV1,NV2,IE,IV
       +  /CGEO/IN,INM,JN,JNM,IMIN(21),IMAX(21),X1(21),X2(21),
       +  R(21),NCORD
         COMMON/CCONST/TR,TW,TL,RR,BETA
C**CALCULATION OF BE,BW,BN,NS
C
C**COMPUTE GRID CO-ORDINATES
C
         DO 10 I=1,IN
   10    X1(I)=FLOAT(I-1)*TL/FLOAT(INM)
         DO 50 J=1,JN
   50    X2(J)=FLOAT(J-1)*RR/FLOAT(JNM)
         DELX2G=X2(JN)-X2(JNM)
         X2(JNM)=X2(JN)-DELX2G/4
         X2(JNM-1)=X2(JN)-DELX2G/2
         X2(JNM-2)=X2(JN)-.75*DELX2G
         X2(JNM-3)=X2(JN)-DELX2G
         JNM3=JNM-3
         DO 51 J=1,JNM3
   51    X2(J)=FLOAT(J-1)*X2(JNM3)/FLOAT(JNM3-1)
C**CALCULATE R(J) ACCORDING TO CHOICE OF CO-ORD SYSTEM
         DO 11 J=1,JN
         R(J)=X2(J)
   11    CONTINUE
C**COMPUTE BE,BW,BN,BS
         DO 21 I=2,INM
         DX1=1./(X1(I+1)-X1(I-1))
         BW(I)=DX1/(X1(I)-X1(I-1))
   21    BE(I)=DX1/(X1(I+1)-X1(I))
         DO 22 J=2,JNM
         DX2=0.5/(X2(J+1)-X2(J-1))
         BS(J)=(1.+R(J-1)/R(J))/(X2(J)-X2(J-1))*DX2
   22    BN(J)=(1.+R(J+1)/R(J))/(X2(J+1)-X2(J))*DX2
C**PRINT OUT CO-ORDINATES
         WRITE(6,101) (X1(I),I=1,IN)
         WRITE(6,102) (X2(J),J=1,JN)
```

```
      RETURN
101   FORMAT(25H DISTANCES IN DIRECTION-1/(1H 4E25.8))
102   FORMAT(25H DISTANCES IN DIRECTION-2/(1H 4E25.8))
      END
C
C**SUBROUTINE FOR CALC. OF INITIAL VALUES AND FIXED B.C.'S
C
      SUBROUTINE INIT (N1,N2,N3,A)
      DIMENSION A(N1,N2,N3)
      COMMON/CNUMBR/NW,NF,NT,NRO,NMU,NL,NV1,NV2,IE,IV
     +  /CGEO/IN,INM,JN,JNM,IMIN(21),IMAX(21),X1(21),X2(21),
     +  R(21),NCORD
     +/CGEN/ROREF,ZMUREF,NMAX,NPRINT,IP,CC,PR(9),RP(9),RSDU(9)
      COMMON/CCONST/TR,TW,TL,RR,BETA
C**SET INITIAL VALUES
      DO 30 K=1,7
      DO 30 J=1,JN
      DO 30 I=1,IN
30    A(I,J,K)=  0.001
C READ IN OLD VALUES
      DO 31 I=1,IN
      DO 31 J=1,JN
      DO 31 K=1,7
      READ(8,134)A(I,J,K)
31    CONTINUE
C**SET DENSITY IN FIELD
      DO 50 I=1,IN
      DO 50 J=1,JN
50    A(I,J,NRO)=ROREF
C**SUPPLY BOUNDARY CONDITIONS
C**BASE
      DO 20 J=1,JN
      A(IN,J,NF)=0.0
      A(IN,J,NT)=TW
      A(IN,J,NV2)=0
      A(IN,J,NV1)=0.0
20    CONTINUE
C**SIDE WALL
      DO 34 I=1,IN
      A(I,JN,NF)=0.0
      A(I,JN,NT)=TW
      A(I,JN,NV1)=0.0
      A(I,JN,NV2)=0.0
      A(IN,J,NV2)=0.0
C**AXIS
      A(I,1,NF)=0.0
34    CONTINUE
      RETURN
134   FORMAT(E13.7)
      END
C
C***OUTPUT SUBROUTINE
```

```
C
      SUBROUTINE PRINT (N1,N2,N3,A,ANAME,IN,JN,NBEGIN,NTOTAL)
      DIMENSION A(N1,N2,N3),ANAME(6,N3)
C
      JX=JN/10
      IF(JX.LT.1)JX=1
      IX=IN/10
      IF(IX.LT.1)IX=1
      K=1
      WRITE(6,100)
      DO 2 L=1,JN,JX
      J=JN+1-L
 2    WRITE(6,101)(A(I,J,K),I=1,IN,IX),J
      WRITE(6,102)(I,I=1,IN,IX)
      K=2
      WRITE(6,103)
      DO 3 L=1,JN,JX
      J=JN+1-L
 3    WRITE(6,101)(A(I,J,K),I=1,IN,IX),J
      WRITE(6,102)(I,I=1,IN,IX)
      K=3
      WRITE(6,104)
      DO 4 L=1,JN,JX
      J=JN+1-L
 4    WRITE(6,101)(A(I,J,K),I=1,IN,IX),J
      K=4
      WRITE(6,105)
      DO 6 L=1,JN,JX
        J=JN+1-L
 6    WRITE(6,101)(A(I,J,K),I=1,IN,IX),J
      K=5
      WRITE(6,106)
      DO 7 L=1,JN,JX
        J=JN+1-L
 7    WRITE(6,101)(A(I,J,K),I=1,IN,IX),J
      INM=IN-1
      DO 47 L=1,JN,2
 47   WRITE(6,108)A(INM,L,1),A(INM,L,2),A(INM,L,3)
 100  FORMAT(/,15X,'VORTICITY')
 101  FORMAT(2X,11E10.2,I8)
 102  FORMAT(/,1X,'I',11I10)
 103  FORMAT(/,15X,'STREAM FUNCTION')
 104  FORMAT(/,15X,'TEMPERATURE')
 105  FORMAT(/,15X,'AXIAL VELOCITY')
 106  FORMAT(/,15X,'RADIAL VELOCITY')
 108  FORMAT(2X,3E12.4)
C     K=NBEGIN
C     DO 10 M=1,NTOTAL
C     WRITE(6,100)  (ANAME(L,K),L=1,6)
C     DO 2 L=1,JN,JX
C     J=JN+1-L
C     WRITE(6,101)  (A(I,J,K),I=1,IN,IX),J
```

```
C      K=K+1
COC    WRITE(6,102) (I,I=1,IN,IX)
C      RETURN
COOC   FORMAT(1H130X,21HTHE DISTRIBUTION OF    ,6A6/
C     231X,57H------------------ ----------------------------/
C     31HO127X,1HJ/127X,3H---//)
CO1C   FORMAT(1HO,3X,11(1PE11.3),3X,I2)
CO2C   FORMAT(1HO//3H I,4X,10(I2,9X),I2/4H ---)
       RETURN
       END
C
C
C***SUBROUTINE FOR SOURCE TERMS
C
C
       SUBROUTINE SORCE(N1,N2,N3,A,SOURCE,I,J,K)
       DIMENSION A(N1,N2,N3)
       COMMON/CNUMBR/NW,NF,NT,NRO,NMU,NL,NV1,NV2,IE,IV
     +  /CGEO/IN,INM,JN,JNM,IMIN(21),IMAX(21),X1(21),X2(21),
     +  R(21),NCORD
       COMMON/CCONST/TR,TW,TL,RR,BETA
C**FOR STREAM FUNCTION
       IF(K.EQ.NF) GOTO 22
       IF(K.EQ.NW) GOTO 33
       SOURCE=0
       RETURN
22      SOURCE= A(I,J,NW)
       RETURN
C**FOR VORTICITY
33     S1=-X2(J)*9.81*A(I,J,NRO)*BETA*(A(I,J+1,NT)
     +    -A(I,J-1,NT))/ (X2(J+1)-X2(J-1))
       S2=(A(I+1,J,NV1)**2+A(I+1,J,NV2)**2-A(I-1,J,NV1)**2
     +    -A(I-1,J,NV2)**2)/(X1(I+1)-X1(I-1))*(A(I,J+1,NRO)
     +    -A(I,J-1,NRO))/(X2(J+1)-X2(J-1))
       S3=(A(I,J+1,NV1)**2+A(I,J+1,NV2)**2-A(I,J-1,NV1)**2
     +    -A(I,J-1,NV2)**2)/(X2(J+1)-X2(J-1))*(A(I+1,J,NRO)
     +    -A(I-1,J,NRO))/(X1(I+1)-X1(I-1))
       SOURCE=-S1
       RETURN
       END
C
C
C***SUBROUTINE FOR CALC OF V1 AND V2
C
C
       SUBROUTINE VELDIS(N1,N2,N3,A)
       DIMENSION A(N1,N2,N3)
       COMMON/CNUMBR/NW,NF,NT,NRO,NMU,NL,NV1,NV2,IE,IV
     +  /CGEO/IN,INM,JN,JNM,IMIN(21),IMAX(21),X1(21),X2(21),
     +  R(21),NCORD
       COMMON/CCONST/TR,TW,TL,RR,BETA
C**INTERIOR NODES
```

```
      DO 50 J=2,JNM
      H2=(X2(J)-X2(J-1))/(X2(J+1)-X2(J))
      RX2=R(J)*(X2(J+1)-X2(J-1))
      IL=IMIN(J)
      IH=IMAX(J)
      DO 50 I=IL,IH
      H1=(X1(I-1)-X1(I))/(X1(I+1)-X1(I))
      RX1=R(J)*(X1(I+1)-X1(I-1))
      A(I,J,NV1)=(A(I,J+1,NF)-A(I,J,NF))*H2+(A(I,J,NF)
     +   -A(I,J-1,NF))/H2
      A(I,J,NV1)=A(I,J,NV1)/RX2/A(I,J,NRO)
      A(I,J,NV2)=(A(I+1,J,NF)-A(I,J,NF))*H1+(A(I,J,NF)
     +   -A(I-1,J,NF))/H1
50    A(I,J,NV2)=A(I,J,NV2)/RX1/A(I,J,NRO)
C**ON PLANE OF SYMMETRY
      J=1
      DO 20 I=1,INM
      A(I,1,NV2)=0.0
20    A(I,1,NV1)=A(I,2,NV1)
C  ORIIFICE
      DELX1=X1(IN)-X1(INM)
      DO 21 J=2,JNM
      H2=(X2(J)-X2(J-1))/(X2(J+1)-X2(J))
      RX2=R(J)*(X2(J+1)-X2(J-1))
      A(1,J,NV1)=(A(1,J+1,NF)-A(1,J,NF))*H2+
     +  (A(1,J,NF)-A(1,J-1,NF))/H2
      A(1,J,NV1)=A(1,J,NV1)/RX2/A(1,J,NRO)
      A(1,J,NV2)=0.0
21    CONTINUE
      RETURN
      END
C
C
C***SUBROUTINE FOR CALCULATION OF EFFECTIVE VISCOSITY
C
C
      SUBROUTINE VISCOS (N1,N2,N3,A)
      DIMENSION A(N1,N2,N3)
      COMMON/CNUMBR/NW,NF,NT,NRO,NMU,NL,NV1,NV2,IE,IV
     +  /CGEO/IN,INM,JN,JNM,IMIN(21),IMAX(21),X1(21),X2(21),
     +  R(21),NCORD
     +/CGEN/ROREF,ZMUREF,NMAX,NPRINT,IP,CC,PR(9),RP(9),RSDU(9)
      DO 10 J=1,JN
      DO 10 I=1,IN
      A(I,J,NMU)=ZMUREF
10    CONTINUE
      RETURN
      END
```

```
C    CONDUCTION IN A CYLINDER
C
      DIMENSION T(12,602),TT(12,602),C1(12),C2(12),C3(12),
     +   C4(12),CP(12),TO(12,602),DT(12),A(12),Q(12)
      INTEGER N,M,L,K
      REAL KK
      DR=0.005
      DZ=0.010
      N=12
      M=202
      TH=60
      KK=0.20
      TC=15
      L=100
      W=1.5
      QSUM=0.0
C   INITIALIZE TEMPERATURES
      DO 100 I=1,N
        DO 200 J=1,M
          IF(J.LE.101.)THEN
            T(I,J)=TC
          ELSE
            T(I,J)=TH
          ENDIF
200     CONTINUE
100   CONTINUE
      DO 50 K=1,L
C   BOUNDARY CONDITIONS
        DO 300 J=2,101
          T(1,J)=2.*TH-T(2,J)
          T(N,J)=T(N-1,J)
          TO(1,J)=T(1,J)
          TO(N,J)=T(N,J)
300     CONTINUE
        DO 400 J=102,M-1
          T(1,J)=2.*TC-T(2,J)
          T(N,J)=T(N-1,J)
          TO(1,J)=T(1,J)
          TO(N,J)=T(N,J)
400     CONTINUE
        DO 500 I=2,N-1
          T(I,1)=2.0*TH-T(I,2)
          TO(I,1)=T(I,1)
500     CONTINUE
        DO 600 I=2,N-1
          T(I,M)=2.*TC-T(I,M-1)
          TO(I,M)=T(I,M)
600     CONTINUE
        DO 700 J=2,M-1
          DO 800 I=2,N-1
            C1(I)=(N-I)*DZ
```

```
                C2(I)=(N-I-1)*DZ
                C3(I)=(N-I-0.5)*DR**2/DZ
                C4(I)=C3(I)
                CP(I)=C1(I)+C2(I)+C3(I)+C4(I)
                TO(I,J)=T(I,J)
                T(I,J)=(C1(I)*T(I-1,J)+C2(I)*T(I+1,J)+C3(I)*
     +                T(I,J-1)+C4(I)*T(I,J+1))/CP(I)
  800         CONTINUE
  700       CONTINUE
            DO 900 I=1,N-1
              DO 910 J=1,M
                T(I,J)=W*T(I,J)+(1-W)*TO(I,J)
  910         CONTINUE
  900       CONTINUE
            WRITE(6,10)( T(I,101),I=1,N)
            WRITE(6,20)( T(I,101+1),I=1,N)
C         WRITE(6,20)( T(I,80),I=1,N)
C         WRITE(6,20)( T(I,120),I=1,N)
  50      CONTINUE
          DO 1000 I=2,N-1
            DT(I)=(T(I,101)-T(I,102))/DZ
            A(I)=3.1416*(((N-I)*DR)**2-((N-I-1)*DR)**2)
            Q(I)=KK*A(I)*DT(I)
            QSUM=QSUM+Q(I)
 1000     CONTINUE
          WRITE(6,30)(Q(I),I=2,N-1)
          WRITE(6,40)QSUM
  30      FORMAT(2X,'Q(I)',2X,10F8.4,/,/)
  40      FORMAT(2X,'QSUM=',F8.4)
  10      FORMAT(2X,10F8.4,/)
  20      FORMAT(2X,12F7.3,/,/)
          STOP
          END
```

```
C
C   COUPLING PROGRAM FOR THE CLOSED THERMOSYPHON
C
      FLUXM=0.310
      QHOT=1006.0
      COND=0.20
      CP=2497.
      PR=6.86
      RHO=786.6
      VIS=0.5514E-03
      THC=20.00
      THW=29.23
      BETA=.12E-02
      RR=0.05
      TL=3.0
      LD=30
      DELTT=THW-THC
      WRITE(6,40)
      DO 10 I=1,40
        RK=FLOAT(I-1)*0.05
        TCC=THC+QHOT*(1.-RK)/(FLUXM*CP*(1.-RK/2.))
        TCW=TCC-DELTT
        RNUD=QHOT/(3.1416*TL*(THW-TCW)*COND)
        TD=BETA*9.81*(THW-TCW)*(RR*2)**4*PR*RHO**2/(VIS**2*TL)
        WRITE(6,30)LD,RK,TD,RNUD,TCC,TCW
   10 CONTINUE
   40 FORMAT(3X,'   L/D        K           TD                 NUD',/)
   20 FORMAT(3X,I4,2F7.2,E10.3,2F8.3)
   30 FORMAT(3X,I4,5X,F8.3,5X,E10.3,5X,F8.3,3X,F8.3,3X,F8.3)
   11 FORMAT(3X,2F8.3)
      END
```